2013

Fabrication and characterisation of conducting fibres for use in biomedical applications

Dorna Esrafilzadeh
University of Wollongong

Intelligent Polymer Research Institute (IPRI), Australian Research Council (ARC) Centre of Excellence for Electromaterials Science (ACES), Australian Institute for Innovative Materials (AIIM)

Fabrication and Characterisation of Conducting Fibres for Use in Biomedical Applications

Dorna Esrafilzadeh

This thesis is presented as part of the requirement for the
Award of the Degree of **Doctor of Philosophy**
of the
University of Wollongong

August 2013

This work is dedicated to my parents, Mrs. Mina Chelabi and Mr. Hemmat Esrafilzadeh and my lovely partner Ali for their love and support.

Certification

I, Dorna Esrafilzadeh, declare that this thesis, submitted in fulfilment of the requirements for the award of Doctor of Philosophy, in the School of Chemistry, Faculty of Science, Health and Medicine, University of Wollongong, is wholly my own work unless otherwise referenced or acknowledged. The document has not been submitted for qualification at any other academic institution.

Dorna Esrafilzadeh
August 2013

ABSTRACT

Fabrication and characterisation of conducting biomaterials in 3-dimensional configuration for biomedical applications have been studied and is presented in this thesis. Different fibre spinning techniques (wet-spinning and electrospinning) were utilised to create multifunctional fibres to be employed for controlled drug delivery and cellular growth supports. Two different classes of organic conductors, namely conducting polymers and graphene, were utilised to induce and develop electrical and electrochemical features in the fibres for their potential applications in drug delivery and cell growth enhancement via electrical stimulation. Physical, mechanical, electrical, electrochemical and biological characterisations of the fibres were investigated.

In chapter two, Poly(3,4-ethylenedioxythiophene) poly(styrene sulfonate) (PEDOT:PSS) and polypyrrole (Ppy) were utilised in conjugation with chitosan for fabrication of conducting biocompatible fibres using wet-spinning. Then, a layer of Ppy with an antibiotic drug Ciprofloxacin hydrochloride (Cipro) as a dopant for Ppy was produced on the PEDOT:PSS-CHI fibres. The wet-spinning of PEDOT:PSS in a chitosan coagulation bath was successfully carried out and the fibres were shown to have an electrical conductivity of 56 ± 7 S/cm with a modulus and strength of 2.0 ± 0.3 GPa and 99 ± 7 MPa, respectively. The PEDOT:PSS-CHI fibres were subsequently employed as an electrode for the electropolymerisation of Ppy.Cipro on their surfaces. Scanning electron microscopy (SEM) of the fibres showed the morphological differences between PEDOT:PSS and Ppy.Cipro layers, confirming the deposition of the Ppy.Cipro. Cyclic voltammograms of fibres exhibited that the Ppy.Cipro was electroactive and showed an oxidation and reduction peak at +0.2 V

and -0.1 V, respectively. The conducting and electroactive fibres were utilised for controlling the release of Cipro using an electrochemical stimulation protocol. The results of electrical stimulation of fibres revealed that Cipro release could be tuned by utilizing the different redox states of PEDOT:PSS-CHI and Ppy.Cipro conducting polymers. The *in vitro* antibacterial studies on the fibres and released Cipro demonstrated that the drug did not lose its antibacterial property during electropolymerisation and electrochemically stimulated release processes. *In vitro* fluorescent staining images revealed that the fibres were not cytotoxic to B35 neuroblastoma cells, however, the cells tended to cluster together rather than attach to the fibres. Moreover, the results of a lactate dehydrogenase (LDH) test revealed that the Cipro concentrations released in this study did not have an adverse effect on B35 neural cell.

In chapter three, the development of a novel and facile system of wet-electrospinning (combined electrospinning and wet-spinning) is presented. This new method was developed in order to improve the attachment behaviour of B35 neuroblastoma cells on wet-spun fibres containing conducting polymers. The process of fibre fabrication consists of simultaneously wet-spinning and electrospinning to form a structure composing of micro-size wet-spun fibres coated in nano-sized electrospun fibres. The new fibre configuration demonstrated increased B35 neuroblastoma cell attachment as well as promising electrochemical property. Extended electrospinning times resulted in a thick coating of poly(D,L-lactic-co-glycolic acid) (PLGA) around the PEDOT:PSS-CHIT fibres which hindered the electroactivity of this conducting inner core. This was attributed to the thick PLGA coating blocking any ions from solution interacting with the PEDOT:PSS. This result had implications on the ability to use these particular fibres in electrical stimulation experiments, and therefore

shorter electrospinning times were investigated. Additionally, the release of Cipro from PLGA electrospun fibres has shown the potential of the fibres in drug delivery applications.

In chapter four, fabrication and characterisation of graphene as an organic conductor in a wet-spun composite fibres structure was studied to induce and develop electrical conductivity and electrochemical activity in the fibres. The graphene dispersion exfoliated in N-Cyclohexyl-2-pyrrolidone (CHP) exhibited dispersion stability over an extended period of time. The free-standing graphene paper fabricated from the dispersion (thickness between 5.0 to 100 μm) demonstrated well-defined layered morphology of graphene. The TEM characterisations of CHP-exfoliated graphene showed that the graphene dispersion consisted of monolayer and few layers of graphene. Additionally, the blend of PLGA with graphene was fabricated using a wet-spinning system. The rheological characterisation of wet-spinning solutions showed that a concentration of 1.5 wt. % PLGA and above, dissolved in 5 mg/ml graphene dispersion in CHP, can provide viscosity of $\geq$ 0.023 Pa s which was found to be spinnable. The wet-spinning of graphene with the biocompatible PLGA was carried out successfully with the fibres demonstrating an electrical conductivity of 1.5 S/cm. The PLGA-graphene fibre showed electroactivity in phosphate buffered saline (PBS) when tested by cyclic voltammetry. The electrical conductivity measurements showed that, once the graphene content was greater than 11.1 wt. % (with respect to PLGA), electrical conductivity increased above the percolation threshold (~30 S/m) and increased to 150 S/m when the graphene content was 24.3 wt. %. The cytocompatibility tests and cryo-SEM images showed that C2C12 myoblast cells were metabolically active on the fibres and attached along the length

of the fibres. Furthermore, the proliferation assessment over 72 hr on the fibres revealed that C2C12 cells proliferated along the fibres.

ACKNOWLEDGEMENTS

I would like to thank my principal supervisor Professor Gordon Wallace and my co-supervisors A/Prof. Simon Moulton and Dr. Joselito Razal for their supervision. I truly appreciate the opportunity that Professor Gordon Wallace gave me to work in a prestigious research environment. A special thanks to A/Prof. Simon Moulton for the time has spent on my work, publications and thesis, as well as encouragement throughout my time in IPRI, thank you; I could not have done it without you.

I would like to thank Dr. Elise Stewart for her collaboration in cells and bacteria studies as well as correcting my chapter and paper, Dr. Brianna Thompson, Dr. Kerry Gilmore and Dr. Robin Gorkin III for their help in correcting my thesis. Huge thanks to Dr. Kerry Gilmore for her generous training on cell culture works. Thanks to Dr. Tony Romeo, Mr. Darren Attard for their help on SEM, TEM and sputter coating. Additionally, the help and guidance from, Dr. David Harman, Dr. Pawel Wagner, Dr. Klaudia Wagner, A/Prof. Peter Innis, Dr. Damia Mawad, Dr. Xiao Liu, Dr. Stephen Beirne and Ms. Sue Ku who provided the background I lacked in different stages of the project, are also gratefully acknowledged.

Thanks to all my friends in IPRI and AIIM, who are still here or have left for new adventures, including Adrian, Alberto, Wen, Grace, Mohammed, Jared, Sima, Hamed, Cameron, Willo, Cathal, Mark, Sara, Sina, Maryam, Peter, Amy, Bo, Nuchalee, Wid and Binbin, for their support in work and other little things that made my Ph.D. journey so much more interesting.

Finally and most important, I would like to thank my family, Dad, Mum and Kimi for their patience, support and unconditional love.

To Ali Jalili, thank you, the last 10 years would not have been the same without you.

PUBLICATIONS

1. **Dorna Esrafilzadeh**, Joselito M Razal, Simon E Moulton, Elise M Stewart, Gordon G Wallace, "*Multifunctional conducting fibres with electrically controlled release of ciprofloxacin*", **Journal of Controlled Release**, 2013, 169 (3), Pages 313-320.

2. Rouhollah Jalili, Seyed Hamed Aboutalebi, **Dorna Esrafilzadeh**, Konstantin Konstantinov, Simon E Moulton, Joselito M Razal, Gordon G Wallace, **"***Organic Solvent-Based Graphene Oxide Liquid Crystals: A Facile Route toward the Next Generation of Self-Assembled Layer-by-Layer Multifunctional 3D Architectures*", **ACS Nano**, 2013, *7* (5), Pages 3981-3990.

3. Rouhollah Jalili, Seyed Hamed Aboutalebi, **Dorna Esrafilzadeh**, Roderick L Shepherd, Jun Chen, Sima Aminorroaya-Yamini, Konstantin Konstantinov, Andrew I Minett, Joselito M Razal, Gordon G Wallace, "*Scalable One-Step Wet-Spinning of Graphene Fibers and Yarns from Liquid Crystalline Dispersions of Graphene Oxide: Towards Multifunctional Textiles*", **Advanced Functional Materials**, 23 (43), 5345–5354, 2013..

4. Rouhollah Jalili, Seyed Hamed Aboutalebi, **Dorna Esrafilzadeh**, Konstantin Konstantinov, Joselito M. Razal, Simon E. Moulton and Gordon G. Wallace, "*Formation and Processability of Liquid Crystalline Dispersions of Graphene Oxide*", **Materials Horizons**, 1 (1), 87-91, 2014.

5. Seyed Hamed Aboutalebi., Rouhollah Jalili, **Dorna Esrafilzadeh**, Maryam Salary, M., Zahra Golamvand, Sima Aminorroaya-Yamini, Konstantin Konstantinov, Roderick L Shepherd, Jun Chen, Simon E Moulton, Peter C Innis, Andrew I Minett, Joselito M Razal, Gordon G Wallace, "*High Performance Multifunctional Graphene Yarns: Towards Wearable all-carbon Energy Storage Textiles*". **ACS Nano**, 8 (3), 2456–2466, 2014.

CONFERENCE PRESENTATIONS

1. **Dorna Esrafilzadeh**, Rouhollah Jalili, Kerry J. Gilmore, Joselito M. Razal, Simon L. Moulton, Gordon G. Wallace, "*Combined Wet-spinning & Electro-spinning: Novel and Facile Method to Fabricate Micro-nano Scale Conducting Fibres*", International Fibre Conference, 22th- 24th May, 2013, Geelong, Australia.

2. **Dorna Esrafilzadeh**, Joselito M. Razal, Simon E. Moulton, Elise M. Stewart & Gordon G. Wallace, "*Conducting polymer wet-spun fibres for bionic applications*", 9th World Biomaterials Congress, Innovative Biomaterials and Crossing Frontiers in Biomaterials and Regenerative Medicine, 1st- 5th June, 2012, Chengdu, China.

3. **Dorna Esrafilzadeh**, Joselito M. Razal, Simon E. Moulton, Elise M. Stewart & Gordon G. Wallace, "*Bio conducting wetspun fibre*", 7th Annual International Electromaterials Science Symposium, 15th- 17th February, 2012, Geelong, Australia.

4. **Dorna Esrafilzadeh**, Joselito M. Razal, Simon E. Moulton & Gordon G. Wallace, "*Controlled release of ciprofloxacin from double layer conducting fibre*", ACES Electromaterials Symposium, 9th-11th February, 2011, Wollongong, Australia.

5. **Dorna Esrafilzadeh**, Joselito M. Razal, Simon E. Moulton & Gordon G. Wallace, "*PEDOT:PSS-CHI wetspun fibres*", 2nd Asia-Pacific Symposium on Nanobionics, 9th -11th June, 2010, Wollongong, Australia.

6. **Dorna Esrafilzadeh**, Joselito M. Razal & Gordon G. Wallace, "*Bi-component wetspun fibres for bionic applications*", ACES Electromaterials Symposium 2nd -4th February 2010, Melbourne, Australia.

ABBREVIATIONS

PEDOT:PSS	poly(3,4-ethylenedioxythiophene) poly(styrene sulfonate)
rpm	revolutions per minute
CHI	Chitosan
EG	ethylene glycol
Degrees Celcius	°C
CV	cyclic voltammetry
EIS	electrochemical impedance spectroscopy
SEM	scanning electron microscopy
Ppy	Polypyrrole
PBS	phosphate Buffer Saline
Cipro	ciprofloxacin hydrochloride
UV.VIS	ultraviolet-visible spectrophotometry
M_t	release mass
E.Coli	Escherichia coli
S. pyogenes	Streptococcus pyogenes
DMEM	dulbecco's modified eagle's medium

FBS	fetal bovine serum
Pt	Platinum
ZOI	zone of inhibition
LDH	lactate dehydrogenase
AECM	artificial extra cellular matrix
PLGA	poly lactic-co-glycolic acid
λmax	wavelength of a maximum absorbance
TCP	tissue culture plate
CHP	cyclohexyl-pyrrolidone
α	extinction coefficient
PVDF	polyvinylidene difluoride
Y	Young's modulus
σ	tensile strength
ε	breaking strain
TGA	thermal gravimetric analysis
DMSO	dimethyl sulfoxide

NMP	*N*-Methyl-2-pyrrolidone
DMF	Dimethylformamide
D	Defect
G	Graphene
TEM	transmission electron microscopy
Ppy.Cipro	polypyrrole doped with ciprofloxacin hydrochloride
PSS	poly(sodium styrene sulfonate)
SWCNT	single-walled carbon nanotube
NaCl	sodium chloride
Hz	hertz, unit of frequency
µl	microliter, a measure of volume 1 µl = 10^{-6} litre
Ag	silver
AgCl	silver chloride
N	nitrogen
S	sulphur
FTIR	fourier transform infrared spectroscopy
mA	milliampere

S	second(s)
min	minute(s)
nm	nanometre, A measure of length 1 nm = 10^{-9} metres
Py	Pyrrole
hr	hour

TABLE OF CONTENTS

LIST OF FIGURES

LIST OF TABLES

1 INTRODUCTION

1.1 Thesis outline

Biomaterials are an exciting class of materials that scientists are using in various biomedical applications such as tissue regeneration and targeted drug delivery. The term biomaterials consist of two words, “bio” and “materials”, each representing an immense category in science. The combination of these two categories brings us new vision in terms of selecting the right precursors, engineering better architectures with desirable characteristics to enhance and control the interaction of living cells, determining appropriate therapeutic triggers or development of novel diagnostic methods.

This thesis describes the fabrication of 3-dimensional conducting biomaterials and characteristics of organic conductors individually or in combination with non-conductive polymers for different biomedical applications such as controlled drug delivery and tissue regeneration. Primarily, wet-spinning methods were used to fabricate composite conducting materials comprising of conducting polymers, graphene and biopolymers. These materials were tested for cyctocompatibility, ability to controllably deliver therapeutic agents, and their applications as templates for cellular growth. In addition, a new combined electrospinning and wet-spinning system was developed and optimised in order to improve cell adhesion on wet-spun fibres.

These studies are summarised in the following sections:

In Chapter 1, organic conductors are introduced and selective applications in biomedical engineering are explained. Conducting polymers (PEDOT:PSS, Ppy) and graphene as examples of organic conductors were studied and their chemical and physical reactions have been described in detail. Then, the importance of engineering

3-dimensional structures has been defined with more details of the fabrication methods used in this project. The chapter concludes with applications of defined architectures with the potential for drug delivery and tissue engineering.

Chapter 2 describes the fabrication of 3-dimensional conducting fibres via wet-spinning. The characteristics of fibres were investigated electrochemically and physically using cyclic voltammetry, electrochemical impedance spectroscopy and mechanical analysis. A novel structure of a double layer of conducting fibres is introduced which enable loading and releasing biological triggers; in this case the controlled release of the antibiotic drug, ciprofloxacin, is demonstrated. The activity of drug and cytocompatibility of conducting fibres are examined using zone of inhibition and fluorescent staining imaging tests.

In Chapter 3, a combined wet-spinning and electrospinning system is introduced, the process is a new combination of electrospinning and wet-spinning in continuous mode. PEDOT:PSS-CHI-PLGA fibres were fabricated and characterised physically and electrochemically using scanning electron microscopy (SEM) and cyclic voltammetry techniques respectively. Moreover, improvement in cell attachment on the fibres produced with the new spinning system has been demonstraed using Calcein AM and cryo-SEM images.

Chapter 4 investigates graphene as another type of organic conductor. In this work graphene is synthesised using solvent exfoliation method and its properties have been characterised. Fabrication of graphene fibres via wet-spinning method blended with PLGA was performed, and physical and electrochemical behaviours of the fibres have been investigated using SEM, conductivity measurements and cyclic

voltammetry. Cytocompatibility of the fibres was tested using fluorescent staining imaging and cryo-SEM on skeletal muscle myoblast (C2C12) cells.

Chapter 5 concludes the thesis by providing final conclusions and recommendations for further research. The reader should note that each relevant chapter includes a short introduction, followed by experimental, results and discussion and conclusion sections.

1.2 Materials in biomedical applications

There are a wide range of materials utilised in biomedical applications including organic and inorganic chemical components, metals, alloys and ceramics. Specific materials have been commonly applied in different biomedical fields such as orthopaedics, dental implants, controlled drug delivery, artificial vascular materials and device housings. In this thesis, the focus is on the role of organic conductors and polymers as biomaterials for drug delivery and cells growth template. Therefore, different categories of polymers and organic conductors will be described in following sections.

1.2.1 Structural polymers

Polymers are a favourite sub-group of organic components, which have been applied in biomedical fields for decades. The first experiment of cells growth on polymers template was performed by Vacanti *et al* in 1988 with harvesting of liver, pancreas and intestine cells on poly anhydride and poly orthoesters discs [1]. The results showed that the cells could be cultured on biocompatible polymer without showing toxicity [1]. It was a promising beginning for the establishment of tissue engineering science. By introducing the concept of tissue engineering in science, cell growth on an external template attracted considerable attention. Vast varieties of classic polymers have been applied for cell growth such as Polycaprolactone (PCL) [2], Poly lactic-co-glycolic acid (PLGA) [3], Polyurethane (PU) [4], etc by synthesis whereas, alginate [5], chitosan [6] and collagen [7], etc have been utilised for cell growth from natural sources. The growth of cells are influenced by various factors such as substrate composition, architecture, biocompatibility and other external stimuli including electrical signals, mechanical pulses and presence of growth factors or other biological agents [8].

In this thesis, polymers are categorised into non-conducting and conducting materials. Non-conducting materials are vastly used as templates for cell growth (scaffolds) and artificial implants. Conducting scaffolds have been used as template for cell growth in addition to applying electrical stimulation of cells to improve functional development.

In the following sections, chemical composition, synthesis and applications of PLGA and chitosan are explored; as they are a focus of several sections of the thesis.

1.2.1.1 Poly lactic-co-glycolic acid (PLGA)

PLGA comes from a family of linear aliphatic polyesters, that are widely applied in biomedical applications. There are different types of PLGA including PLGA (50:50), PLGA (75:25) and PLGA (85:15), that have different ratios of lactic to glycolic acid, with various degradation timeframes from a few weeks to a few months [9]. The chemical structure of PLGA is presented in Figure 1.1. The versatile degradation timeframe in conjunction with biocompatibility of PLGA encourages its application in biomedical researches such as tissue engineering [10], scaffolds [3] and drug delivery [11].

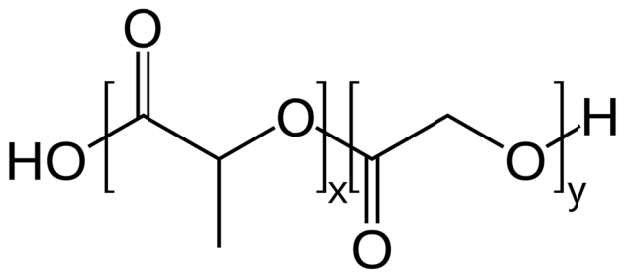

Figure 1.1. Chemical structure of poly (lactic-co-glycolic acid). X is the number of lactic acid and y is number of glycolic acid units.

Uematsu *et al.* applied PLGA for cartilage regeneration by culturing mesenchymal stem cells (MSCs) on the polymer scaffold and implanting into a rabbit's injured knee [12]. The results demonstrated that the defect area was filled by new cartilage after 12 weeks implantation [12].

1.2.1.2 Chitosan

A de-acylated derivation of chitin (chitosan) is a type of linear polysaccharide. It has a very broad range of molecular weights, from 50 to 1000 kDa, that could be tuned on the basis of sources and preparation procedures [13]. Chitosan is a semi-crystalline polymer. Due to its crystalline structure, it normally does not dissolve in aqueous solution at pH≈7 however, it dissolves in dilute acid (pH≈ 5) easily [13]. Its cationic nature and high charge density with its enzymatic hydrolysis degradation in combination with biocompatibility makes it a suitable choice for biomedical applications. The ability to process it in a porous structure and its applications in cells transplantation is one of the chitosan features [14]. Chitosan was utilised for treatment of periodontitis and was absorbed by the host tissue perfectly. It kept its honeycomb structure based on the evidence received from biopsy of 10 patients [6]. It has also been applied in controlled drug delivery using different methods such as spheres (micro, nano), spray coating, emulsion droplets [15].

1.2.2 Electro-active materials

Conducting substrates are often utilised as connector between cells and electrical sources to pass or receive electrical signals to and from cells [16]. In 1791, Luigi Galvani applied the electrical pulse on muscle for the first time to investigate the phenomena of "animal electricity" [17]. Conducting platforms include metals (gold, platinum and stainless steel), or organic conductors (inherently conducting polymers

and graphene). It is usually thought that organic materials are electrical insulators. However, the progress made in chemical synthesis and molecular modification has brought a rich variety of conducting organic materials [18-20]. These materials can be classified into inherently conducting polymers and carbon derivatives such as carbon nanotubes (CNTs) and graphene [18, 21]

The chemical structures, synthesis methods, and electrochemical properties of the conducting polymers used in this work, specifically poly (3,4-ethylenedioxythiophene) poly (styrene sulfonate) **(**PEDOT:PSS), polypyrrole (Ppy) and graphene, will be described in the following sections..

1.2.2.1 Inherently conducting polymers

It is viable to have highly conducting polymers in a charge transfer complex as long as suitable combination of an organic electron donor or acceptor molecules with counter-ions or other organic molecules provide charge carriers, known as dopants [18]. During the chemical doping process, these charge transfer complexes provide high electrical conductivity [18]. These complexes known as inherently conducting polymers (ICPs), or synthetic metals, have attracted considerable attention soon after their discovery by Shirakawa *et al.* [18]. Subsequently, extensive characterisations of the ICPs including electrical, thermal and environmental stability as well as their processability indicate their potential for their use in electronic, renewable energy, composites and biomedical applications. Over the last 30 years a wide range of ICPs based on, anilines, pyrroles and thiophenes have been developed [22-25].

ICPs can be polymerised by either chemical [26] or electrochemical [27] methods, with chemical synthesis being the preferred method when large quantities of polymer are required. The procedure involves the addition of a strong oxidising agent (such as

$FeCl_3$) to the monomer solution [28] to initiate the free radical polymerisation process. Electrochemical synthesis is typically performed in a 3-electrode cell comprising of a working, auxiliary and reference electrodes, whereby polymerisation is initiated by the application of either a voltage or current and an insoluble ICP film forms on the working electrode, driven by electrostatic forces [29]. This method of synthesis is usually chosen for research purposes because of the ease of the system and the ability to have control over of the amount of material deposited. In addition, using electrochemical polymerisation, it is possible to deposit the polymer on any shape of electrode and it provides a broad choice of existing dopant ions and the production of fine quality films [29].

Figure 1.2 shows the polymerisation of polypyrrole (Ppy) (one of the most important classes of ICPs) from a bulk solution containing pyrrole monomer. The electrodeposition proceeds by adsorption of a monomer unit onto the surface of the working electrode, the positively polarised electrode, to form a pyrrole cation radical through the oxidation process. These cations combine together or with neutral monomers present in the solution [30] to form a dimer, which undergoes double deprotonation to provide a neutral molecule. Dimer radicals are more stable and have a lower oxidation potential compared with the monomer units and polymer chain growth then occurs by favoured coupling between the dimers and monomers. The electrical conductivity and chemical stability of ICPs occurs as a result of extended π-conjugated backbone and its hetero aromatic structure [30]. As positive charges are developed along the polymer during polymerisation, the incorporation of negatively charged counter-ions become necessary to maintain charge balance within the ICP backbone. This latter process is known as doping [31].

The conductivity of ICPs can be enhanced to metallic levels by chemical or electrochemical `p-doping' (oxidation) [22], or `n-doping' (reduction) [22]. The conductivity enhancement of ICPs is due to movement of electrons along the backbone of the polymer after the doping process [29]. During oxidative doping of ICPs, “holes” are created throughout the polymeric chain and electrons move freely to these holes and it assists electron movement and conductivity eventually [29]. This hole, which is basically a molecule or part of a macromolecular chain containing two positive charges in the conjugated system (known as bipolaron), is responsible for high conductivity of an ICP after oxidative doping [19].

In contrast with metals, the electrical, electrochemical and physical properties of ICPs can be tailored for particular applications by changing the dopant and doping process [19, 32, 33]. ICPs have been utilised for biosensors [34], drug delivery [35], cells host template [36], and stimulation of cells or tissues to enhance cells survival or direction [37]. ICPs such as PPy and PANI are not biodegradable; therefore they are often used in combination with other biodegradable polymers such as PLGA, PVA and PCL for use in biomedical applications, where biodegradability required. Polypyrrole is one of the most preferred conducting polymer used in biomedical applications due to its ability to be synthesised at neutral pH and its ability to support cell growth. Rivers et al. used the strategy of tethering conductive pyrrole-thiophene oligomers to degradable ester linkages using an aliphatic linker. They demonstrated that these ICP-blends were biocompatible with human neuroblastoma cells and that they also demonstrated degradability in PBS [38]. Conducting polymers including, PEDOT have been utilised in cellular growth support and implantable cochlear [5, 39]. Several studies have also reported utilising PANI [40-43] and PT [44] as cellular growth templates and neural electrode respectively.

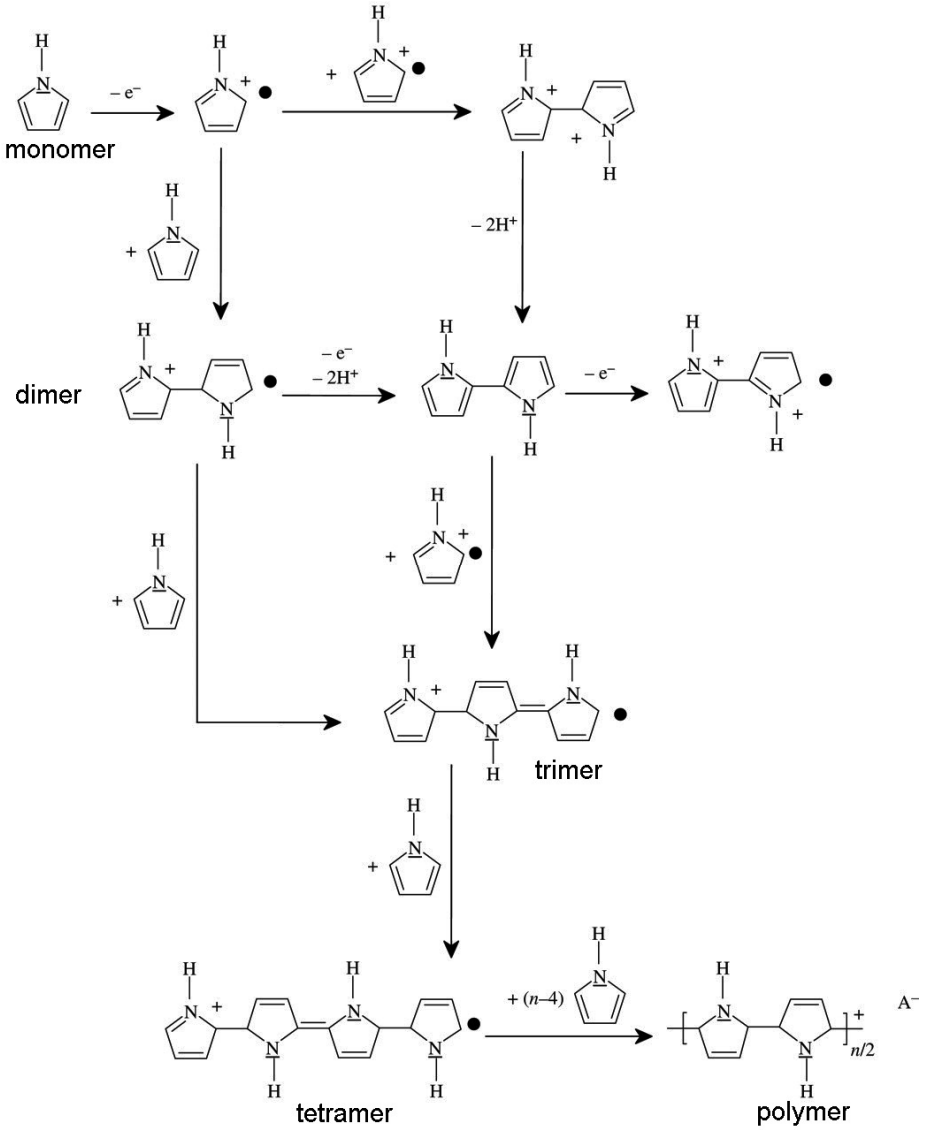

Figure 1.2. Mechanism of polypyrrole polymerisation

1.2.2.1.1 Polypyrrole

Polypyrrole (Ppy) is an ICP which has been greatly explored due to its high electrical conductivity, biocompatibility, low production cost and suitable environmental stability [42]. Ppy has been considered in a variety of applications including, capacitors [23], electronic devices [45], actuators [46], sensors [47], corrosion-protection materials [48], electrochromic devices [49], electrodes for rechargeable batteries [50], super capacitors [51], controlled drug delivery [52], 3D scaffold [39].

The oxidation potential at which pyrrole is polymerised into Ppy is normally above +600mV versus an Ag/AgCl reference. The morphology and electrochemical property of the resulting film depend on several processing parameters including the nature of supporting electrolyte, crystallographic structure of underlying anode, potential used for deposition, nature of dopant, monomer concentration, temperature and pH of the solution [53, 54]. Figure 1.3 illustrates some examples of different surface topographies due to variation of counter-ions and synthesis durations. The shorter polymerisation times (10 min) (A, C, E and G) create thin films with very little surface features while at longer times (60 min) (B, D, F and H), thicker films with distinctive topography are observed [55].

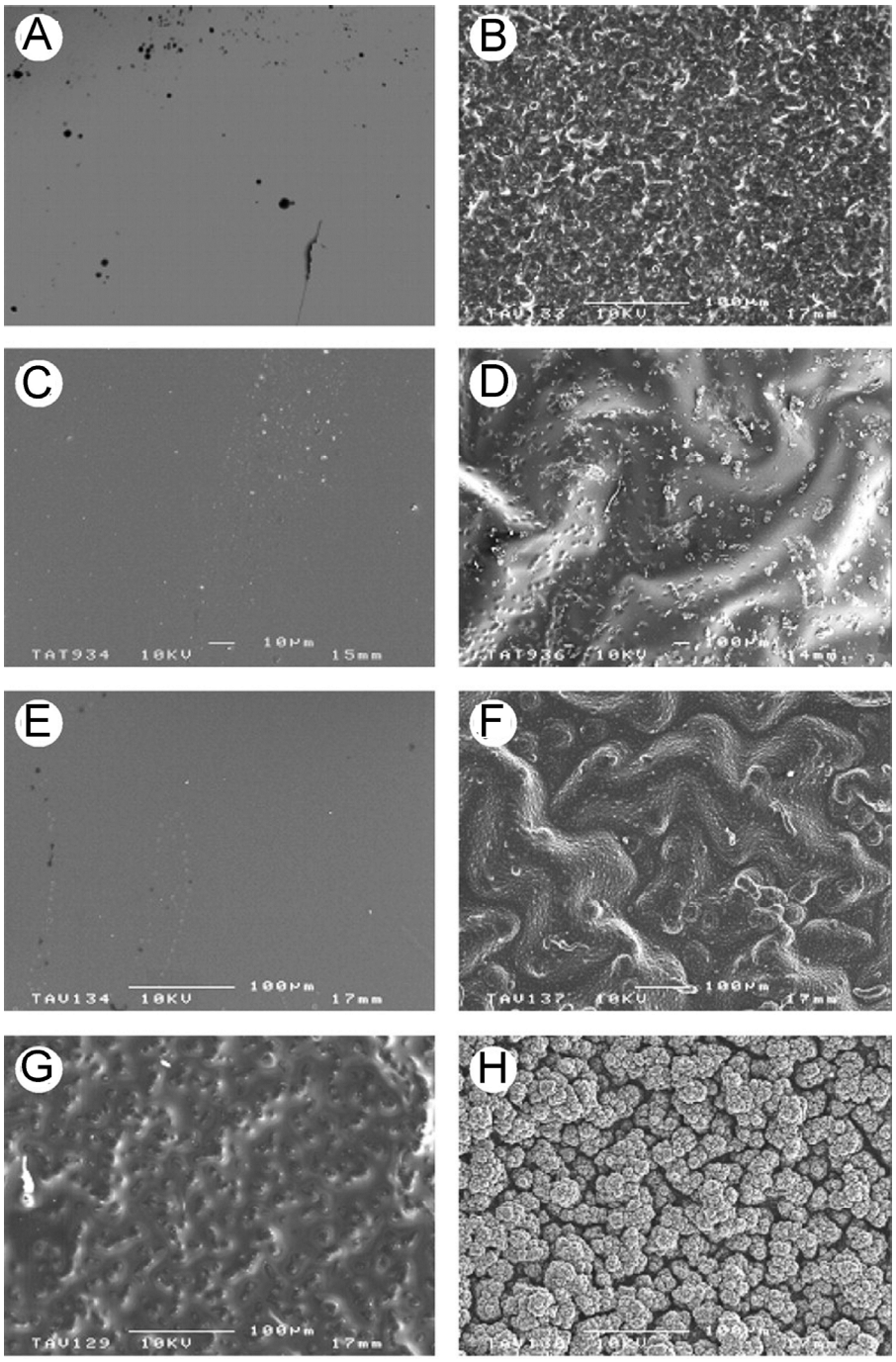

Figure 1.3. SEM images of Ppy surface topography as a function of counter-ions and electropolymerisation durations. Left column is short time (10 min) synthesis while right column is longer polymerisation duration (60 min). (*A–B*) Ppy/chloride, (*C–D*) Ppy/polyvinyl sulphate, (*E–F*) Ppy/dextran and (*G–H*) Ppy/collagen (Figure adapted from Ref.[55]).

The interaction of the polymer conjugated chain is strong resulting to the insolubility and infusibility of Ppy. In addition, the ionic interaction between the oxidised segments of the Ppy chains also contributes to the insolubility of doped Ppy [28]. Ppy can undergo a dedoping and doping process involving either chemical or electrochemical processes. Through this doping process the conductivity of neutral Ppy is enhanced from insulator to a metallic state due to the tuning of the Ppy band gap. This feature is one of the advantages of conducting polymers over metals when there is a need to control the electronic properties of the material [56]. Figure 1.4 shows the doping process of Ppy from a neutral and non-conductive state of Ppy with the benzenoid structure to the metallic and conducting state. In the neutral state (Figure 1.4-A), the band gap of Ppy is 3.6 eV, making it difficult for electrons to transfer from the valence to the conduction band. Upon doping and extraction of the first electron from the neutral part of a Ppy chain, the quinoid resonance becomes favourable (Figure 1.4-B). The presence of a positive charge and an unpaired electron are referred to as a polaron with the spin of $^1/_2$. After removing the second electron by further oxidation of the Ppy chain, a bipolaron is formed; which is broadly more encouraged than formation of two polarons (Figure 1.4-C). Each bipolaron usually extends over four pyrrole rings and sets the polymer chain to zero spin [56].

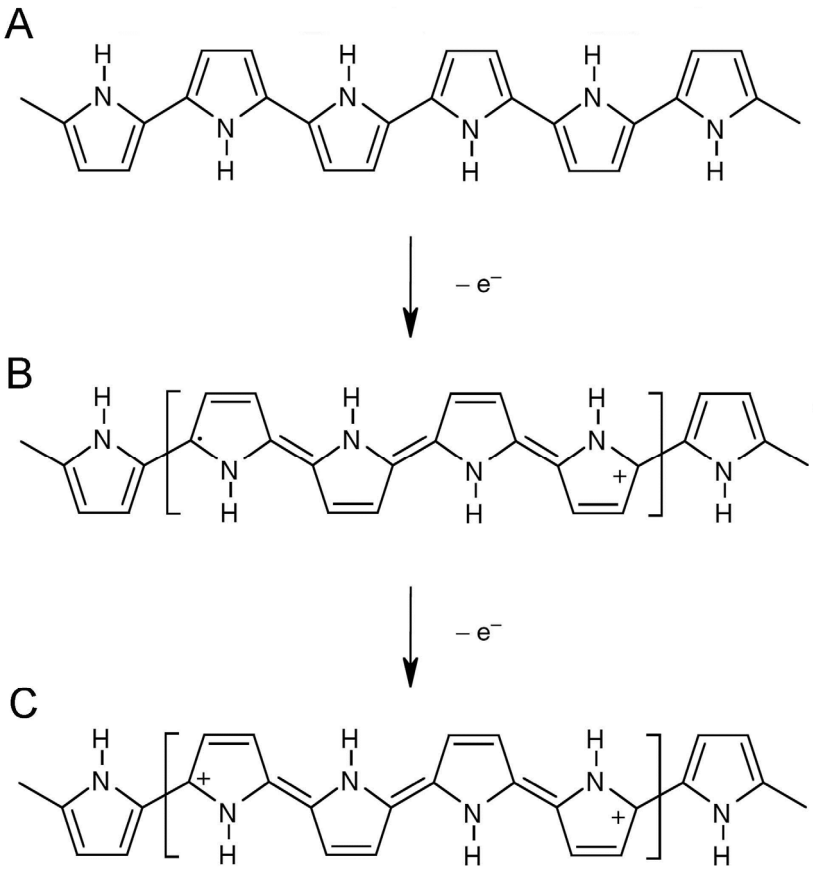

Figure 1.4. Doping/dedoping of Ppy. A) neutral, B) polaron in partially doped, and C) bipolaron in fully doped polymer.

The ability to polymerise Ppy at neutral pH in aqueous solutions makes it an appropriate polymer to include biological molecules and living cells within its structure [57].For example, Ppy with functionalised chondroitin sulphate (CS), an extracellular matrix molecule, has advantages for different biomedical and organic bioelectronic applications, such as cell stimulation, as it allows facile incorporation of bio-regulative cues to provide bio-mimicry and conductive environments for promotion of cell functionality [58].

1.2.2.1.2 PEDOT

Poly (3,4-ethylenedioxythiophene) (PEDOT) is an ICP from the polythiophene family and possesses a low band gap (between 1.4 to 2.5 eV) and is electrochemically and thermally stable [59]. In particular, PEDOT:PSS has been utilised in a wide range of applications including transparent conducting electrodes, antistatic coatings, electrochromic devices, organic photovoltaic devices, inkjet printing, rechargeable batteries, super capacitors, sensors and fibre spinning [60-64].

One of the most commonly used PEDOTs is the polymer doped with PSS (PEDOT:PSS) and can be synthesised either chemically [65] or through electrochemical polymerisation [66]. The conductivity of PEDOT:PSS depends on the method of polymerisation used and/or post-treatment of PEDOT:PSS with other reagents such as ethylene glycol (EG) [3]. In the chemical method, the EDOT monomer is mixed with an oxidant such as ferric chloride with polymerisation leading to highly conducting PEDOT whilst, in electrochemical polymerisation EDOT monomer is polymerised using a three electrode cell.

PEDOT has been utilised in biomedical applications such as cells host template [67], biosensor [68] and neural prosthetics [69]. PEDOT film was able to control cells density gradient which influences cells interaction with their neighbour environment for intracellular interaction [70].

1.2.2.2 Graphene

Graphene is a two-dimensional single atom thick monolayer of carbon, which **is** tightly packed in a honeycomb crystal lattice of sp^2-bonded carbon [71, 72]. This structure is the basic building block of all other graphitic nanostructured materials [71]. As shown in Figure 1.5, if it is wrapped up into 0D it will form a fullerene, rolling into 1D makes a nanotube or if stacked into 3D it builds graphite [21]. 2D graphite (or graphene) has been the subject of theoretical studies for over 60 years [73]. The theory behind graphene was first introduced by the theoretical physicist Philip Wallace in 1947 [73] and was then further explored by Hanns-Peter Boehm, who described single-layer carbon foils in 1962 [74]. However, not much attention was given to practical applications of graphene due to the fact that it was presumed not to exist in the free state [71]. It was believed that graphene was unstable with respect to its curved structures such as nanotubes and was described as an 'academic' material [75]. This was until isolation of individual graphene planes was realised using micromechanical cleavage by Novoselov *et al*. [72].

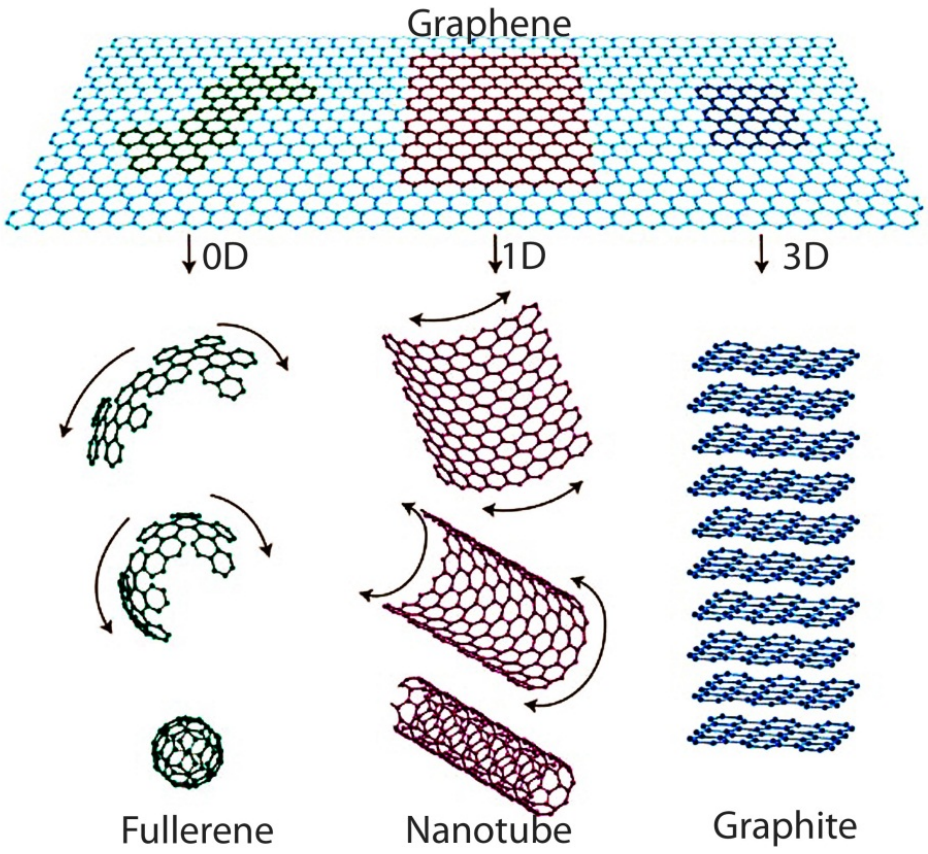

Figure 1.5. Graphene is a 2D building material for carbon materials of all other dimensions (Figure adapted from ref.[21]).

The unique electronic properties of isolated layers of graphene were measured [72] and its outstanding electronic [76], mechanical [77], thermal [78] and chemical properties were realised resulting in graphene receiving increasing attention in the scientific community. Therefore, graphene became an interesting candidate for a wide range of applications including composites [79], optics [80] and electronic devices [81]; however, the first step to exploit these superlative properties of graphene is its synthesis on a large scale with low cost, high yield, reliable, mild environmentally friendly method.

Graphene was initially produced by micromechanical cleavage of bulk graphite, which involves peeling off layers of highly ordered pyrolitic graphite (HOPG) using scotch tape and then depositing on to a silicon wafer [72]. Although this method can produce high quality graphene with dimensions as high as 10 μm, both the yield and throughput are extremely low. More recently, other methods such as mechanical exfoliation [72], epitaxial growth [82], unzipping of carbon nanotubes [83], single layer graphene growth on carbon melts [84], pyrolysis of ethoxides [85], graphene processing of sucrose [86], chemical reduction of graphene oxide (GO) [87, 88] and liquid phase exfoliation of graphite [89] have been developed.

So far, the most promising method for production and processing of graphene is solution based graphene which is advantageous in terms of yield, cost and performance [87]. To this end, one of the most efficient methods for large scale and low-cost production of graphene is oxidative exfoliation of natural graphite followed by chemical reduction [90, 91]. The oxidation process introduces various functional groups such as hydroxyl, epoxide, carbonyl and carboxyl in-plane and around the edges of graphene crystals [92]. These functional groups make GO hydrophilic and dispersible in aqueous media. Reduction processes removes most of the chemical functional groups and renders reduced graphene oxide (rGO) hydrophobic and insoluble in aqueous media. The former product is conducting but its low solubility sometimes causes irreversible aggregation and limits further processing. Although the chemical reduction method is a practical and high throughput method for making graphene, a significant amount of irreversible lattice defects are introduced by the oxidation process, which adversely affects the electronic properties of graphene [93, 94]. Liquid phase exfoliation of graphite using surfactants or organic solvents provides a practical method to produce a significant amount of defect-free, high

quality monolayer or few layers un-oxidized graphene [95]. This method deals with exfoliation of powdered graphite with the aid of sonication to give graphene in the liquid phase without any additional oxidation steps [96].

Table 1.1 compares some of the researches that have been carried out to produce graphene through the solution exfoliation of graphite. In this method, graphite source (i.e graphite powder) is added to water (containing dispersant) or organic solvent followed by sonication (bath, probe). The choice of surfactant or dispersant as stabilizer is important with surfactants such as SDBS [97], sodium cholate [96], 1-pyrenemethylamine hydrochloride [98], perylene-based bola amphiphilic detergent [99], and 7,7,8,8-tetracyanoquinodimethane [100] being utilised for successful liquid phase exfoliation of graphene and few layers of graphene. Probe sonication required much lower processing time (up to 4 hr), while the bath sonication was applied for up to 400 hr. The advantages of the bath sonication over the probe sonication are the formation of less defects and production of larger graphene flakes [95, 101-103]. NMP and DMF were the most effective solvents for dispersing graphene when concentrations higher than 1mg/ml were obtained after bath sonication of up to 400 hr [101]. Liquid phase exfoliation of graphite results in a mixture of graphite, few-layers graphene and mono-layer graphene. Large particles have been removed through the use of centrifugation. Different centrifugation speeds (from 500 rpm to 13000 rpm) and durations (from 30 min to 90 min) were applied (Table 1.1).

Table 1.1. Comparison of different methods for production of liquid phase exfoliated graphene

Graphite precursor	Dispersant Solvent/surfactant	Sonication method	Sonication time (h)	Centrifugation speed (rpm)	Centrifugation time (min)	Graphene concentration (mg ml^{-1})	Application	Reference
Natural graphite	N-methyl-pyrrolidone (NMP)	Bath	0.5	500	90	0.01	Transparent thin film	[95]
Natural graphite	Dimethylformamide (DMF)	Probe	3	13000	10	-	Liquid crystal devices	[104]
Natural graphite	Hexafluorobenzene	Bath	1	-	-	0.05-0.1	-	[105]
Different types	Ortho-dichlorobenzene	Probe	0.5	4400	-	0.02-0.03	-	[106]
Natural graphite	40 Different solvents	Bath	0.5	500	90	Up to 0.008	-	[107]
Natural graphite	Sodium cholate	Probe	-	15000	60	0.09	Transparent thin film	[108]
Expanded graphite	NMP	Probe	0.5	600	30	Up to 0.1	-	[109]
Natural graphite	1-Hexyl-3-methylimidazolium Hexafluorophosphate	Probe	Up to 24	-	-	Up to 5.33	-	[109]
Highly ordered pyrolytic Graphite	Cetyltrimethylammonium Bromide in DMF	Probe	4	-	-	-	-	[110]
Natural graphite	Sodium dodecylbenzene Sulfonate	Bath	0.5	500	90	Up to 0.1	-	[97]
Natural graphite	NMP	Bath	Up to 460	500	90	1.2	-	[103]
Natural graphite	Sodium cholate	Bath	Up to 400	500	90	0.3	-	[96]
Natural graphite	n 1-Propanol	Probe	0.3	4500	10	0.025	-	[111]
Natural graphite	Chloroform and Isopropanol	Bath	Up to 300	2000	45	0.5	-	[112]
Natural graphite	Organic solvents and NaOH	Probe	1.5	3000	60	0.07	-	[113]
Natural graphite	NMP, DMF	Bath	Up to 400	500	90	>1	Low defect graphene	[101]
Expanded graphite	NMP	Probe	2	3000	90		Composite with PU	[114]
Natural graphite	NMP	Bath	144	1000	45	-	Composite with Polyethylene Terephthalate and SWNTs	[115]
Natural graphite	PVA	Bath	100	1000	45	-	Composite with PVA	[116]

Direct exfoliation of graphite is also possible by utilising organic solvents [105, 112]. The advantage of using organic solvents over surfactants is the avoidance of the addition of dispersing agents, which can cause adverse effect on the electrical properties of graphene. NMP has been reported as the most effective solvent for graphene, dispersing more than 1 mg/ml of graphene and few layers graphene after 460 hours mild sonication [103]. Figure 1.6 shows transmission electron microscopy (TEM) images of solvent (NMP) exfoliated graphene [103]. Figure 1.6-A shows a graphene monolayer whereas Figure 1.6-C shows a multilayer [103]. Utilising TEM images provides the possibility to do edge-counting to evaluate the number of graphene layers. The well-defined edges are representative of graphene monolayer while multilayers, typical of larger objects, are observed regularly [103]. It should be noted that, very thick multilayers also can be observed and these need to be removed by subsequent centrifugation [115]. Another confirmation for the presence of graphene monolayer is analysis of the electron-diffraction patterns, such as that presented in the inset of Figure 1.6-A [103]. Confirmation of graphene monolayer occurs when the inner spots are more intense than the outer spots [95].

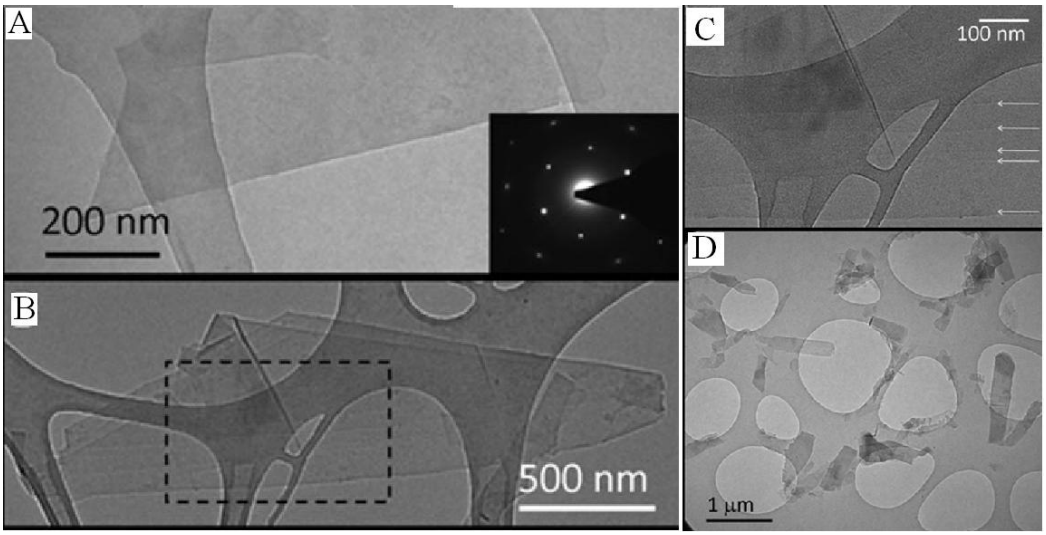

Figure 1.6. TEM images of solvent exfoliated graphene flakes. A) A typical monolayer. Inset: a diffraction pattern taken from the monolayer. B) One few layers graphene, and C) a magnification of the part identified by a dashed box in image B. The arrows in this image demonstrate the spot of the edges of the individual sheets comprising this multilayer. D) A wide-field image illustrating the bulk quantities of graphene prepared after long sonication times (180 h) (Figure adapted from ref. [103]).

The choice of solvent is crucial during the exfoliation process, as no dispersing agent is used. Coleman *et al.* investigated the dispersability of graphene in 40 solvents and suggested that good solvents for graphene are characterised by surface tensions close to 40 mJ/m^2 (equivalent to surface energies of ~70 mJ/m^2) and Hildebrand solubility parameter close to 23 $MPa^{1/2}$ [107]. Figure 1.7 compares the effectiveness of solvents to disperse graphene as a function of the solvent surface energy. According to this graph, NMP and DMF (their chemical structure are shown in Figure 1.7) are the most effective solvents to disperse graphene [101].

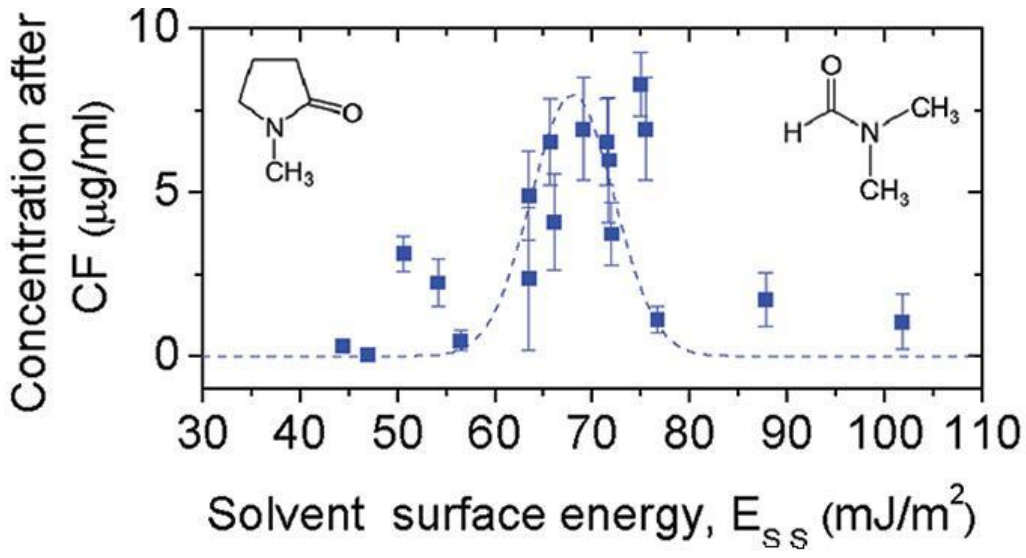

Figure 1.7. Graphene concentration as a function of solvent surface energy. The chemical structure of NMP (left) and DMF (right) are presented in the graph (Figure adapted from ref. [101]).

Centrifugation is another key point affecting the quality of graphene dispersion, by separating large aggregate particles and non-exfoliated graphite from monolayer/few layers graphene. Higher centrifugation rate and duration were found to produce better quality graphene sheets, but smaller size with lower concentration [96, 103]. The sonication method and condition also play important roles in production of solvent exfoliated graphene. Both intense tip sonication for short time and mild bath sonication for long periods have been used to produce graphene in organic solvents or in water [102]. Tip sonication method is fast but introduces more lattice defects to the graphene whereas bath sonication is time consuming, but, causes less defects [96, 108]. In order to enhance the efficiency of production procedure, it is also possible to utilise different graphene precursors such as thermally expanded graphite (EG) [106] and functionalised graphite such as fluorinated graphite [117].

One of the main advantages of the solution processing method for producing graphene, in contrast with other methods, is the easy processing of the final product [118]. Processing in solution not only permits the fabrication of paper like structures (Figure 1.8) and/or thin films but also, permits the introduction of graphene into polymer host material and simplifies the fabrication of composites [119]. The graphene paper shown in Figure 1.8**,** afforded high electrical conductivity and tensile strength of 180 S/cm and 15 MPa, respectively [103]. As such, solvent or surfactant-exfoliated graphene has the potential to be employed in many applications in both research and industry.

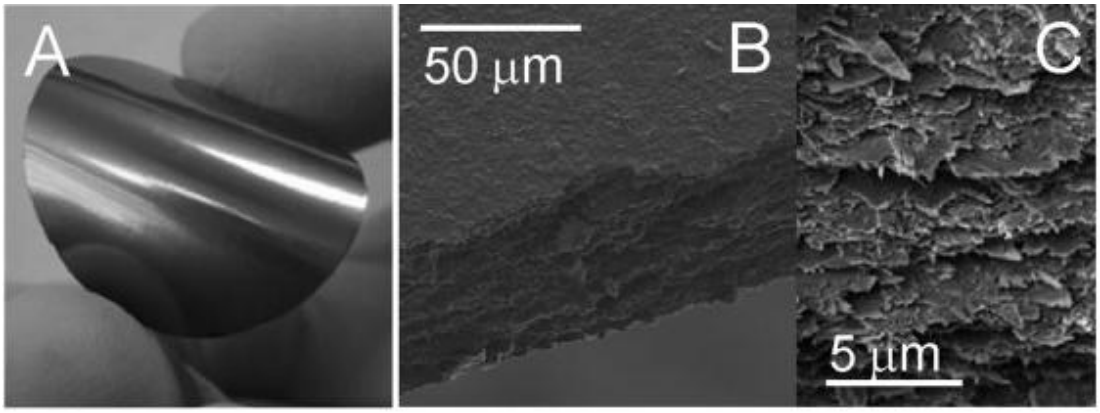

Figure 1.8. A) photograph of a free-standing paper prepared from solvent exfoliated graphene. B) SEM image of the edge of the paper in (A). C) Close up image of (B) (Figure adapted from ref. [103]).

A summary of the fabrication of three-dimensional structures for biomedical applications is presented in the following sections.

1.3 Fabrication

The fabrication techniques and utilising of 3-dimensional structures for assessing biological based applications are rising due to the inability of 2-dimensional structures to accurately mimic the extracellular matrix (ECM) [120]. In biology, the extracellular matrix is a part tissue in 3D form, which supports cells attachment and their functionalities [120]. Parameters such as geometry, biocompatibility, mechanical properties and surface properties [7] need to be carefully considered when designing three-dimensional architectures for biomedical applications.

Structures that have circular [121], tubular [4] and nano [122] architectures show similarities with human ECM, therefore are favourable for tissue engineering applications.

The following sections describe the fabricated structures that have been utilised in this thesis.

1.3.1 Wet-spun fibres

Fibres are another class of 3-dimensional structures, which are the primary product in the garments industry. Wet-spinning is a particular industrial method to produce continuous fibres during extrusion of synthetic or naturally made fluid polymers into a spinneret followed by injecting into a coagulation bath which could be water based or organic solvent based. During this process, first, the polymer fluid is being converted into a rubbery gel state and then, to a solid-state fibre. This process of extrusion and solidification/coagulation of filaments is called wet-spinning [123, 124]. Wet-spinning is the oldest spinning method and was initially used for the spinning of rayon fibres [123]. Rayon was the first man-made fibre spun from a synthetic polymer in the 19th century. Prior to this, the spinning precursors were

limited to naturally occurring materials [123, 124]. The principle of wet-spinning (Figure 1.9) relies on the coagulation precipitation of a fluid polymer to form a fibre; with rayon, aramid, acrylic, modified acrylic, polyaniline and spandex fibres all being manufactured by this process [123, 124].

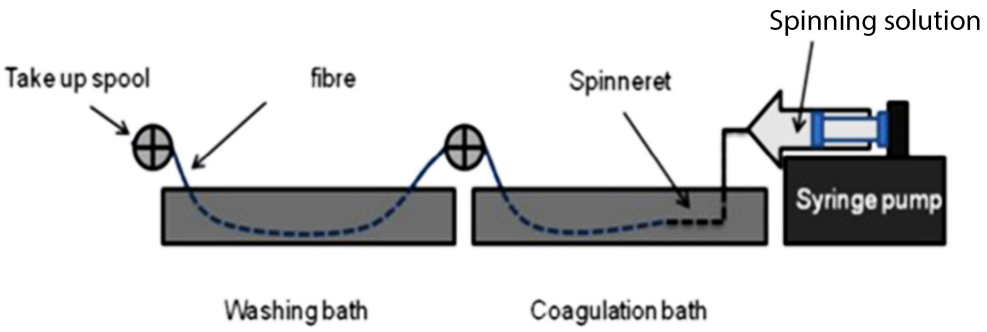

Figure 1.9. Schematic of wet-spinning technique used in this thesis to produce wet-spun fibres.

Wet-spinning can be sub-divided into three methods based on different spinning strategies as follows: (i) phase separation, (ii) gel formation and (iii) liquid crystal spinning [123]. (i) During phase separation (sometimes referred to as non-solvent method), fibre formation occurs rapidly as the polymer fluid is injected through the spinneret into a coagulation bath. As the polymer fluid is exposed to the non-solvent, the solvent is extracted from the polymer solution and this causes the polymer to coagulate in the bath, then precipitate to form a semi-solid fibre. This process is followed by further solidification into the coagulation bath to provide sufficient cohesion and strength for the fibre to be collected continuously out of the coagulation bath. (ii) In the gel formation method, the polymer solution is coagulated due to

intermolecular bonds such as ionic cross-linking by a salt or other reacting agent. (iii) In the case of liquid crystal spinning, lyotropic liquid crystalline solution provides sufficient alignment and cohesiveness for fibres to form a solid crystalline phase. The ultimate physical properties of wet-spun fibres are influenced by a number of process and solution parameters such as solution viscosity and concentration, coagulation strategy, pumping rate, pH, temperature and winding speed [123, 124].

While wet-spun fibres were utilised in tissue regeneration [125], their applications in other fields of biomedical engineering such as drug delivery [126] are under progress. Flexibility, appropriate mechanical properties, processability into devices by knitting and braiding methods provide huge opportunities for wet-spun fibres to be utilised in biomedical fields. For example, PLGA wet-spun fibres were knitted and braided into artificial anterior cruciate ligament (ACL) structures by Larencin *et al.* [127]. PLGA wet-spun fibres possessing appropriate biocompatibility and mechanical properties have been braided into scaffolds which exhibited cells attachment efficiency for ligament replacement [127]. Razal *et al.* wet spun hyaluronic acid (HA) and chitosan (CHI) with carbon nanotube (CNTs) to form a composite fibre that was shown to support the growth of L-929 mouse fibroblast cells [125]. Cell adhesion to the fibres was promising and they mimicked the geometry of the wet-spun fibres [125]. Lee and colleagues developed a method to fabricate PLGA micro-fibres as platforms for tissue regeneration [128] by precipitating a solution of PLGA prepared in DMSO into a glycerol-containing water solution in PDMS-based micro fluid system, and cultured L-929 fibroblast on the surface of fibres without fibronectin up to 3 days. Cell attachment to the fibres structure and their alignment proved the potential of wet-spun fibres in tissue engineering [128].

In addition, wet-spun fibres can be used as a substrate for drug delivery [126]. Biological molecules such as therapeutic drugs or growth factors can be incorporated into and/or onto fibres with ionic, covalent bonding or by physical blending into polymer solutions prior to forming the fibre [129]. Mack *et al*. utilised PLGA wet-spun fibres as platforms for controlled release of levofloxacin and dexamethasone using the degradation property of PLGA [126]. They implanted certain lengths of fibres containing levofloxacin into the eye of rabbits. The burst release of the drug was detected through the rabbit's tears, and correlation between *in vitro* and *in vivo* levofloxacin release profiles was demonstrated. The burst release of levofloxacin was favourable, as a high amount of drug is needed right after implantation. Fibres can also be knitted or braided into mats or cylindrical platforms to accommodate a range of different applications in biomedical engineering.

1.3.2 Electrospun fibres

Nanotechnology provides a means to advance the fabrication of sub-micron or nano-structured 3D dimensional structures [130]. Combining nanotechnology with micro-scale fabrication processes provides the opportunities to discover new aspects of materials for tissue engineering, diagnosis and monitoring [131]. Electrospinning is one of the versatile methods for production of sub-micron or nano-scale fibres, which greatly facilitates the fabrication of biomaterials [131].

Doshi and Reneker were the first researchers in 1995 to report the electrospinning method to produce nanofibres [132]. Electrospinning requires a high voltage power supply (up to 30 kV), syringe pump and conducting collectors (target). In a typical electrospinning process, a high voltage is applied between a droplet of polymer solution, extruded from the tip of a metal syringe needle, and a grounded target

[133]. Upon applying the electrical voltage, electrostatic charge forms on the surface of the polymer droplet and increases as the voltage is increased until the electrostatic charge overcomes the surface tension of the droplet upon which a charged polymer fluid jet is ejected toward the target. The jet exhibits bending instabilities due to the repulsion of mutual surface charges, which is carried by the jet, and follows a looping and spiral path (Figure 1.10). This repulsion elongates the jet thousands of times so that it becomes extremely thin. Eventually, the solvent evaporates and long nanofibres are collected on the grounded target.

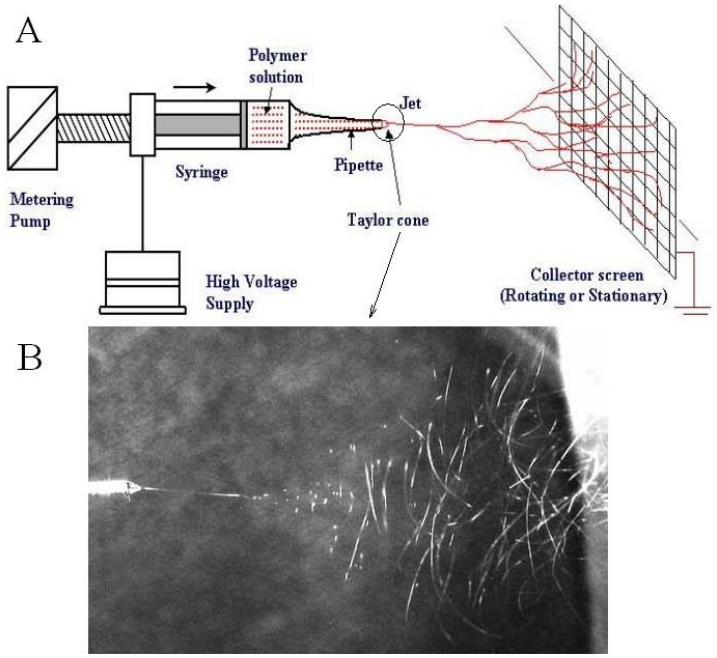

Figure 1.10. A) Schematic of electrospinning set-up. B) Photograph of the electrospinning jet.

The morphology and diameter of electrospun nanofibres are dependent on a number of processing and solution parameters [134] as follows: (a) the intrinsic properties of the solution such as the type of polymer and solvent, polymer molecular weight, viscosity (or concentration), elasticity, conductivity, and surface tension, and (b) the operational conditions such as the applied voltage, the distance between spinneret

and collector (tip-target distance), and the feeding rate of the polymer solution. Additionally, the morphology and the diameter of electrospun nanofibres are affected by ambient humidity and temperature [134]. For example, for the electrospinning of poly (ethylene oxide) (PEO), the concentration of polymer solution must be high enough (between 298 to 1835 cP) to afford polymer entanglements, but not so high that the viscosity prevents polymer motion induced by the electric field. The lower surface tension (~ 76 mN/m) and higher electrical conductivity of spinning solution (between 200-250 Ω m) are also favorable [135].

Due to the chaotic oscillation of the electrospinning jet, the nanofibres are usually collected as a nonwoven mat, which are used in various applications such as filtration [136], tissue scaffolds [137], wound dressing [138], and drug delivery [139, 140]. However, in some of the biomedical applications where cell alignment is favourable, well-aligned and highly ordered nanofibres are required [141, 142].

Different geometries such as highly aligned [143], yarns (twisted [144] or untwisted [145]) and arrays [146] of electrospun fibres have been achieved by modifying the electrospinning set up. There have been many attempts to achieve aligned nanofibres either with electrostatic or mechanical forces. Oriented polyamide nanofibres formation was demonstrated by Dersch *et al.* as a result of the polymeric jet moving back and forth on the collecting site due to electrostatic forces [147]. In the other method, aligned polyethylene oxide nanofibres were collected on the rotating drum in aligned and cross-bars shape [148].

Electrospinning of PEDOT:PSS has been performed from a mixture with other polymers such as polyvinylpyrrolidone (PVP) [149] and polyacrylonitrile (PAN) [150], as polymerisation templates in different polymerisation methods such as

vapour phase [149] and electrochemical polymerisation [151]. The versatility of electrospinning and nanofibres helps in designing more appropriate structures when fibres are required for biomedical research. Although the electrospinning and wet-spinning system has led to the fabrication of fibres with low mechanical properties, the fibres can be modified by addition of different additives such as polymers (e.g. PLGA, PCL, and chitosan), carbon nanotubes or graphene. Moreover, the feasibility to tune the morphology in terms of design, size and thickness facilities generation of fibres with increased mechanical properties [152, 153]. Many studies have been published where the formed fibres have been evaluated for their implant biocompatibility. Shin et al. has shown that electrospun fibres were biocompatible when implanted into the omenta of rats for 4 weeks [154]. In addition Requicha et al. showed similar biocompatibility after implanting wet-spun fibres into 10-weeks old Wistar rats [155]. These studies clearly demonstrate the biocompatibility of these produced fibres with not inflammatory response reported. The following section describes in detail the role of 3D structures in different architectures in biomedical engineering.

1.4 Biomedical Applications

Artificial extracellular matrixes (AECM) have been designed and fabricated to support the growth of cells and eventually be utilised in tissue regeneration [156]. In order to reduce post-surgery inflammation and infection, biomaterial scaffolds have been designed to incorporate drugs in the structure [157].

1.4.1 Drug delivery

Drug delivery is a technique or process to deliver therapeutic triggers such as drug, protein, growth factor and enzyme, into target organs in a desirable release profile in animal or human [158, 159]. Localised drug delivery offers several advantages over conventional oral or parenteral (systemic) dosage forms. First, localised delivery allows site specific drug administration where the drug is needed most. Examples include implants used in the treatment of brain tumors or prostate cancer. This may also allow for significantly lower doses of the drug, which can minimize potential side effects. In addition localised delivery systems minimize drug degradation and loss, increase drug bioavailability and the fraction of the drug accumulated in the required zone. These advantages have led to increase research activity in the development of various drug delivery and drug targeting systems.[160]. Although, traditional delivery systems (orally or semi-localised) are still the current methods for treatment of diseases, new drug delivery methods are in the central focus of researches to achieve highest therapeutics efficiency with lowest side effects [161].

Advances in the design of biocompatible structures with capability to maintain different therapeutic triggers, in conjunction with knowledge of diseases mechanism, led to the creation of different delivery systems either in biodegradable or non-biodegradable strategies [129]. In biodegradable structures, therapeutic components

are released with the assistance of degradation, diffusion and dissolution, however, in non-degradable materials, external factors such as electrical stimulation [159], pH [162], light [163] and mechanical signals [164] are the main elements to drive the release process.

1.4.1.1 Drug delivery from degradable polymers

Biodegradable polymers are attractive materials for drug delivery since, once they have performed their drug delivery role they degrade away [165]. Degradation of these polymer types occur when the release medium penetrate the polymer structure and in turn breaks down the polymer backbone and converts it to simple components [166]. Several factors such as molecular weight, chemical composition, structural configuration and physicochemical factors (i.e., ionic strength and pH) influence the degradation rate of polymers [167]. Poly lactic-co-glycolic acid (PLGA) is one of the most common degradable polymers applied in a variety of biomedical applications in a wide range of architectures due to its biocompatibility and processability [168].

Bodmeier *et al.* investigated the release of progesterone from poly (D-lactic) films and studied the release kinetics of progesterone due to degradation of the polymer. The results showed that 0.8 μg of progesterone was released during the first 60 min of the experiment followed by the release profile plateauing out [169]. Multilayers of chitosan-PLGA-chitosan were fabricated and loaded with ipriflavone and compared to monolayer films of PLGA and chitosan and characterised i*n vitro*. In addition, the drug release properties over 20 days from chitosan-PLGA-chitosan structures were shown to be biocompatible *in vitro* [170].

Drug delivery from a biodegradable polymer usually resulted in a sustained release profile, however, in some medications patients need to have a higher concentration of drug in specific time points. In these cases, other drug delivery systems need to be considered.

1.4.1.2 Drug delivery from conducting polymers

Controlled delivery of drugs from a conducting platform was performed for the first time in 1984 [171]. This process entailed passing electrical charge through the platform loaded with the drugs. This electrical stimulation triggered a response in the conducting materials such that the drug is released. To use electrical stimulation to release incorporated drugs in a controlled way, the material must be conducting and more importantly, their conductivity should not change during the release process [172]. In order to tune the release profile of therapeutics components, electrical stimulation can be applied to the conducting material with direct connection [29].

It is important to know if the drug of interest for the intended application is itself electroactive and likely to be influenced by the magnitude of the applied electrical stimulation [161]. In addition, the pKa of the drug should be considered as this will influence the incorporation and release of drug from the conducting platform [173].

Conducting materials that have been utilized in drug release include functionalised metal (e.g., gold and silver) [174], conducting polymers [175] and carbon nanostructures [176] (e.g., carbon nanotubes and recently graphene). The use of conducting polymers and other carbon nanostructures are becoming more desirable

for drug delivery since polymers have softer and more flexible surfaces than metals [157, 161]. The mechanism for drug release is proposed to involve electrostatic interactions as the application of electrical stimulation protocol changes the amount of drug release [52]. Figure 1.11 shows the schematic reaction associated with the electrochemical polymerisation of PPy. During polymerisation (Figure 1.11. A) the negatively charged A^- molecules (that can be a drug) acts as counter ion and is incorporated into PPy structures during synthesis. Drug release from the PPy structures can be facilitated by applying a reducing potential to the polymer (Figure 1.11. B).

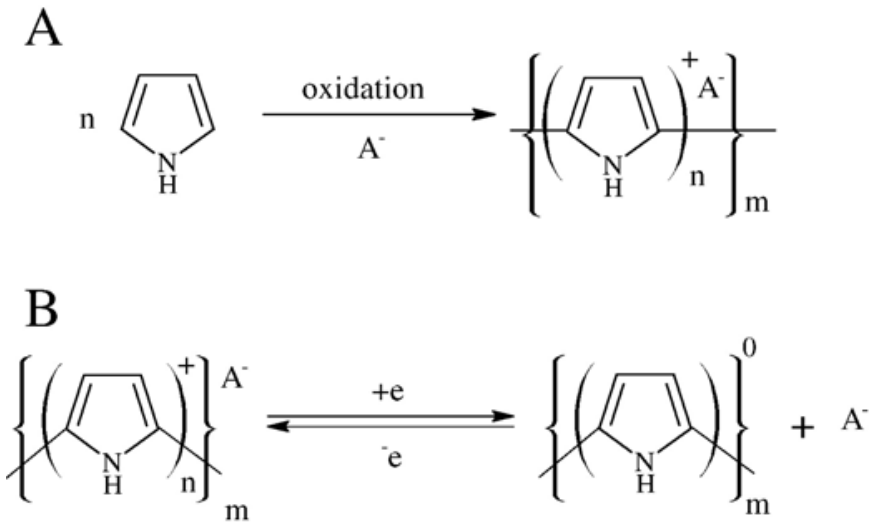

Figure 1.11., A) Synthesis of ICP showing the incorporation of the dopant A^-. B, Release of the dopant A^- during redox cycling of the ICP. Figure adapted from ref [52].

Table 1.2 presents some of the significant works that have utilised conducting polymers for controlled release of biomolecules. The delivery of nerve growth factors has also been demonstrated from conducting polymer films via electrical stimulation [177, 178]. These studies showed that Ppy could incorporate and release

the nerve growth factors NT3 and BDNF using electrical pulses or constant currents and potentials. It is also reported that different types of counter-ions (anionic [179], cationic [158] and neutral [180]) can be incorporated during electropolymerisation therefore, anionic drugs according to their chemical structure can be utilised as a dopant in electropolymerisation, and cationic and neutral drugs can be associated during the polymerisation process with the aid of a co-dopant which has a negatively charged functional group [161]. Polypyrrole was electropolymerised with the assistance of biotin to load nerve growth factor as a neural trigger. The biocompatibility of Ppy suggests that it is possible to use these materials for implantable drug delivery systems [52, 161].

Table 1.2. Some of the significant works that utilised conducting polymer for controlled release of bio-active molecules.

Type of conducting polymer	Synthetic method	Structural form	Released components	Stimulation conditions	Reference
Ppy	Electrochemical	Film on GCE	Glutamate (Glu)	CV	[181]
Ppy	Electrochemical	Film on GM	Neurotrophin-3 (NT-3)	CV, pulsed potential & Current	[177]
Ppy	Electrochemical	Double layer film	Risperidone	Pulse potential, CV	[182]
Ppy	Electrochemical	Film	Chlorpromazine (CPZ)	Pulse potential & QCM	[183]
Ppy	Electrochemical	Film	Nerve Growth Factor (NGF)	Constant potential	[180]
Ppy	Electrochemical	Film	Tosylate, salicylate, nicoside, naproxen	Constant potential	
Ppy	Electrochemical	Film	Heparin	Mechanical pressure	[184]
PEDOT	Electrochemical	Film on GE	Dexamethasone	Pulse potential in	[179]
PEDOT	Electrochemical	Layer on Pt/Ir alloy	BDNF	Passive, Better cochlear Functionality with PEDOT	[5]

1.4.2 Scaffolds for Cellular Interactions

Cellular studies performed on engineered extracellular matrix (ECM) scaffolds have increased the understanding of cells interaction with tissue in the micro- and nano-scale domains [156]. Scaffolds as ECMs can be fabricated in a variety of architectures such as printed layers [185], electrospun mats [3], wet-spun fibres [12], however, important factors such as composition, dimension, mechanical properties and flexibility may interfere with the cell interaction. This section will introduce some successfully fabricated scaffolds with emphasis on their cellular interaction.

One method for the production of scaffolds is electrospinning which produces connected 3D porous mats that exhibit a high surface area with ability to mimic features of the ECM structure. Biocompatibility and biodegradability are the most important necessities for electrospun nanofibres as a scaffold [131]. These properties will determine the scaffolds' ability to degrade within a timeframe *in vivo* and be replaced with newly regenerated tissues [131]. Figure 1.12 compares cell interaction between microfibres and nanofibres. Nanofibres have superior surface areas to adsorb proteins, providing more binding sites to cell membrane receptors resulting in improvement in cells attachment, proliferation and expression of matrix components [186].

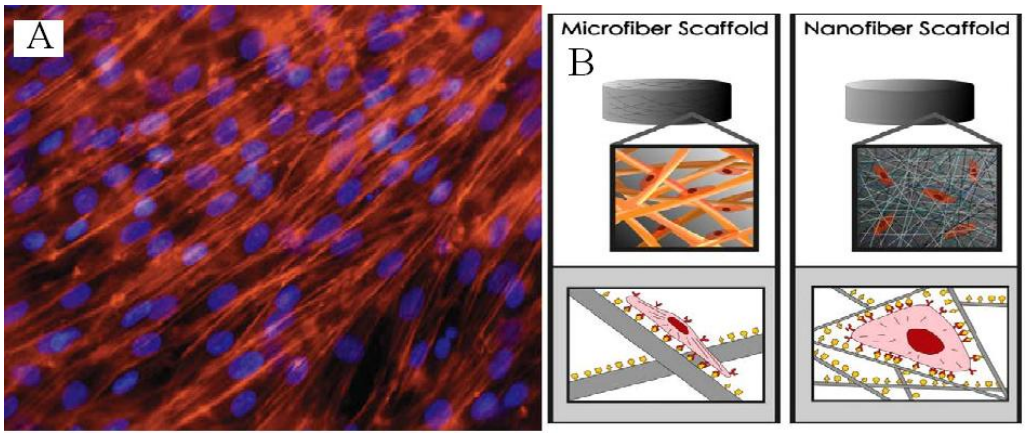

Figure 1.12. A) Fluorescence graphs of confluent H9C2 myoblast cells on PLGA nanofibres. B) Cell binding and spreading with respect to scaffold architecture. Cells binding to microfibres flatten and spread. (Figure adapted from ref. [131] and [186]).

Mats which are prepared by the electrospinning method and employed as temporary platforms for cells regeneration can be optimised in terms of thickness, morphology, and structure by selection of right architectures. A high porosity and specific surface area of an electrospun mat provides more cells attachment with multiple adhesion points; as a result of its three-dimensional structure [187]. Moreover, because the size of cells are approximately one magnitude larger than individual electrospun fibres, cells are capable of attaching around the fibres and extend along its length [188]. For instance, PLGA electrospun fibres were fabricated by Ko *et al.* to be used as an human bone-marrow-derived mesenchymal stem cells (hMSCs) template and showed cell attachment and proliferation on a PLGA electrospun mat [10]. Hsiao *et al.* investigated the interaction of primary cardiomyocytes (CMs) with electrospun PLGA fibres and showed that an aligned electrospun mat can direct cells for cardiac tissue [3].

In some cases, the scaffold is capable of enhancing the growth of attached cells with electrical stimulation. For example, electrospun nanofibres of polyaniline (PANI) with a mixture of polycaprolactone (PCL) and gelatin (G) were utilised to apply electrical stimulation to nerve stem cells (NSCs) [189]. The results showed the proliferation rate of cells was slightly higher in PCL and graphene nanofibres without PANI whereas, the proliferation rate of cells on PCL-G electrospun fibres with and without PANI was higher compared to tissue culture plate (TCP). They also applied an electrical stimulation protocol with 1.5 V on cells for 15, 30 and 60 min. The results demonstrated no significant cells proliferation for samples exposed to the electrical field for 15 and 30 min, however, there was significant cells growth for samples with 60 min electrical stimulation. Furthermore, they reported that the average neurite length for NSCs grown on PANI/PCL/G with application of electrical stimulation for 1 hr and without electrical stimulation was found to be 30 ± 1.1 and 22 ± 0.97 μm, respectively, indicating that the application of electrical stimulus for 1 hr to NSCs cultured on PANI/PG significantly ($p \leq 0.05$) enhanced the neurite outgrowth. It is worth noting that the electrical stimulation did not show a significant influence on neurite outgrowth for samples that were stimulated electrically for 15 and 30 min [189].

Kam *et al.* reported cell growth on a single-walled carbon nanotube (SWCNT) and laminin composite when electrical stimulation was applied [190]. The presence of SWCNTs permitted the use of electrical stimulation of the neural stem cells (NSCs). They indicated that 98% of cells on the surface of the SWCNT−laminin composite were viable. The electrical stimulation of NSCs comprised a series (10−15) of 1 ms pulses spaced at 1−10 s intervals. Ion-sensitive dyes undergo a change in fluorescence intensity as a result of changes in ion concentrations upon application of

an action potential. Confocal microscopy images of a cell cluster demonstrated a clear increase in fluorescence dye (Fluo-4 a.m.) indicating an increase in population of live cells after electrical stimulation [190].

The attachment of functional groups to a synthesised Ppy film has shown to be advantageous for different biomedical and organic bioelectronic applications, such as cell stimulation. This approach allows facile incorporation of bio-regulative cues to provide a bio-mimicry and conductive environment for the promotion of cell functionality [58]. For example, cell attachment on chlorine-doped polypyrrole (Ppy.Cl) films has been improved by the immobilization of peptides (T59-GRGDS) on the Ppy surface [191]. Relative cell attachment to Ppy.Cl film was analysed using the rat pheochromocytoma cell line (PC12) as this cell line has been shown not to adhere to Ppy.Cl in serum-free medium [191]. However, when the Ppy.Cl surface was modified with the T59-GRGDS peptide, significant attachment was observed [191]. Table 1.3 presents some of the significant biomedical applications of Ppy.

Table 1.3. Some studies using Ppy in biomedical applications along with synthesis method and dopant used.

Synthesis method	Structure	Dopant	Application	Advantages	Reference
Electrochemical	Film on ITO glass	Cl	Promotion of cells attachment	Peptide immobilization on Ppy.Cl	[191]
Chemical	Nanoparticles	SDS	Cells stimulation	Conducting template with PDLLA polymer	[192]
Electrochemical	Layer on micro-patterns	pGlu*	Neurite guidance	Conducting micro-patterns	[193]
Chemical	Coating on membrane	Chloride (from Ferric chloride oxidant)	Biosensor	Higher electrochemical stability of PEDOT in longer term applications	[68]

*pGlu = poly-l-glutamic acid

Ppy doped with chondroitin sulfate (CS) has been electrochemically synthesised and conjugated with type I collagen [58]. The collagen modification formed a 3-dimensional fibrillar matrix at the surface of Ppy. However, no significant reduction in the electroactivity of the fibrillar collagen-modified Ppy substrates was observed [58]. The differentiation and neurite outgrowth of PC12 cells was improved due to the collagen modification and electrical stimulation of the underlying Ppy substrate (Figure 1.13).

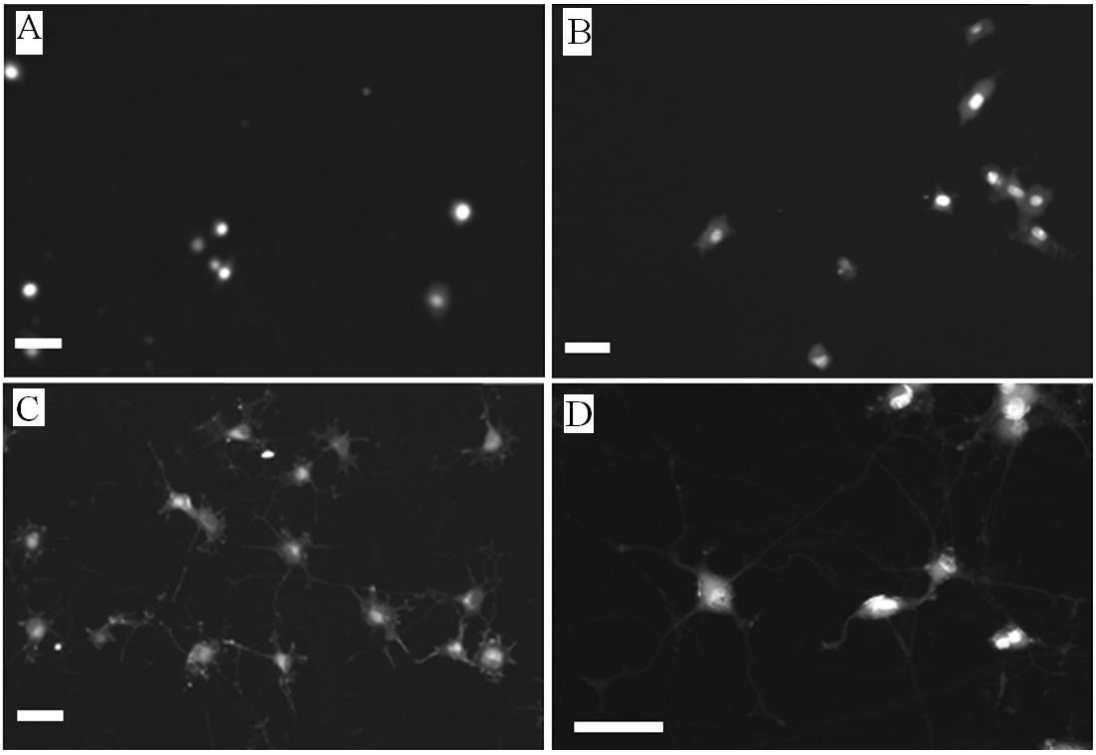

Figure 1.13. Fluorescence micrographs of PC12 cells cultured on surface modified Ppy at A) 2h, B) 24h, C) 144h and D) At 144 h after being subjected to electrical stimulation applied with charge-balanced biphasic ± 1 mA current pulses with 100 μs pulse width, 20 μs open-circuit interphase gap and 3.78 ms short-circuit phase between pulses at 250 Hz. Scale bars represent100 μm. (Figure adapted from Ref.[58].)

Thompson *et al.* [194] showed elongation of neural explants from the rat pup cochlea as a function of electrical stimulation. Neurite outgrowth from cochlea neural explants grown on Ppy containing growth factors showed synergistic effect on both neurotrophins. Neurite outgrowth was significantly improved when the polymers containing growth factors (NT3 and BDNF) were electrically stimulated (Figure 1.14) [194].

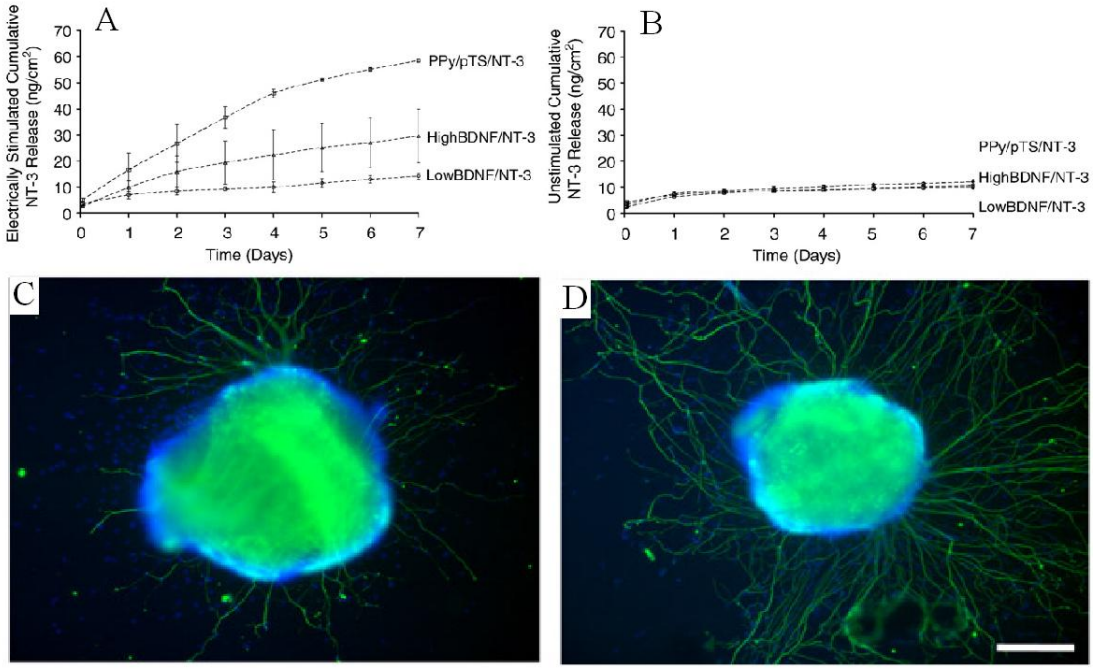

Figure 1.14. Release of NT-3 and BDNF from Ppy films. A) With and B) without electrical stimulation. A representative image of cochlea neural explants grown on Ppy.pTS. C) Without electrical stimulation and B) with electrical stimulation (Figure adapted from ref.[159]).

Vapour phase polymerised Ppy on poly (styrene-b-isobutylene-b-styrene) (SIBS) electrospun fibres also exhibit potential in biomedical applications due to their ability

to align PC12. This alignment was facilitated by the aligned patterns of the electrospun material as well as the application of electrical stimulation [195, 196]. Highly aligned PC12 neurite outgrowth was achieved by applying electrical stimulation to aligned electroactive Ppy coated SIBS nanofibres (Figure 1.15) [195].

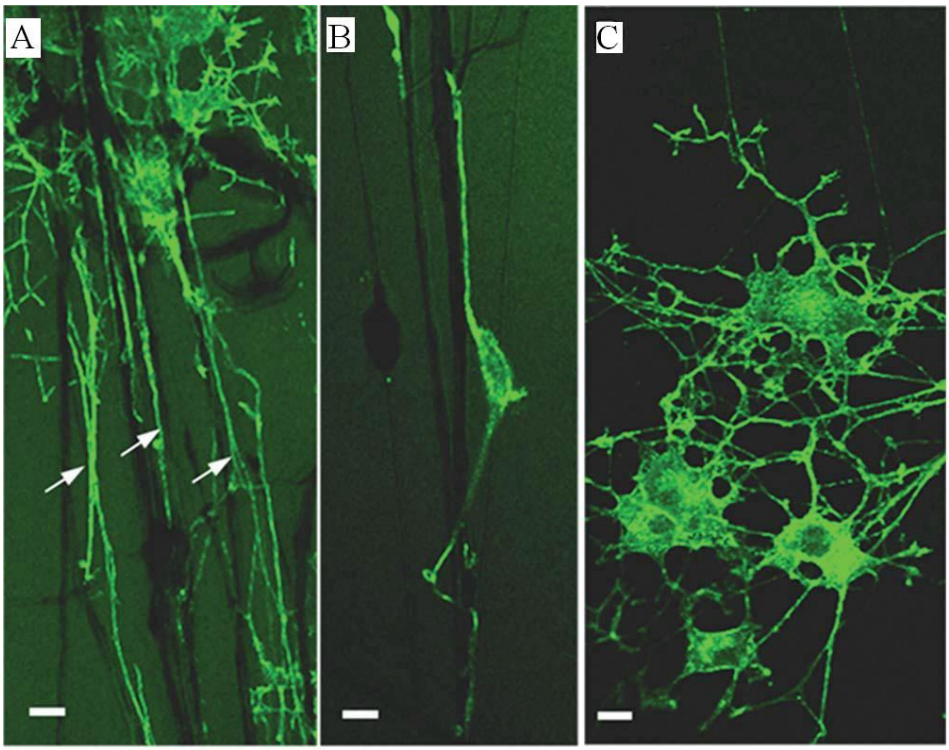

Figure 1.15. A and B) Fluorescence images of PC12 cells on aligned Ppy/SIBS **electrospun** fibres. The F-actin filaments in PC12 cell bodies and neurite outgrowths are shown by arrows in A. C) Fluorescence images of PC12 cells on Ppy films without Ppy/SIBS fibres. Scale bars represent 10 μm (Figure adapted from Ref.[195]).

PEDOT film was shown to be capable of controlling cell density gradient which in turn influenced cells interaction with their neighbour environment [70]. A poly(3,4-ethylenedioxythiophene) doped with *p*-toluenesulfonate (PEDOT-TOS) film,

exhibiting a redox gradient, was deposited by vapour phase polymerization onto indium tin oxide (ITO) with varying thicknesses [70]. Varying the polymer film thickness resulted in a gradient density of normal and cancerous cells, their attachment and proliferation. Moreover, Abidian *et al*. deposited PEDOT using lithium perchlorate as the dopant on the surface of platinum (Pt/Ir) electrode to enhance the electroactive surface area of neural electrodes, and reported a lower impedance for the modified neural electrode compared with a traditional metal electrode [197]. Table 1.4 demonstrates some examples of the role PEDOT in biomedical applications.

Table 1.4. Some of studies using PEDOT in biomedical applications along with synthesis method and dopant used.

Synthesis	Structure	Dopant	Application	Advantages	Reference
Electrochemical	Coated on neural probes	PSS	Neural recording	Peptide incorporation on probe	[69]
Chemical	Coating on membrane	Ferric chloride	Biosensor	Higher electrochemical stability of PEDOT in longer term applications	[68]
Electrochemical	Coating on neural probe	Lithium perchlorate, TEAP	Neural recording	Lowering impedance and ability to control release of dexamethasone	[179, 198]
Electrochemical	Coating on tissue culture plate	Tosylate	Cells host template	Electrically controlling cells attachment	[67]
Electrochemical	Film	Heparin	Stem cells templates	Electrochemically controlling the stem cells Microenvironment	[199]
Vapour phase	Film on ITO	p-Toluenesulfonate (PTS)	Cells template	Controlling cells gradient	[70]

The use of graphene and graphene oxide without any polymer or additives to produce composites for biomedical applications is relatively new, with only limited number of publications reporting their use. However, their use to form composites containing biocompatible and biodegradable polymers is becoming more widely studied [200, 201]. These composites are mostly utilised as scaffolds for tissue engineering [200, 201]. For instance, a group of researchers in the University of Louisiana investigated cellular interaction with a composite of graphene oxide-chitosan [14]. They showed that pre-osteoblasts could attach and proliferate well on the surface and inside of chitosan pores and it presented these composites as potential scaffolds for bone regeneration due to the fact that graphene oxide enhanced the mechanical properties of the composite [14]. In addition, these scaffolds containing graphene oxide had a lower rate of enzymatic degradation compared with a pure chitosan scaffold, due to reaction between amine groups of chitosan with hydroxyl groups of graphene oxide [14]. Other work introduced graphene oxide (GO) as filler for the enhancement of mechanical properties, and as a template for biological attachment in a gelatin-GO film [113]. Li *et al.* reported preparation of graphene papers made from highly ordered graphene sheets with the biocompatibility of these papers proven using L-929 (mouse fibroblast) cells (Figure 1.16) [202].

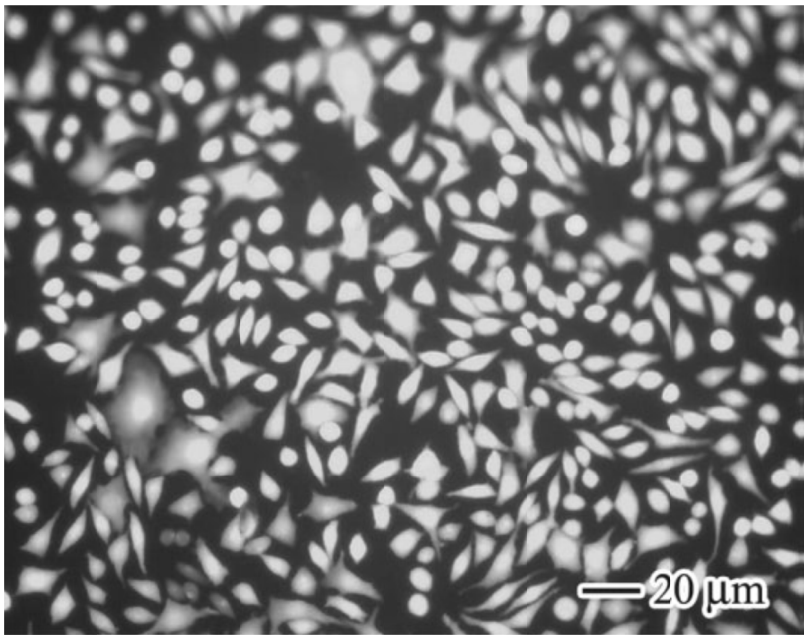

Figure 1.16. Fluorescence microscopy image of Calcein AM stained L-929 cells grown on reduced graphene oxide paper (Figure adapted from Ref. [202]).

Graphene and its derivatives are increasingly having an impact as organic conductors in tissue engineering to convert non-conducting biocompatible polymers to conducting composites. These conducting composites may be used to modulate cellular activity through electrical stimulation of cells.

Heo *et al.* reported the use of a composite of polyethylene terephthalate (PET) and graphene to control SHSY5Y human neuroblastoma cell-to-cell interaction using electrical stimulation. They utilised charge-balanced biphasic pulses with a frequency of 1 Hz for a total time period of 32 min to generate an electric field ranging from ±4.5 mV/mm to ±450 mV/mm. They imaged cells every 50 seconds using fluorescent microscopy and showed that the graphene-PET composite films had no toxicity for SHSY5Y human neuroblastoma cells and that the largest percentage of shrunken cells was observed at the ±450 mV/mm electric field while,

the smallest percentage of shrunken cells was observed at the 4.5 mV/mm electric field. Hartig *et al.* investigated the effect of electrical field on proliferation rate of osteoblast-like primary cells and found that an external voltage signal with electric field of 6kV/m can enhance proliferation, maturation and ECM protein synthesis of osteoblast in vitro [203]. Ahadian et al. showed that protein expression profoundly increases by applying electrical stimulation on C2C12 myotubes using an integrated methacrylated gelatin (GelMA) hydrogel with aligned carbon nanotubes as a conducting platform [204]. They reported myosin heavy chain protein was significantly found after electrical stimulation that performed on the day 8^{th} of cell culture experiments for two consecutive days [204]. Researchers in National University of Singapore showed that the cells proliferation and expression of CX43 were improved after applying electrical stimulation. It is worth to note that CX43 is a cardiac-muscle-specific intermediate lament protein which has an important role in cardiac contractility [205].

In conclusion, the overall aim of this thesis is to develop a range of fibrous 3D architectures of composite biomaterials. These composites were prepared from conducting and non-conducting materials and were evaluated for their suitability and use in drug delivery and support of cellular growth.

1.5 References

[1] Vacanti JP, Morse MA, Saltzman WM, Domb AJ, Perez-Atayde A, Langer R. "*Selective cell transplantation using bioabsorbable artificial polymers as matrices*". Journal of Pediatric Surgery. 1988;**23**(1):3-9.

[2] Brett Runge M, Dadsetan M, Baltrusaitis J, Knight AM, Ruesink T, Lazcano EA, Lu L, Windebank AJ, Yaszemski MJ. "*The development of electrically conductive polycaprolactone fumarate–polypyrrole composite materials for nerve regeneration*". Biomaterials. 2010;**31**(23):5916-26.

[3] Zong X, Bien H, Chung C-Y, Yin L, Fang D, Hsiao BS, Chu B, Entcheva E. "*Electrospun fine-textured scaffolds for heart tissue constructs*". Biomaterials. 2005;**26**(26):5330-8.

[4] Jung J-H, Choi C-H, Chung S, Chung Y-M, Lee C-S. "*Microfluidic synthesis of a cell adhesive Janus polyurethane microfiber*". Lab on a Chip. 2009;**9**(17):2596-602.

[5] Chikar JA, Hendricks JL, Richardson-Burns SM, Raphael Y, Pfingst BE, Martin DC. "*The use of a dual PEDOT and RGD-functionalized alginate hydrogel coating to provide sustained drug delivery and improved cochlear implant function*". Biomaterials. 2012;**33**(7):1982-90.

[6] Muzzarelli R, Biagini G, Pugnaloni A, Filippini O, Baldassarre V, Castaldini C, Rizzoli C. "*Reconstruction of parodontal tissue with chitosan*". Biomaterials. 1989;**10**(9):598-603.

[7] Cukierman E, Pankov R, Yamada KM. "*Cell interactions with three-dimensional matrices*". Current Opinion in Cell Biology. 2002;**14**(5):633-40.

[8] Hutmacher DW. "*Scaffolds in tissue engineering bone and cartilage*". Biomaterials. 2000;**21**(24):2529-43.

[9] Wang Y, Challa P, Epstein DL, Yuan F. "*Controlled release of ethacrynic acid from poly(lactide-co-glycolide) films for glaucoma treatment*". Biomaterials. 2004;**25**(18):4279-85.

[10] Li W-J, Laurencin CT, Caterson EJ, Tuan RS, Ko FK. "*Electrospun nanofibrous structure: A novel scaffold for tissue engineering*". Journal of Biomedical Materials Research. 2002;**60**(4):613-21.

[11] Panyam J, Labhasetwar V. "*Biodegradable nanoparticles for drug and gene delivery to cells and tissue*". Advanced Drug Delivery Reviews. 2012;**64, Supplement**(0):61-71.

[12] Uematsu K, Hattori K, Ishimoto Y, Yamauchi J, Habata T, Takakura Y, Ohgushi H, Fukuchi T, Sato M. "*Cartilage regeneration using mesenchymal stem cells and a three-dimensional poly-lactic-glycolic acid (PLGA) scaffold*". Biomaterials. 2005;**26**(20):4273-9.

[13] Rathke TD, Hudson SM. "*Review of Chitin and Chitosan as Fiber and Film Formers*". Journal of Macromolecular Science, Part C. 1994;**34**(3):375-437.

[14] Depan D, Girase B, Shah JS, Misra RDK. "*Structure–process–property relationship of the polar graphene oxide-mediated cellular response and stimulated growth of osteoblasts on hybrid chitosan network structure nanocomposite scaffolds*". Acta Biomaterialia. 2011;**7**(9):3432-45.

[15] Agnihotri SA, Mallikarjuna NN, Aminabhavi TM. "*Recent advances on chitosan-based micro- and nanoparticles in drug delivery*". Journal of Controlled Release. 2004;**100**(1):5-28.

[16] Abidian MR, Martin DC. "*Multifunctional Nanobiomaterials for Neural Interfaces*". Adv Funct Mater. 2009;**19**(4):573-85.
[17] Piccolino M. "*Animal electricity and the birth of electrophysiology: the legacy of Luigi Galvani*". Brain Research Bulletin. 1998;**46**(5):381-407.
[18] Shirakawa H, Louis EJ, MacDiarmid AG, Chiang CK, Heeger AJ. "*Synthesis of electrically conducting organic polymers: halogen derivatives of polyacetylene, (CH)*". Journal of the Chemical Society, Chemical Communications. 1977(16):578-80.
[19] Skotheim TJ, RLE, Reynolds JR. Handbook of conducting polymers. 2nd ed: Marcel Dekker; 1998.
[20] Kotov NA, Winter JO, Clements IP, Jan E, Timko BP, Campidelli S, Pathak S, Mazzatenta A, Lieber CM, Prato M, Bellamkonda RV, Silva GA, Kam NWS, Patolsky F, Ballerini L. "*Nanomaterials for neural interfaces*". Adv Mater. 2009;**21**(40):3970-4004.
[21] Geim AK, Novoselov KS. "*The rise of graphene*". Nature Materials. 2007;**6**:183 - 91.
[22] Chandrasekhar P. Conducting polymers, fundamentals and applications: A practical approach: Kluwer Academic Publishers; 1999.
[23] Terje AS, John RR. Handbook of Conducting Polymers: CONJUGATED POLYMERS PROCESSING AND APPLICATIONS. 3rd ed: CRC Press Taylor & Francis Group; 2007.
[24] R. Andersson M, Thomas O, Mammo W, Svensson M, Theander M, Inganas O. "*Substituted polythiophenes designed for optoelectronic devices and conductors*". Journal of Materials Chemistry. 1999;**9**(9):1933-40.
[25] Pernites RB, Ponnapati RR, Advincula RC. "*Superhydrophobic–Superoleophilic Polythiophene Films with Tunable Wetting and Electrochromism*". Advanced Materials. 2011;**23**(28):3207-13.
[26] Duchet J, Legras R, Demoustier-Champagne S. "*Chemical synthesis of polypyrrole: structure–properties relationship*". Synthetic Metals. 1998;**98**(2):113-22.
[27] West K, Jacobsen T, Zachau-Christiansen B, Careem MA, Skaarup S. "*Electrochemical synthesis of polypyrrole: Influence of current density on structure*". Synthetic Metals. 1993;**55**(2–3):1412-7.
[28] J. SATRR, ed. Conjugated Polymers: Processing and Applications. Third ed: CRC Press 2006.
[29] Svirskis D, Travas-Sejdic J, Rodgers A, Garg S. "*Electrochemically controlled drug delivery based on intrinsically conducting polymers*". Journal of Controlled Release. 2010;**146**(1):6-15.
[30] Sadki S, Schottland P, Brodie N, Sabouraud G. "*The mechanisms of pyrrole electropolymerization*". Chemical Society Reviews. 2000;**29**(5):283-93.
[31] Gordon G. Wallace GMS, Leon A.P. Kane-Maguire, Peter R. Teasdale. Conductive Electroactive Polymers: Intelligent Polymer Systems. Third ed: CRC Press; 2008.
[32] Chiang CK, Fincher CR, Park YW, Heeger AJ, Shirakawa H, Louis EJ, Gau SC, MacDiarmid AG. "*Electrical Conductivity in Doped Polyacetylene*". Physical Review Letters. 1977;**39**(17):1098.
[33] Tourillon G, Garnier F. "*New electrochemically generated organic conducting polymers*". Journal of Electroanalytical Chemistry. 1982;**135**(1):173-8.
[34] Gerard M, Chaubey A, Malhotra BD. "*Application of conducting polymers to biosensors*". Biosensors and Bioelectronics. 2002;**17**(5):345-59.

[35] Bajpai AK, Shukla SK, Bhanu S, Kankane S. "*Responsive polymers in controlled drug delivery*". Progress in Polymer Science. 2008;**33**(11):1088-118.
[36] Jager EWH, Inganäs O, Lundström I. "*Microrobots for Micrometer-Size Objects in Aqueous Media: Potential Tools for Single-Cell Manipulation*". Science. 2000;**288**(5475):2335-8.
[37] Kotwal A, Schmidt CE. "*Electrical stimulation alters protein adsorption and nerve cell interactions with electrically conducting biomaterials*". Biomaterials. 2001;**22**(10):1055-64.
[38] Rivers TJ, Hudson TW, Schmidt CE. "*Synthesis of a Novel, Biodegradable Electrically Conducting Polymer for Biomedical Applications*". Advanced Functional Materials. 2002;**12**(1):33-7.
[39] Bolin MH, Svennersten K, Wang X, Chronakis IS, Richter-Dahlfors A, Jager EWH, Berggren M. "*Nano-fiber scaffold electrodes based on PEDOT for cell stimulation*". Sensors and Actuators B: Chemical. 2009;**142**(2):451-6.
[40] Humpolicek P, Kasparkova V, Saha P, Stejskal J. "*Biocompatibility of polyaniline*". Synthetic Metals. 2012;**162**(7–8):722-7.
[41] Bidez PR, Li S, MacDiarmid AG, Venancio EC, Wei Y, Lelkes PI. "*Polyaniline, an electroactive polymer, supports adhesion and proliferation of cardiac myoblasts*". Journal of Biomaterials Science, Polymer Edition. 2006;**17**(1-2):199-212.
[42] Wang X, Gu X, Yuan C, Chen S, Zhang P, Zhang T, Yao J, Chen F, Chen G. "*Evaluation of biocompatibility of polypyrrole in vitro and in vivo*". Journal of Biomedical Materials Research Part A. 2004;**68A**(3):411-22.
[43] Li M, Guo Y, Wei Y, MacDiarmid AG, Lelkes PI. "*Electrospinning polyaniline-contained gelatin nanofibers for tissue engineering applications*". Biomaterials. 2006;**27**(13):2705-15.
[44] Widge AS, Jeffries-El M, Cui X, Lagenaur CF, Matsuoka Y. "*Self-assembled monolayers of polythiophene conductive polymers improve biocompatibility and electrical impedance of neural electrodes*". Biosensors and Bioelectronics. 2007;**22**(8):1723-32.
[45] Otero TF, Cantero I, Grande H. "*Solvent effects on the charge storage ability in polypyrrole*". Electrochimica Acta. 1999;**44**(12):2053-9.
[46] Madden JD, Cush RA, Kanigan TS, Hunter IW. "*Fast contracting polypyrrole actuators*". Synt Met. 2000;**113**(1-2):185-92.
[47] Partridge AC, Jansen ML, Arnold WM. "*Conducting polymer-based sensors*". Materials Science and Engineering: C. 2000;**12**(1–2):37-42.
[48] Tallman D, Spinks G, Dominis A, Wallace G. "*Electroactive conducting polymers for corrosion control*". J Solid State Electrochem. 2002;**6**(2):73-84.
[49] Sapp SA, Sotzing GA, Reddinger JL, Reynolds JR. "*Rapid switching solid state electrochromic devices based on complementary conducting polymer films*". Advanced Materials. 1996;**8**(10):808-11.
[50] Otero TF, Cantero I. "*Conducting polymers as positive electrodes in rechargeable lithium-ion batteries*". Journal of Power Sources. 1999;**81-82**(0):838-41.
[51] Ghosh S, Inganäs O. "*Conducting Polymer Hydrogels as 3D Electrodes: Applications for Supercapacitors*". Advanced Materials. 1999;**11**(14):1214-8.
[52] Thompson BC, Moulton SE, Ding J, Richardson R, Cameron A, O'Leary S, Wallace GG, Clark GM. "*Optimising the incorporation and release of a neurotrophic factor using conducting polypyrrole*". J Control Release. 2006;**116**(3):285-94.

[53] Li J, Wang E. "*Scanning tunneling microscopy (STM) and lateral force microscopy (LFM) investigation of the structure and character of conductive polypyrrole film*". Synthetic Metals. 1994;**66**(1):67-74.
[54] Fonner JM, Forciniti L, Nguyen H, Byrne JD, Kou Y-F, Syeda-Nawaz J, Schmidt CE. "*Biocompatibility implications of polypyrrole synthesis techniques*". Biomedical Materials. 2008;**3**(3):034124.
[55] Ateh DD, Navsaria HA, Vadgama P. "*Polypyrrole-based conducting polymers and interactions with biological tissues*". Journal of The Royal Society Interface. 2006;**3**(11):741-52.
[56] Brédas JL, Scott JC, Yakushi K, Street GB. "*Polarons and bipolarons in polypyrrole: Evolution of the band structure and optical spectrum upon doing*". Physical Review B. 1984;**30**(2):1023-5.
[57] Wallace GG, Kane-Maguire LAP. "*Manipulating and Monitoring Biomolecular Interactions with Conducting Electroactive Polymers*". Advanced Materials. 2002;**14**(13-14):953-60.
[58] Liu X, Yue Z, Higgins MJ, Wallace GG. "*Conducting polymers with immobilised fibrillar collagen for enhanced neural interfacing*". Biomaterials. 2011;**32**(30):7309-17.
[59] Okuzaki H, Harashina Y, Yan H. "*Highly conductive PEDOT/PSS microfibers fabricated by wet-spinning and dip-treatment in ethylene glycol*". European Polymer Journal. 2009;**45**(1):256-61.
[60] Kirchmeyer S, Reuter K. "*Scientific importance, properties and growing applications of poly(3,4-ethylenedioxythiophene)*". Journal of Materials Chemistry. 2005;**15**(21):2077-88.
[61] Argun AA, Cirpan A, Reynolds JR. "*The First Truly All-Polymer Electrochromic Devices*". Advanced Materials. 2003;**15**(16):1338-41.
[62] de Kok MM, Buechel M, Vulto SIE, van de Weijer P, Meulenkamp EA, de Winter SHPM, Mank AJG, Vorstenbosch HJM, Weijtens CHL, van Elsbergen V. "*Modification of PEDOT:PSS as hole injection layer in polymer LEDs*". physica status solidi (a). 2004;**201**(6):1342-59.
[63] Yang Y, Yu G, Cha JJ, Wu H, Vosgueritchian M, Yao Y, Bao Z, Cui Y. "*Improving the Performance of Lithium–Sulfur Batteries by Conductive Polymer Coating*". ACS Nano. 2011;**5**(11):9187-93.
[64] Huang L-M, Wen T-C, Gopalan A. "*Electrochemical and spectroelectrochemical monitoring of supercapacitance and electrochromic properties of hydrous ruthenium oxide embedded poly(3,4-ethylenedioxythiophene)–poly(styrene sulfonic acid) composite*". Electrochimica Acta. 2006;**51**(17):3469-76.
[65] Winther-Jensen B, Winther-Jensen O, Forsyth M, MacFarlane DR. "*High Rates of Oxygen Reduction over a Vapor Phase–Polymerized PEDOT Electrode*". Science. 2008;**321**(5889):671-4.
[66] Damlin P, Kvarnström C, Ivaska A. "*Electrochemical synthesis and in situ spectroelectrochemical characterization of poly(3,4-ethylenedioxythiophene) (PEDOT) in room temperature ionic liquids*". Journal of Electroanalytical Chemistry. 2004;**570**(1):113-22.
[67] Svennersten K, Bolin MH, Jager EWH, Berggren M, Richter-Dahlfors A. "*Electrochemical modulation of epithelia formation using conducting polymers*". Biomaterials. 2009;**30**(31):6257-64.
[68] Kros A, Sommerdijk NAJM, Nolte RJM. "*Poly(pyrrole) versus poly(3,4-ethylenedioxythiophene): implications for biosensor applications*". Sensors and Actuators B: Chemical. 2005;**106**(1):289-95.

[69] Cui X, Martin DC. "*Electrochemical deposition and characterization of poly(3,4-ethylenedioxythiophene) on neural microelectrode arrays*". Sensors and Actuators B: Chemical. 2003;**89**(1–2):92-102.
[70] Wan AMD, Brooks DJ, Gumus A, Fischbach C, Malliaras GG. "*Electrical control of cell density gradients on a conducting polymer surface*". Chemical Communications. 2009(35):5278-80.
[71] Geim AK, Novoselov KS. "*The rise of graphene*". Nat Mater. 2007;**6**(3):183-91.
[72] Novoselov KS, Geim AK, Morozov SV, Jiang D, Zhang Y, Dubonos SV, Grigorieva IV, Firsov AA. "*Electric Field Effect in Atomically Thin Carbon Films*". Science. 2004;**306**(5696):666-9.
[73] Wallace PR. "*The Band Theory of Graphite*". Physical Review. 1947;**71**(9):622-34.
[74] Boehm HP, Clauss A, Fischer GO, Hofmann U. "*Das Adsorptionsverhalten sehr dünner Kohlenstoff-Folien*". Zeitschrift für anorganische und allgemeine Chemie. 1962;**316**(3-4):119-27.
[75] Fradkin E. "*Critical behavior of disordered degenerate semiconductors. II. Spectrum and transport properties in mean-field theory*". Physical Review B. 1986;**33**(5):3263-8.
[76] Balog R, Jorgensen B, Nilsson L, Andersen M, Rienks E, Bianchi M, Fanetti M, Laegsgaard E, Baraldi A, Lizzit S, Sljivancanin Z, Besenbacher F, Hammer B, Pedersen TG, Hofmann P, Hornekaer L. "*Bandgap opening in graphene induced by patterned hydrogen adsorption*". Nat Mater. 2010;**9**(4):315-9.
[77] Lee C, Wei X, Kysar JW, Hone J. "*Measurement of the Elastic Properties and Intrinsic Strength of Monolayer Graphene*". Science. 2008;**321**(5887):385-8.
[78] Balandin AA, Ghosh S, Bao W, Calizo I, Teweldebrhan D, Miao F, Lau CN. "*Superior Thermal Conductivity of Single-Layer Graphene*". Nano Letters. 2008;**8**(3):902-7.
[79] Huang X, Qi X, Boey F, Zhang H. "*Graphene-based composites*". Chemical Society Reviews. 2012;**41**(2):666-86.
[80] Vakil A, Engheta N. "*Transformation Optics Using Graphene*". Science. 2011;**332**(6035):1291-4.
[81] Eda G, Chhowalla M. "*Graphene-based composite thin films for electronics*". Nano Lett. 2009;**9**(2):814-8.
[82] Sutter PW, Flege J-I, Sutter EA. "*Epitaxial graphene on ruthenium*". Nat Mater. 2008;**7**(5):406-11.
[83] Kosynkin DV, Higginbotham AL, Sinitskii A, Lomeda JR, Dimiev A, Price BK, Tour JM. "*Longitudinal unzipping of carbon nanotubes to form graphene nanoribbons*". Nature. 2009;**458**(7240):872-6.
[84] Amini S, Garay J, Liu G, Balandin AA, Abbaschian R. "*Growth of large-area graphene films from metal-carbon melts*". Journal of Applied Physics. 2010;**108**(9):094321--7.
[85] Choucair M, Thordarson P, Stride JA. "*Gram-scale production of graphene based on solvothermal synthesis and sonication*". Nat Nano. 2009;**4**(1):30-3.
[86] Sun Z, Yan Z, Yao J, Beitler E, Zhu Y, Tour JM. "*Growth of graphene from solid carbon sources*". Nature. 2010;**468**(7323):549-52.
[87] Li D, Muller MB, Gilje S, Kaner RB, Wallace GG. "*Processable aqueous dispersions of graphene nanosheets*". Nat Nano. 2008;**3**(2):101-5.

[88] Guo S, Dong S. "*Graphene nanosheet: synthesis, molecular engineering, thin film, hybrids, and energy and analytical applications*". Chemical Society Reviews. 2011;**40**(5):2644-72.
[89] Hernandez Y, Nicolosi V, Lotya M, Blighe FM, Sun Z, De S, McGovern IT, Holland B, Byrne M, Gun'Ko YK, Boland JJ, Niraj P, Duesberg G, Krishnamurthy S, Goodhue R, Hutchison J, Scardaci V, Ferrari AC, Coleman JN. "*High-yield production of graphene by liquid-phase exfoliation of graphite*". Nat Nano. 2008;**3**(9):563-8.
[90] Rao CNR, Sood AK, Subrahmanyam KS, Govindaraj A. "*Graphene: The New Two-Dimensional Nanomaterial*". Angewandte Chemie International Edition. 2009;**48**(42):7752-77.
[91] Zhu Y, Murali S, Cai W, Li X, Suk JW, Potts JR, Ruoff RS. "*Graphene and Graphene Oxide: Synthesis, Properties, and Applications*". Adv Mater. 2010;**22**(35):3906-24.
[92] Xu Y, Shi G. "*Assembly of chemically modified graphene: methods and applications*". Journal of Materials Chemistry. 2011;**21**(10):3311-23.
[93] Eda G, Fanchini G, Chhowalla M. "*Large-area ultrathin films of reduced graphene oxide as a transparent and flexible electronic material*". Nat Nano. 2008;**3**(5):270-4.
[94] Stankovich S, Dikin DA, Piner RD, Kohlhaas KA, Kleinhammes A, Jia Y, Wu Y, Nguyen ST, Ruoff RS. "*Synthesis of graphene-based nanosheets via chemical reduction of exfoliated graphite oxide*". Carbon. 2007;**45**(7):1558-65.
[95] Hernandez Y, Nicolosi V, Lotya M, Blighe FM, Sun Z, De S, McGovern IT, Holland B, Byrne M, Gun'Ko YK, Boland JJ, Niraj P, Duesberg G, Krishnamurthy S, Goodhue R, Hutchison J, Scardaci V, Ferrari AC, Coleman JN. "*High-yield production of graphene by liquid-phase exfoliation of graphite*". Nat Nanotechnol. 2008;**3**(9):563-8.
[96] Lotya M, King PJ, Khan U, De S, Coleman JN. "*High-Concentration, Surfactant-Stabilized Graphene Dispersions*". ACS Nano. 2010;**4**(6):3155-62.
[97] Lotya M, Hernandez Y, King PJ, Smith RJ, Nicolosi V, Karlsson LS, Blighe FM, De S, Wang Z, McGovern IT, Duesberg GS, Coleman JN. "*Liquid Phase Production of Graphene by Exfoliation of Graphite in Surfactant/Water Solutions*". Journal of the American Chemical Society. 2009;**131**(10):3611-20.
[98] Zhang M, Parajuli RR, Mastrogiovanni D, Dai B, Lo P, Cheung W, Brukh R, Chiu PL, Zhou T, Liu Z, Garfunkel E, He H. "*Production of Graphene Sheets by Direct Dispersion with Aromatic Healing Agents*". Small. 2010;**6**(10):1100-7.
[99] Englert JM, Röhrl J, Schmidt CD, Graupner R, Hundhausen M, Hauke F, Hirsch A. "*Soluble Graphene: Generation of Aqueous Graphene Solutions Aided by a Perylenebisimide-Based Bolaamphiphile*". Advanced Materials. 2009;**21**(42):4265-9.
[100] Hao R, Qian W, Zhang L, Hou Y. "*Aqueous dispersions of TCNQ-anion-stabilized graphene sheets*". Chemical Communications. 2008(48):6576-8.
[101] Coleman JN. "*Liquid Exfoliation of Defect-Free Graphene*". Accounts of Chemical Research. 2012.
[102] Jonathan NC. "*Liquid-Phase Exfoliation of Nanotubes and Graphene*". Advanced Functional Materials. 2009;**19**(23):3680-95.
[103] Khan U, O'Neill A, Lotya M, De S, Coleman JN. "*High-Concentration Solvent Exfoliation of Graphene*". Small. 2010;**6**(7):864-71.

[104] Blake P, Brimicombe PD, Nair RR, Booth TJ, Jiang D, Schedin F, Ponomarenko LA, Morozov SV, Gleeson HF, Hill EW, Geim AK, Novoselov KS. "*Graphene-Based Liquid Crystal Device*". Nano Letters. 2008;**8**(6):1704-8.
[105] Bourlinos AB, Georgakilas V, Zboril R, Steriotis TA, Stubos AK. "*Liquid-Phase Exfoliation of Graphite Towards Solubilized Graphenes*". Small. 2009;**5**(16):1841-5.
[106] Hamilton CE, Lomeda JR, Sun Z, Tour JM, Barron AR. "*High-Yield Organic Dispersions of Unfunctionalized Graphene*". Nano Letters. 2009;**9**(10):3460-2.
[107] Hernandez Y, Lotya M, Rickard D, Bergin SD, Coleman JN. "*Measurement of Multicomponent Solubility Parameters for Graphene Facilitates Solvent Discovery*". Langmuir. 2009;**26**(5):3208-13.
[108] Green AA, Hersam MC. "*Solution Phase Production of Graphene with Controlled Thickness via Density Differentiation*". Nano Letters. 2009;**9**(12):4031-6.
[109] Gu W, Zhang W, Li X, Zhu H, Wei J, Li Z, Shu Q, Wang C, Wang K, Shen W, Kang F, Wu D. "*Graphene sheets from worm-like exfoliated graphite*". Journal of Materials Chemistry. 2009;**19**(21):3367-9.
[110] Vadukumpully S, Paul J, Valiyaveettil S. "*Cationic surfactant mediated exfoliation of graphite into graphene flakes*". Carbon. 2009;**47**(14):3288-94.
[111] Choi E-Y, Choi WS, Lee YB, Noh Y-Y. "*Production of graphene by exfoliation of graphite in a volatile organic solvent*". Nanotechnology. 2011;**22**(36):365601.
[112] O'Neill A, Khan U, Nirmalraj PN, Boland J, Coleman JN. "*Graphene Dispersion and Exfoliation in Low Boiling Point Solvents*". The Journal of Physical Chemistry C. 2011;**115**(13):5422-8.
[113] Liu WW, Wang JN. "*Direct exfoliation of graphene in organic solvents with addition of NaOH*". Chemical Communications. 2011;**47**(24):6888-90.
[114] Jung YC, Kim JH, Hayashi T, Kim YA, Endo M, Terrones M, Dresselhaus MS. "*Fabrication of Transparent, Tough, and Conductive Shape-Memory Polyurethane Films by Incorporating a Small Amount of High-Quality Graphene*". Macromolecular Rapid Communications. 2012;**33**(8):628-34.
[115] Khan U, Young K, O'Neill A, Coleman JN. "*High strength composite fibres from polyester filled with nanotubes and graphene*". Journal of Materials Chemistry. 2012;**22**(25):12907-14.
[116] May P, Khan U, O'Neill A, Coleman JN. "*Approaching the theoretical limit for reinforcing polymers with graphene*". Journal of Materials Chemistry. 2012;**22**(4):1278-82.
[117] Lee JH, Shin DW, Makotchenko VG, Nazarov AS, Fedorov VE, Kim YH, Choi J-Y, Kim JM, Yoo J-B. "*One-Step Exfoliation Synthesis of Easily Soluble Graphite and Transparent Conducting Graphene Sheets*". Advanced Materials. 2009;**21**(43):4383-7.
[118] Behabtu N, Lomeda JR, Green MJ, Higginbotham AL, Sinitskii A, Kosynkin DV, Tsentalovich D, Parra-Vasquez ANG, Schmidt J, Kesselman E, Cohen Y, Talmon Y, Tour JM, Pasquali M. "*Spontaneous high-concentration dispersions and liquid crystals of graphene*". Nat Nano. 2010;**5**(6):406-11.
[119] Stankovich S, Dikin DA, Dommett GHB, Kohlhaas KM, Zimney EJ, Stach EA, Piner RD, Nguyen ST, Ruoff RS. "*Graphene-based composite materials*". Nature. 2006;**442**(7100):282-6.
[120] Geiger B, Bershadsky A, Pankov R, Yamada KM. "*Transmembrane crosstalk between the extracellular matrix and the cytoskeleton*". Nat Rev Mol Cell Biol. 2001;**2**(11):793-805.

[121] García Cruz DM, Escobar Ivirico JL, Gomes MM, Gómez Ribelles JL, Sánchez MS, Reis RL, Mano JF. "*Chitosan microparticles as injectable scaffolds for tissue engineering*". Journal of Tissue Engineering and Regenerative Medicine. 2008;**2**(6):378-80.
[122] Ramalingam M, Ramakrishna S. "*Nano-Featured Scaffolds for Tissue Engineering: A Review of Spinning Methodologies* ". Tissue Engineering. 2006;**12**(3):435-47.
[123] Dogine K. Formation of fibers and development their structure: (II) wet spinning and dry spinning: The society of fiber science and technology; 1970.
[124] Nakajima T. Advanced fiber spinning technology: Woodhead; 1994.
[125] Razal JM, Gilmore KJ, Wallace GG. "*Carbon Nanotube Biofiber Formation in a Polymer-Free Coagulation Bath*". Advanced Functional Materials. 2008;**18**(1):61-6.
[126] Mack BC, Wright KW, Davis ME. "*A biodegradable filament for controlled drug delivery*". Journal of Controlled Release. 2009;**139**(3):205-11.
[127] Lu HH, Cooper Jr JA, Manuel S, Freeman JW, Attawia MA, Ko FK, Laurencin CT. "*Anterior cruciate ligament regeneration using braided biodegradable scaffolds: in vitro optimization studies*". Biomaterials. 2005;**26**(23):4805-16.
[128] Hwang CM, Khademhosseini A, Park Y, Sun K, Lee S-H. "*Microfluidic Chip-Based Fabrication of PLGA Microfiber Scaffolds for Tissue Engineering*". Langmuir. 2008;**24**(13):6845-51.
[129] G.Wallace G, Moulton S, Kapsa RMI, MichaelHiggins. Organic Bionics. Weinheim: Wiley-VCH Verlag GmbH & Co. KGaA
2012.
[130] Li D, Xia Y. "*Electrospinning of Nanofibers: Reinventing the Wheel?*". Advanced Materials. 2004;**16**(14):1151-70.
[131] Agarwal S, Wendorff JH, Greiner A. "*Use of electrospinning technique for biomedical applications*". Polymer. 2008;**49**(26):5603-21.
[132] Doshi J, Reneker DH. "*Electrospinning process and applications of electrospun fibers*". Journal of Electrostatics. 1995;**35**(2–3):151-60.
[133] Ramakrishna WETaS. "*A review on electrospinning design and nanofibre assemblies*". Nanotechnology. 2006;**17**(14):R89-R106

[134] Naficy S, Razal JM, Spinks GM, Wallace GG, Whitten PG. "*Electrically Conductive, Tough Hydrogels with pH Sensitivity*". Chemistry of Materials. 2012;**24**(17):3425-33.
[135] Fong H, Chun I, Reneker DH. "*Beaded nanofibers formed during electrospinning*". Polymer. 1999;**40**(16):4585-92.
[136] Qin X-H, Wang S-Y. "*Filtration properties of electrospinning nanofibers*". Journal of Applied Polymer Science. 2006;**102**(2):1285-90.
[137] Jin H-J, Fridrikh SV, Rutledge GC, Kaplan DL. "*Electrospinning Bombyx mori Silk with Poly(ethylene oxide)*". Biomacromolecules. 2002;**3**(6):1233-9.
[138] Rho KS, Jeong L, Lee G, Seo B-M, Park YJ, Hong S-D, Roh S, Cho JJ, Park WH, Min B-M. "*Electrospinning of collagen nanofibers: Effects on the behavior of normal human keratinocytes and early-stage wound healing*". Biomaterials. 2006;**27**(8):1452-61.
[139] Kenawy E-R, Bowlin GL, Mansfield K, Layman J, Simpson DG, Sanders EH, Wnek GE. "*Release of tetracycline hydrochloride from electrospun*

poly(ethylene-co-vinylacetate), poly(lactic acid), and a blend". Journal of Controlled Release. 2002;**81**(1–2):57-64.
[140] Huang Z-M, Zhang YZ, Kotaki M, Ramakrishna S. "*A review on polymer nanofibers by electrospinning and their applications in nanocomposites*". Composites Science and Technology. 2003;**63**(15):2223-53.
[141] Chris A. Bashur RDS, Linda A. Dahlgren, Scott A. Guelcher, and Aaron S. Goldstein. "*Effect of Fiber Diameter and Alignment of Electrospun Polyurethane Meshes on Mesenchymal Progenitor Cells*". Tissue Engineering Part A. 2009;**15**(9):2435-45.
[142] Barnes CP, Sell SA, Boland ED, Simpson DG, Bowlin GL. "*Nanofiber technology: Designing the next generation of tissue engineering scaffolds*". Advanced Drug Delivery Reviews. 2007;**59**(14):1413-33.
[143] Jalili R, Morshed M, Ravandi SAH. "*Fundamental parameters affecting electrospinning of PAN nanofibers as uniaxially aligned fibers*". Journal of Applied Polymer Science. 2006;**101**(6):4350-7.
[144] Dalton PD, Klee D, Möller M. "*Electrospinning with dual collection rings*". Polymer. 2005;**46**(3):611-4.
[145] Ramakrishna WETaS. "*Electrospun fibre bundle made of aligned nanofibres over two fixed points*". Nanotechnology. 2005;**16**:1878.
[146] Sundaray B, Subramanian V, Natarajan TS, Xiang R-Z, Chang C-C, Fann W-S. "*Electrospinning of continuous aligned polymer fibers*". Applied Physics Letters. 2004;**84**(7):1222-4.
[147] Dersch R, Liu T, Schaper AK, Greiner A, Wendorff JH. "*Electrospun nanofibers: Internal structure and intrinsic orientation*". Journal of Polymer Science Part A: Polymer Chemistry. 2003;**41**(4):545-53.
[148] E. Zussman, Theron A, Yarin AL. "*Formation of nanofiber crossbars in electrospinning*". Appl Phys Lett. 2003; **82**(973):3.
[149] Laforgue A. "*All-textile flexible supercapacitors using electrospun poly(3,4-ethylenedioxythiophene) nanofibers*". Journal of Power Sources. 2011;**196**(1):559-64.
[150] Laforgue A, Robitaille L. "*Production of Conductive PEDOT Nanofibers by the Combination of Electrospinning and Vapor-Phase Polymerization*". Macromolecules. 2010;**43**(9):4194-200.
[151] Kim D-H, Abidian M, Martin DC. "*Conducting polymers grown in hydrogel scaffolds coated on neural prosthetic devices*". Journal of Biomedical Materials Research Part A. 2004;**71A**(4):577-85.
[152] Young K, Blighe FM, Vilatela JJ, Windle AH, Kinloch IA, Deng L, Young RJ, Coleman JN. "*Strong Dependence of Mechanical Properties on Fiber Diameter for Polymer−Nanotube Composite Fibers: Differentiating Defect from Orientation Effects*". ACS Nano. 2010;**4**(11):6989-97.
[153] Tamayol A, Akbari M, Annabi N, Paul A, Khademhosseini A, Juncker D. "*Fiber-based tissue engineering: Progress, challenges, and opportunities*". Biotechnology Advances. 2013;**31**(5):669-87.
[154] Michael Shin, Hiroshi Yoshimoto, Vacanti JP. "*In Vivo Bone Tissue Engineering Using Mesenchymal Stem Cells on a Novel Electrospun Nanofibrous Scaffold*". Tissue Engineering. 2004;**10**(1-2):33-41.
[155] Requicha JF, Moura T, Leonor IB, Martins T, Muñoz F, Reis RL, Gomes ME, Viegas CA. "*Evaluation of a starch-based double layer scaffold for bone regeneration in a rat model*". Journal of Orthopaedic Research. 2014.

[156] Nisbet DR, Forsythe JS, Shen W, Finkelstein DI, Horne MK. "*A Review of the Cellular Response on Electrospun Nanofibers for Tissue Engineering*". Journal of Biomaterials Applications. 2009;**24**(1):7-29.
[157] Wadhwa R, Lagenaur CF, Cui XT. "*Electrochemically controlled release of dexamethasone from conducting polymer polypyrrole coated electrode*". J Control Release. 2006;**110**(3):531-41.
[158] Thompson BC, Chen J, Moulton SE, Wallace GG. "*Nanostructured aligned CNT platforms enhance the controlled release of a neurotrophic protein from polypyrrole*". Nanoscale. 2010;**2**(4):499-501.
[159] Thompson BC, Richardson RT, Moulton SE, Evans AJ, O'Leary S, Clark GM, Wallace GG. "*Conducting polymers, dual neurotrophins and pulsed electrical stimulation -- Dramatic effects on neurite outgrowth*". Journal of Controlled Release. 2010;**141**(2):161-7.
[160] Allen TM, Cullis PR. "*Drug Delivery Systems: Entering the Mainstream*". Science. 2004;**303**(5665):1818-22.
[161] Svirskis D, Travas-Sejdic J, Rodgers A, Garg S. "*Electrochemically controlled drug delivery based on intrinsically conducting polymers*". J Control Release. 2010;**146**(1):6-15.
[162] Nasongkla N, Bey E, Ren J, Ai H, Khemtong C, Guthi JS, Chin S-F, Sherry AD, Boothman DA, Gao J. "*Multifunctional Polymeric Micelles as Cancer-Targeted, MRI-Ultrasensitive Drug Delivery Systems*". Nano Letters. 2006;**6**(11):2427-30.
[163] Sershen SR, Westcott SL, Halas NJ, West JL. "*Temperature-sensitive polymer–nanoshell composites for photothermally modulated drug delivery*". Journal of Biomedical Materials Research - Part B Applied Biomaterials. 2000;**51**(3):293–8.
[164] Lee KY, Peters MC, Anderson KW, Mooney DJ. "*Controlled growth factor release from synthetic extracellular matrices*". Nature. 2000;**408**:998-1000.
[165] Viry L, Moulton SE, Romeo T, Suhr C, Mawad D, Cook M, Wallace GG. "*Emulsion-coaxial electrospinning: designing novel architectures for sustained release of highly soluble low molecular weight drugs*". Journal of Materials Chemistry. 2012;**22**(22):11347-53.
[166] Wu XS, Wang N. "*Synthesis, characterization, biodegradation, and drug delivery application of biodegradable lactic/glycolic acid polymers. Part II: Biodegradation*". Journal of Biomaterials Science, Polymer Edition. 2001;**12**(1):21-34.
[167] Göpferich A. "*Mechanisms of polymer degradation and erosion*". Biomaterials. 1996;**17**(2):103-14.
[168] Bala I, Hariharan S, Kumar MN. "*PLGA nanoparticles in drug delivery: the state of the art*". Critical reviews in therapeutic drug carrier systems. 2004;**21**(5):387-422.
[169] Bodmeier R, Oh KH, Chen H. "*The effect of the addition of low molecular weight poly(dl-lactide) on drug release from biodegradable poly(dl-lactide) drug delivery systems*". International Journal of Pharmaceutics. 1989;**51**(1):1-8.
[170] Perugini P, Genta I, Conti B, Modena T, Pavanetto F. "*Periodontal delivery of ipriflavone: new chitosan/PLGA film delivery system for a lipophilic drug*". International Journal of Pharmaceutics. 2003;**252**(1–2):1-9.
[171] Zinger B, Miller LL. "*Timed release of chemicals from polypyrrole films*". Journal of the American Chemical Society. 1984;**106**(22):6861-3.

[172] Green RA, Lovell NH, Wallace GG, Poole-Warren LA. "*Conducting polymers for neural interfaces: Challenges in developing an effective long-term implant*". Biomaterials. 2008;**29**(24–25):3393-9.
[173] Staples M, Daniel K, Cima MJ, Langer R. "*Application of micro- and nanoelectromechanical devices to drug delivery*". Pharm Res. 2006;**23**(5):847–63.
[174] Liong M, Lu J, Kovochich M, Xia T, Ruehm SG, Nel AE, Tamanoi F, Zink JI. "*Multifunctional Inorganic Nanoparticles for Imaging, Targeting, and Drug Delivery*". ACS Nano. 2008;**2**(5):889-96.
[175] Pernaut J-M, Reynolds JR. "*Use of Conducting Electroactive Polymers for Drug Delivery and Sensing of Bioactive Molecules. A Redox Chemistry Approach*". The Journal of Physical Chemistry B. 2000;**104**(17):4080-90.
[176] Zhang L, Xia J, Zhao Q, Liu L, Zhang Z. "*Functional Graphene Oxide as a Nanocarrier for Controlled Loading and Targeted Delivery of Mixed Anticancer Drugs*". Small. 2010;**6**(4):537-44.
[177] Thompson BC, Moulton SE, Ding J, Richardson R, Cameron A, O'Leary S, Wallace GG, Clark GM. "*Optimising the incorporation and release of a neurotrophic factor using conducting polypyrrole*". Journal of Controlled Release. 2006;**116**(3):285-94.
[178] Stevenson G, Moulton SE, Innis PC, Wallace GG. "*Polyterthiophene as an electrostimulated controlled drug release material of therapeutic levels of dexamethasone*". Synthetic Metals. 2010;**160**(9-10):1107-14.
[179] Abidian MR, Kim DH, Martin DC. "*Conducting-Polymer Nanotubes for Controlled Drug Release*". Advanced Materials. 2006;**18**(4):405-9.
[180] George PM, LaVan DA, Burdick JA, Chen CY, Liang E, Langer R. "*Electrically Controlled Drug Delivery from Biotin-Doped Conductive Polypyrrole*". Advanced Materials. 2006;**18**(5):577-81.
[181] Miller LL, Zinger B, Zhou QX. "*Electrically controlled release of hexacyanoferrate(4-) from polypyrrole*". Journal of the American Chemical Society. 1987;**109**(8):2267-72.
[182] Svirskis D, Wright BE, Travas-Sejdic J, Rodgers A, Garg S. "*Development of a Controlled Release System for Risperidone Using Polypyrrole: Mechanistic Studies*". Electroanalysis. 2010;**22**(4):439-44.
[183] Hepel M, Mahdavi F. "*Application of the Electrochemical Quartz Crystal Microbalance for Electrochemically Controlled Binding and Release of Chlorpromazine from Conductive Polymer Matrix*". Microchemical Journal. 1997;**56**(1):54-64.
[184] Li Y, Neoh KG, Kang ET. "*Controlled release of heparin from polypyrrole-poly(vinyl alcohol) assembly by electrical stimulation*". Journal of Biomedical Materials Research Part A. 2005;**73A**(2):171-81.
[185] Weng B, Liu X, Higgins MJ, Shepherd R, Wallace G. "*Printing: Fabrication and Characterization of Cytocompatible Polypyrrole Films Inkjet Printed from Nanoformulations Cytocompatible, Inkjet-Printed Polypyrrole Films (Small 24/2011)*". Small. 2011;**7**(24):3401-.
[186] Stevens MM, George JH. "*Exploring and Engineering the Cell Surface Interface*". Science. 2005;**310**(5751):1135-8.
[187] Geng X, Kwon O-H, Jang J. "*Electrospinning of chitosan dissolved in concentrated acetic acid solution*". Biomaterials. 2005;**26**(27):5427-32.
[188] Chengyu Xu RI, Masaya Kotaki, and Seeram Ramakrishna. "*Electrospun Nanofiber Fabrication as Synthetic Extracellular Matrix and Its Potential for Vascular Tissue Engineering*". Tissue Engineering. 2004;**10**(7-8):1160-8.

[189] Ghasemi-Mobarakeh L, Prabhakaran MP, Morshed M, Nasr-Esfahani MH, Ramakrishna S. "*Electrical Stimulation of Nerve Cells Using Conductive Nanofibrous Scaffolds for Nerve Tissue Engineering* ". Tissue Engineering Part A 2009;**15**(11):3605-19.
[190] Kam NWS, Jan E, Kotov NA. "*Electrical Stimulation of Neural Stem Cells Mediated by Humanized Carbon Nanotube Composite Made with Extracellular Matrix Protein*". Nano Letters. 2008;**9**(1):273-8.
[191] Sanghvi AB, Miller KPH, Belcher AM, Schmidt CE. "*Biomaterials functionalization using a novel peptide that selectively binds to a conducting polymer*". Nat Mater. 2005;**4**(6):496-502.
[192] Shi G, Rouabhia M, Wang Z, Dao LH, Zhang Z. "*A novel electrically conductive and biodegradable composite made of polypyrrole nanoparticles and polylactide*". Biomaterials. 2004;**25**(13):2477-88.
[193] Song HK, Toste B, Ahmann K, Hoffman-Kim D, Palmore GTR. "*Micropatterns of positive guidance cues anchored to polypyrrole doped with polyglutamic acid: A new platform for characterizing neurite extension in complex environments*". Biomaterials. 2006;**27**(3):473-84.
[194] Thompson BC, Richardson RT, Moulton SE, Evans AJ, O'Leary S, Clark GM, Wallace GG. "*Conducting polymers, dual neurotrophins and pulsed electrical stimulation -- Dramatic effects on neurite outgrowth*". J Control Release. 2010;**141**(2):161-7.
[195] Liu X, Chen J, Gilmore KJ, Higgins MJ, Liu Y, Wallace GG. "*Guidance of neurite outgrowth on aligned electrospun polypyrrole/poly(styrene-β-isobutylene-β-styrene) fiber platforms*". Journal of Biomedical Materials Research Part A. 2010;**94A**(4):1004-11.
[196] Lee JY, Bashur CA, Goldstein AS, Schmidt CE. "*Polypyrrole-coated electrospun PLGA nanofibers for neural tissue applications*". Biomaterials. 2009;**30**(26):4325-35.
[197] Abidian MR, Martin DC. "*Multifunctional Nanobiomaterials for Neural Interfaces*". Advanced Functional Materials. 2009;**19**(4):573-85.
[198] Yang J, Kim DH, Hendricks JL, Leach M, Northey R, Martin DC. "*Ordered surfactant-templated poly(3,4-ethylenedioxythiophene) (PEDOT) conducting polymer on microfabricated neural probes*". Acta Biomaterialia. 2005;**1**(1):125-36.
[199] Moulton SE, Higgins MJ, Kapsa RMI, Wallace GG. "*Organic Bionics: A New Dimension in Neural Communications*". Advanced Functional Materials. 2012;**22**(10):2003-14.
[200] Sayyar S, Murray E, Thompson BC, Gambhir S, Officer DL, Wallace GG. "*Covalently linked biocompatible graphene/polycaprolactone composites for tissue engineering*". Carbon. (0).
[201] Fan H, Wang L, Zhao K, Li N, Shi Z, Ge Z, Jin Z. "*Fabrication, Mechanical Properties, and Biocompatibility of Graphene-Reinforced Chitosan Composites*". Biomacromolecules. 2010;**11**(9):2345-51.
[202] Chen H, Müller MB, Gilmore KJ, Wallace GG, Li D. "*Mechanically Strong, Electrically Conductive, and Biocompatible Graphene Paper*". Advanced Materials. 2008;**20**(18):3557-61.
[203] Hartig M, Joos U, Wiesmann H-P. "*Capacitively coupled electric fields accelerate proliferation of osteoblast-like primary cells and increase bone extracellular matrix formation in vitro*". Eur Biophys J. 2000;**29**(7):499-506.
[204] Ahadian S, RamÃ³n-AzcÃ³n J, Estili M, Liang X, Ostrovidov S, Shiku H, Ramalingam M, Nakajima K, Sakka Y, Bae H, Matsue T, Khademhosseini A.

"*Hybrid hydrogels containing vertically aligned carbon nanotubes with anisotropic electrical conductivity for muscle myofiber fabrication*". Sci Rep. 2014;**4**.
[205] Kai D, Prabhakaran MP, Jin G, Ramakrishna S. "*Biocompatibility evaluation of electrically conductive nanofibrous scaffolds for cardiac tissue engineering*". Journal of Materials Chemistry B. 2013;**1**(17):2305-14.

2 FABRICATION OF MULTIFUNCTIONAL CONDUCTING POYMERIC FIBRES AND THEIR POSSIBLE APPLICATION IN CONTROLLED RELEASE OF DRUG

The results of this chapter have been published as a full paper in the Journal of Controlled Release:

Esrafilzadeh D, Razal M. J., Moulton E. S., Stewart M. E., Wallace G. G., "Multifunctional conducting fibres with electrically controlled release of ciprofloxacin", *Journal of Controlled Release*, Vol. 169, No.3, pp. 313–320, 2013.

2.1 Introduction

The fabrication of conducting biomaterials for different applications such as neuroprosthetic electrode has been investigated [1, 2]. This kind of electrode is capable of electrical stimulation of cells as well as recording cells signals. The electrode can be fabricated in the form of different architectures and geometry including pads, cuffs or longitudinal intra-fascicular electrodes [1, 3-5].

Some of the critical factors for the application of these structures *in vivo* include their biocompatibility, stable conductivity, low impedance, appropriate mechanical properties and flexibility [3]. The risk of infection and inflammatory complication after electrode implantation [4] raised the idea of incorporating anti-inflammatory or antibiotic drugs during bio-electrode development [6].

There is a wide range of drug delivery formulations such as polymeric structures that are capable of responding to external stimuli including thermal transition [7, 8], pH [9, 10] or electrical stimuli [11], and result in holding or releasing of biological components. Controlled drug release by electrical stimulation is becoming an attractive option in the treatment of acute disease or chronic illness as it has the ability to tune the release profile based on the stimulation conditions employed [12, 13].

Inherently conducting polymers (ICPs) are a type of organic conductors that has been investigated for use in conducting bio-structures. ICPs in conjunction with biopolymers simultaneously introduce conductivity and biocompatibility into bioelectrodes. These structures are capable of recording neural cells activity [14] as

well as responding to electrical stimulation to release therapeutic components [15, 16]. One of the advantages of conducting polymers in comparison to metals as a substrate for biomedical applications is their lower electrochemical impedance [2]. This helps to hold or release appropriately sized biomolecule/drug, which leads to controlled release via electrical stimulation with higher efficiency. Previously, controlled release of dexamethasone (DEX) has been carried out using Poly (3,4-ethylenedioxythiophene) PEDOT and applied for neural recording [17]. In addition, the release of the neurotrophin NT-3 from a polypyrrole film has been reported by Wallace *et al.* [18-20]. The incorporation and release of different types of antibiotics and anti-inflammatory drugs such as penicillin, streptomycin and dexamethasone have also been applied to polypyrrole matrixes [21]. The incorporation of ICPs in biopolymers has currently been limited to 2-dimensional films either in metal supported or coated films. Moreover, some drawbacks relating to applications of ICPs films include their brittleness, firmness, need for structural support and competent charge carrier (i.e. gold mylar), and their delamination from the support substrate during redox processes. Each of these parameters could influence the quality of films during drug delivery processes [5, 22].

Efforts for the fabrication of ICPs in 3-dimensional structures have been performed to introduce more flexibility as well as self-support capabilities for the structures [22]. Among different fabrication methods, wet-spinning is one method capable of producing 3-dimensional, flexible architectures for bionic applications. Recently, highly conducting PEDOT:PSS fibres produced by a wet-spinning method have been shown to possess stable electrochemical properties [23]. Doped polypyrrole has also been fabricated by a wet-spinning method into conducting micro-scale fibres with

appropriate electrochemical and mechanical properties [24]. To the best of our knowledge, ICP micro-scale fibres have not previously been applied for drug delivery systems.

This chapter presents a novel method to produce coaxial ICP fibres wherein electrically controlled release of the antibiotic ciprofloxacin hydrochloride is achievable. Firstly, PEDOT:PSS-chitosan hybrid fibres were fabricated employing an ionic complexation fibre spinning strategy involving the coagulation of PEDOT:PSS using chitosan as the coagulant. Ciprofloxacin hydrochloride (antibiotic drug) was selected as a drug model. The hybrid fibre was subsequently used as a working electrode for the electropolymerisation of a ciprofloxacin hydrochloride doped Ppy layer (Ppy.Cipro). The PEDOT:PSS-chitosan acts as structural support and electronic conductor to electrochemically switch the Ppy.Cipro layer between reduced and oxidised states to controllably release (or retain) Cipro. The bioactivity of wet-spun fibres and the released antibiotic drug (Cipro) were evaluated *in vitro.* Furthermore, the cytotoxicity of the fibres and their components was tested against B35 neuroblastoma cell lines.

2.2 Experimental

2.2.1 Wet-spinning of PEDOT:PSS-CHI fibres

Poly (3,4-ethylenedioxythiophene) poly(styrene sulfonate) (PEDOT:PSS) pellets were obtained from Agfa (Orgacon dry, Lot A6 0000 AC). A spinning solution of 25 mg/ml in water was prepared by dispersing the required amount of PEDOT:PSS pellets in water followed by homogenizing at 10,000 rpm for 10 min [23]. PEDOT:PSS dispersion was loaded into a syringe with a detachable needle (20 gauge) as the spinneret. The feeding ratio applied for wet-spinning was 15 ml/hr using a syringe pump (KDS-Scientific 100). A concentration of 1.0 wt. % chitosan (CHI) was dissolved in 2.0 wt. % acetic acid to prepare the coagulation bath. In order to perform wet-spinning, PEDOT:PSS was injected into the chitosan coagulation bath to form gel-state fibres as a result of ionic cross-linking between chitosan and PSS. Then fibres were passed through an ethanol-washing bath before collecting on a spool. Oven dried PEDOT:PSS-CHI fibres were post-treated via ethylene glycol (EG) followed by heat treatment in 120 °C for 30 min to enhance fibre conductivity [25].

2.2.2 Electrical and electrochemical characterisations

The electrochemical properties of PEDOT:PSS-CHI, PEDOT:PSS-CHI-Ppy.Cipro films (control) and fibres have been investigated using cyclic voltammetry (CV) and electrochemical impedance spectroscopy (EIS). The conductivity of fibres was measured using a linear four-point probe conductivity cell with uniform 2.3 mm spacing between probes. A galvanostat current source (Princeton Applied research Model ED402) and digital multimeter (HP Agilent 34401A) were used to obtain the conductivity (under laboratory humidity and temperature conditions).

Cyclic voltammetry of the fibres was performed in a 3-electrode cell, using a potentiostat source (Princeton Applied research Model ED402) with EChem version 1.5 software. The electrochemical impedance spectroscopy (EIS) was carried out in a two-electrode cell in phosphate buffered saline (PBS) electrolyte using a Gamry Instruments Framework (V.5.5).

2.2.3 Scanning electron microscopy

Physical characterisations of the fibres were performed using scanning electron microscopy (FESEM) (JEOL JSM-7500FA). Samples for cross-section imaging were prepared by breaking a frozen fibre, after dipping into liquid nitrogen, to observe fibre morphology. The chemical elements present in the surface and cross-section of PEDOT:PSS-CHI and PEDOT:PSS-CHI-Ppy.Cipro fibres were investigated using energy-dispersive x-ray spectroscopy (EDX), and the presence of sulphur (PEDOT:PSS) was traced to determine the component of fibres.

2.2.4 Elemental analysis of fibres

In order to determine the mass ratio between PEDOT:PSS and chitosan in the fibres, elemental analysis for nitrogen (N) and sulphur (S) was performed using an automatic analyser (Carlo Erba 1106) technique at the Australian National University (ANU, Canberra). In this case, four different samples were examined including dry PEDOT:PSS powder, dry chitosan powder, a PEDOT:PSS-CHI film prepared by blending solutions of PEDOT:PSS with chitosan (1.0 wt. %) at a ratio of 9:1, and PEDOT:PSS-CHI fibres.

2.2.5 Synthesis of Ppy.Cipro layer on the surface of PEDOT:PSS-CHI fibres

The synthesis of Ppy.Cipro was performed galvanostatically in a glass vial using a platinum mesh (counter electrode), an Ag/AgCl reference electrode and a gold-coated substrate as the working electrode [26]. The polymerisation solution contained 0.2 M pyrrole monomer and 50 mM ciprofloxacin hydrochloride as a dopant that was selected according to the previous monomer and dopant selection carried out in our group [18-20]. A potentiostat (Princeton Applied research Model ED 402) with EChem version 1.5 software was utilised for electropolymerisation. All current densities were normalised by geometric surface area of the working electrode. All films grown on gold mylar were washed in Milli-Q water for 5 min after electropolymerisation to remove any unincorporated dopant on the surface of fibres.

Different current densities (0.5, 1.0 and 2.0 mA/cm^2) and polymerisation times (30 sec, 10 and 20 min) were utilised for Ppy.Cipro growth.

2.2.6 Mechanical property testing

The tensile properties of the fibres were measured using a Shimadzu EZ-S tensile tester at a strain rate of 0.5 %/min. Samples were mounted on aperture cards (1.0 cm length window) with commercial super glue and allowed to air dry. Young's modulus, tensile strength and breaking strain were obtained and the mean and standard deviation calculated for n = 10.

2.2.7 *In vitro* ciprofloxacin release study

The profile of ciprofloxacin release from wet-spun fibres was determined by collection of Cipro aliquots in PBS at different time points (0-72 hr) in different redox states (reduced, passive & oxidised) of the Ppy.Cipro layer using a 3-electrode cell set-up. Ciprofloxacin is an antibiotic from fluoroquinolone class that are effective against broad range of bacteria (gram-negative and gram-positive). It is not electroactive in the range of potential that electrical stimulation applies in our experiments set-up for controlled drug release. It is negatively charge in aqueous solution and performs as a counter ion over electrochemically polymerisation of Ppy. The release medium was collected by micropipette at specific time points and replaced with the same volume of fresh PBS solution. To be able to calculate the percentage of released drug, known concentrations of Cipro in PBS (0.01 μg/ml to 8 mg/ml) were prepared and the absorbance of Cipro at its λmax 270 nm (by UV.Vis spectroscopy) was used to form a calibration curve. The UV-Vis spectra of PBS solutions were recorded between 200 nm and 300 nm using a Shimadzu UV 1601 spectrophotometer in order to construct the absorbance/concentration calibration curve. The release potential conditions were selected according to the cyclic voltammogram of the PEDOT:PSS-CHI-Ppy.Cipro fibre (Figure 2.9). In order to reduce and oxidise the conducting polymer (Ppy), constant potentials of -0.26 V and +0.3 V were used, respectively.

The loading efficiency of Cipro per 1.0 cm length of fibre was estimated by dissolving 1 cm length of fibre in PBS solution. The drug loaded fibre was bath sonicated for 5 days until the fibre completely dissolved and the Ppy.Cipro coating broke down, then the solution was filtered and the Cipro concentration was obtained by UV-Vis spectroscopy. To monitor the effect of sonication on the absorption

properties of Cipro, control solutions of known concentrations of Cipro in PBS were treated under the same conditions as the fibres. All cumulative Cipro release data are plotted as a percentage of (M_t) release relative to the Cipro loading (M_{tot}). Cipro release was investigated under passive diffusion and electrical stimulation conditions in two different patterns. In the first one, constant potential (reduced or oxidised) was applied to fibres during 72 hr whilst, in the second pattern, an alternating potential was applied by switching between reduced and oxidised potentials every 24 hr for 72 hr. For electrically stimulated release, a platinum mesh and Ag/AgCl electrode were utilised as the counter electrode and the reference electrode, respectively, while the PEDOT:PSS-CHI-Ppy.Cipro fibre was the working electrode. The release solution was gently stirred at constant speed (50 rpm) during the release experiments to assist diffusion of Cipro from the surface of the fibres. Fibres with consistent lengths (1 cm in PBS) and thicknesses (diameter of PEDOT:PSS-CHI fibres was 65 ± 7 μm with 1.3± 0.3 μm thickness of Ppy.Cipro layer) were selected for testing.

2.2.8 Antibacterial activity of released ciprofloxacin

The activity of the Ciprofloxacin hydrochloride released from the fibres was tested against both Gram-negative *Escherichia coli* (JM109) and Gram-positive *Streptococcus pyogenes* (NS5448). Bacterial lawns were prepared by firstly inoculating 5 ml of Luria-Bertani (LB) medium or Todd Hewitt (TH) broth with *E. coli* or *S. pyogenes* respectively for overnight incubation at 37 °C. This culture was then used to inoculate a 10 ml culture, which was grown to mid-log phase (OD_{600} 0.6-0.8; determined using an Ultrospec10 spectrophotometer). This culture was then diluted 1/5 in sterile 0.9 % (w/v) NaCl in Milli-Q, and 200 μl of this suspension was

spread onto LB or TH agar plates. The bacterial suspension was air dried prior to application of either fibres or discs.

Following fibre production, dried fibres were prepared in 1.0 cm lengths for antibacterial testing. To test the efficacy of Cipro released from fibres, lengths were carefully placed onto the surface of the prepared plates which were then inverted and incubated at 37 °C overnight prior to examination. Both PEDOT:PSS-CHI and PEDOT:PSS-CHI-Ppy.Cl fibres were tested as controls to ensure no antibacterial activity was exhibited by other components of the fibres. The bioactivity of Cipro released from the fibres either passively or under electrical stimulation was also tested. The fibres were placed in 500 μL PBS for 72 hr. Release samples were then loaded onto sterile 6 mm discs of Whatman No.1 filter paper and allowed to air dry at room temperature. The loaded discs were then carefully placed onto prepared bacterial plates. Discs placed on *E. coli* lawns were loaded with 10 μl of release media, and discs placed on *S. pyogenes* lawns were loaded with 20 μl of release media to account for the different susceptibilities of the bacterial strains to Cipro. Control discs were also prepared by preloading with 1 μg of ciprofloxacin hydrochloride for efficacy comparisons.

2.2.9 Cytotoxicity testing

The cytotoxicity of PEDOT:PSS-CHI, PEDOT:PSS-CHI-Ppy.Cl and PEDOT:PSS-CHI-Ppy.Cipro fibres were tested against a B35 neuroblastoma cell line (ATCC) as an available neural cell line in our laboratory. Cells were cultured in DMEM medium supplemented with 10 % (v/v) fetal bovine serum (FBS, Invitrogen). The fibres were aligned on glass slide substrates and an 8-well cell culture chamber was glued onto

the substrate to immobilise the fibres at the substrate surface. The fibre surfaces were sterilised by rinsing in 70 % (v/v) ethanol followed by air-drying. The fibres in each well were coated with Type IV rat tail collagen by exposing the surface to 50 µg/ml collagen prepared in 0.02 % acetic acid solution for 1 hr at room temperature. Each well was then rinsed twice in serum free medium prior to cell seeding at a density of 10,000 cells/cm^2. Cells were incubated at 37 °C in a humidified 5 % CO_2 environment for 72 hr prior to staining and imaging. Cells were stained for metabolic activity by the addition of Calcein AM (Invitrogen) to a final concentration of 1 µg/ml in cell culture media, followed by incubation as above for 15 min. Propidium iodide (Invitrogen) was then added to a final concentration of 1 µg/ml and the cells incubated for 5.0 min at room temperature. The medium was then gently removed and replaced with fresh PBS prior to imaging with an AxioImager fitted with a Mrm AxioCam, and images were overlayed using AxioVision Software (Zeiss). An LDH release assay was also performed to determine the IC50 for Cipro against B35 cells. B35 cells were seeded at a density of 5,000 cells/well into a 96 well plate. Following 24 hr incubation as described above, cell media were replaced with complete media containing a dilution series of Cipro starting at the highest concentration of 1.0 mg/ml. Following 48 hr incubation, cell media were collected and assayed for LDH activity using the CytoTox 96® Non-Radioactive Cytotoxicity Assay (Promega).

2.3 Results and discussion

2.3.1 Wet-spinning of PEDOT:PSS-Chitosan

Polyionic complexation coagulation strategy was utilised to wet-spin PEDOT:PSS fibres. PEDOT:PSS dispersion (25 mg/ml) was injected into a chitosan (CHI) coagulation bath. Based on the polyionic complexation coagulation strategy [27], the "free" negatively charged polystyrene sulphonate acid (PSS) groups of PEDOT:PSS react with the positively charged amino groups of chitosan to form a gel fibre. Different concentrations of CHI (from 0.5 to 2.0 wt. %) were tested as the coagulation bath. Table 2.1 shows the spinnability of the PEDOT:PSS dispersion as a function of chitosan coagulation bath concentrations. Results showed that PEDOT:PSS fibres could not be coagulated at CHI concentrations of less than 1.0 wt. %. The spinability of PEDOT:PSS fibres was improved significantly by increasing the concentration of CHI to 1.0 wt. %. However, as the concentration of CHI increased, increase in viscosity made the spinning harder until the concentration of 2.0 wt. %, which prevented the spinning of PEDOT:PSS fibres. Therefore, the minimum CHI concentration (1.0 wt. %) needed for effective spinning was chosen as the coagulation bath. This also can minimise the uptake of CHI (an insulator) via PEDOT:PSS during the coagulation process which may have less adverse effect on the conductivity of the resultant fibres.

Table 2.1**.** Comparision on spinability with respect to the concentration of the coagulation solution.

Chitosan conc. (wt.%)	**Feeding rate (ml/hr)**	**Spinability**
0.5	25	No
1.0	25	Yes
2.0	25	Yes

Following coagulation, the fibres were passed through an ethanol bath to remove excess chitosan, which remained un-reacted and only stuck on the surface of the fibres (Figure 2.1). This washing process was critical since the unreacted chitosan can form an insulating layer around the fibre, which is detrimental for both electrical and electrochemical properties of the final fibres. It is worth mentioning that, in contrast with solvent/non-solvent prepared PEDOT:PSS fibres [23], PEDOT:PSS-CHI fibres are insoluble and stable in aqueous media (pH ≃ 7.4) due to the presence of insoluble chitosan in pH ≃ 7.4 and polyionic complexation between positively charged chitosan and negatively charge PSS.

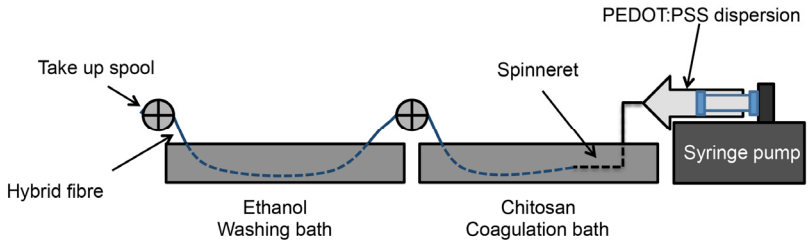

Figure 2.1. Schematic picture of wet-spinning process of PEDOT:PSS-CHI fibre.

2.3.2 Physical characterisation of PEDOT:PSS-CHI fibres

SEM micrographs of a representative PEDOT:PSS-CHI fibre and its cross-section are shown in Figure 2.2. The PEDOT:PSS-CHI fibre was dense and non-porous with a smooth surface and a circular cross-section (diameter = 65 ± 7 μm) upon drying under tension.

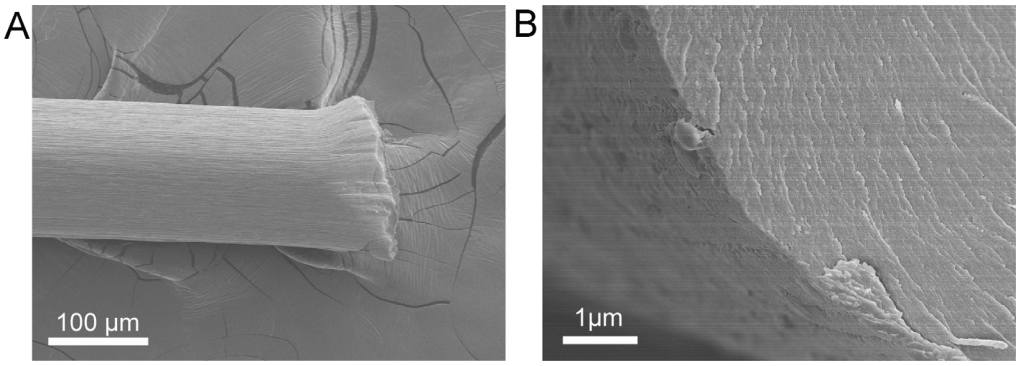

Figure 2.2. A) SEM images of PEDOT:PSS-CHI fibre, B) cross-section of fibre.

The scalability of this wet-spinning method was confirmed by spinning of continuous and long lengths of fibres. It is worth noting that PEDOT:PSS fibres which were spun by utilising solvent/non-solvent strategy (i.e. acetone or isopropanol) are soluble in PBS, the fluid which mimics the physiological body fluid in our *in vitro* tests [25]. However, the stability of chitosan in pH $\backsimeq$ 7.4 and the crosslink reaction between PSS and chitosan provide enough stability of PEDOT:PSS-CHI fibres in PBS which facilitates the following drug delivery and cell culture experiments.

The elemental composition of the fibres was evaluated using energy-dispersive X-ray (EDX) spectroscopy. The EDX spectrum showed sulphur peaks which confirmed the presence of PEDOT:PSS on the surface of the fibre. However, the cross-sectional EDX suggests a hybrid structure of PEDOT:PSS-CHI fibre (Figure 2.3).

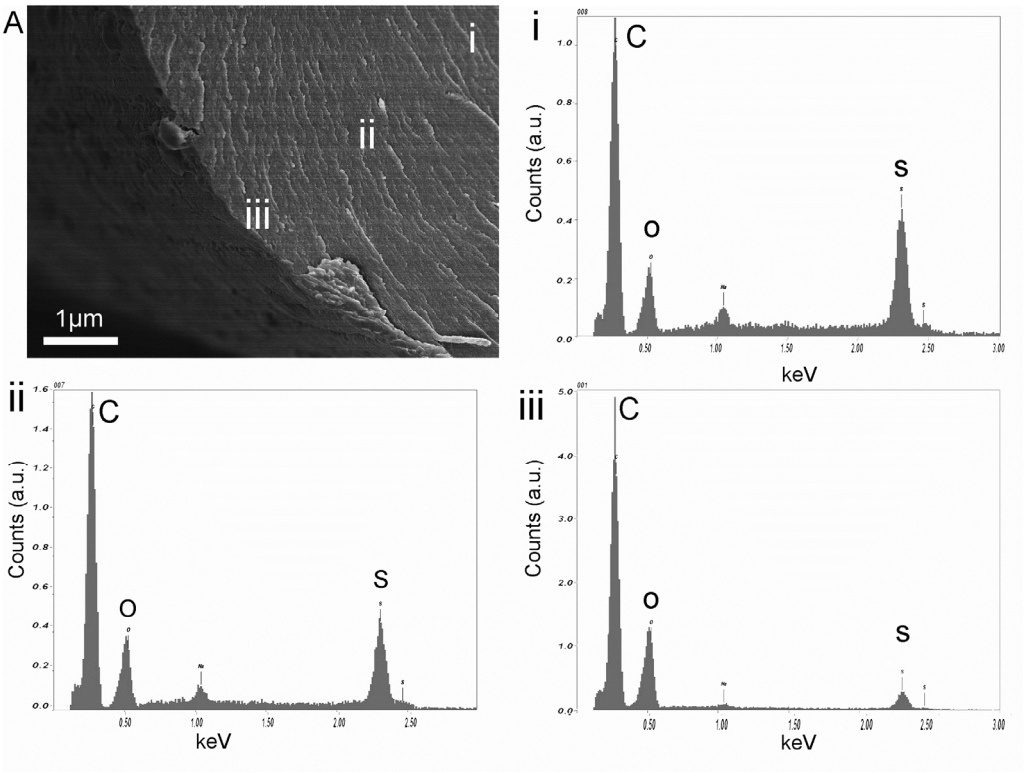

Figure 2.3. A) Scanning electron microscopy (SEM) images of the cross-section of PEDOT:PSS-CHI fibres. i, ii and iii) Energy-dispersive X-ray (EDX) spectrum recorded from the cross-section of PEDOT:PSS-CHI fibre.

Figure 2.3 shows sulphur peaks for all the three different selected spots on the cross section of the fibres. The results show sulphur peaks in both the surface and cross-section of the fibres, which suggests that PEDOT:PSS was present in all of the fibre's regions. In addition, the presence of sulphur on the surface of fibres (presence of PEDOT:PSS) provided surface conductivity. The surface conductivity of fibres is crucial to be utilised as a working electrode in a 3-electrode cell.

Elemental analysis was carried out to determine the overall percentages of PEDOT:PSS and chitosan in the dried fibre (base on the sulphur (S) and nitrogen content (N)). Table 2.2 shows the elemental analysis of different compositions of

PEDOT:PSS-CHI film and fibres and the calculated percentages of N and S. In order to calculate the percentage of PEDOT:PSS in the dried fibres, first the percentage of N and S that solely existed in CHI and PEDOT:PSS respectively were measured for control samples. Then, a known composition of both components was produced (90:10) and the amount of both S and N in this known composition determined. Finally, based on the percentage of nitrogen from chitosan and sulphur from PEDOT:PSS in the control samples (Table 2.2), a calibration curve was provided and was used to determine the ratio of chitosan to PEDOT:PSS in the fibres. The composition was calculated to be 3.2% to 96.7%, respectively. Such a low mass ratio of chitosan in the fibres is favourable as it would have a lower negative impact on the electrical conductivity of the hybrid fibre. The percentage of chitosan in the fibres is critical, as a lower amount of chitosan does not coagulate PEDOT:PSS and a higher proportion can adversely affect the conductivity.

Although, the spinning of fibres is the first step in the fabrication of 3-dimensional structures, the electrical and electrochemical properties of the as-spun fibres are much more important as the goal of using organic conductors is to utilise these properties in 3-dimensional architectures.

Table 2.2. Elemental analysis results of PEDOT:PSS-CHI fibres on the basis of nitrogen (N) and sulphur (S).

Sample	N%	S%
Chitosan Sheet	5.9±0.0	0.0±0.0
PEDOT:PSS Powder	0.0±0.0	16.1±0.5
PEDOT:PSS-CHI Sheet Ratio (90:10)	0.8±0.0	13.8±0.1
PEDOT:PSS-CHI fibre	3.2±0.0	96.7±0.0

2.3.3 Electrochemical characterisation of PEDOT:PSS-CHI fibres

The electrochemical behaviour of the fibres was investigated through cyclic voltammetry (CV) using PEDOT:PSS-CHI hybrid fibres as the working electrode in PBS buffer (Figure 2.4). In order to improve the electrical and electrochemical properties of the fibres, ethylene glycol (EG) treatment was carried out (see experimental section for more details). The conductivity of EG-treated fibres measured by the four-point probe method was 56 ± 7 S/cm. EG-treated fibres also exhibited well-defined electrochemical responses corresponding to oxidation (-0.3 V) and reduction (-0.5 V) of the PEDOT backbone (Figure 2.4). The improved electrochemistry after EG treatment is attributed to a change in the conducting polymer conformation from a compact coil to an extended coil configuration followed by phase separation between excess PSS and PEDOT [23].

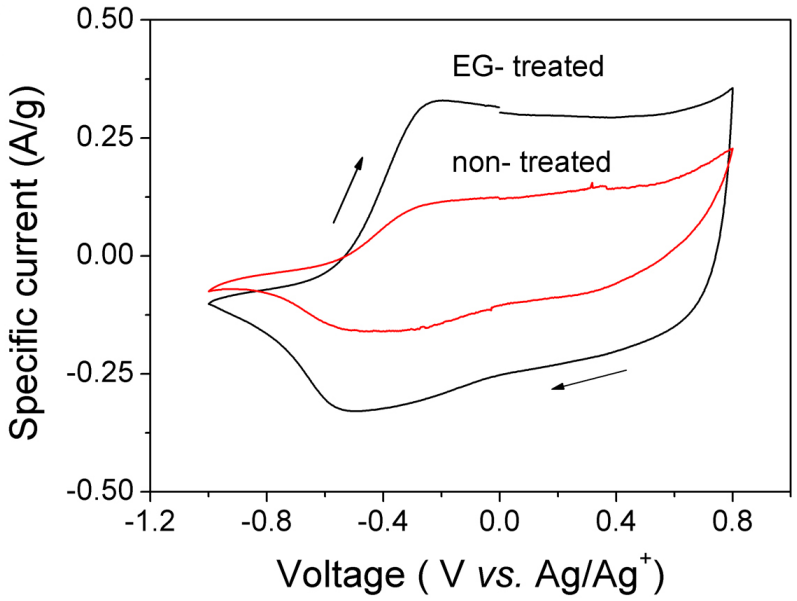

Figure 2.4. Cyclic voltammograms of PEDOT:PSS-CHI fibre in PBS (pH ~ 7.4) between -1.0 V and +0.8 V at scan rate of 50 mV/s (B). Arrows indicate the direction of potential scan.

The electrical and electrochemical properties of the EG-treated PEDOT:PSS-CHI fibres demonstrated high electrical conductivity and stable electrochemistry in aqueous media. Therefore, this fibre was chosen as a micro-dimensional electrode onto which a drug loaded polypyrrole (Ppy) conducting polymer was electrochemically polymerised.

Additionally, the stability of electrochemical performance of EG-treated PEDOT:PSS-CHI fibres is evidenced by negligible electrochemical changes after 100 cycles in PBS (Figure 2.5).

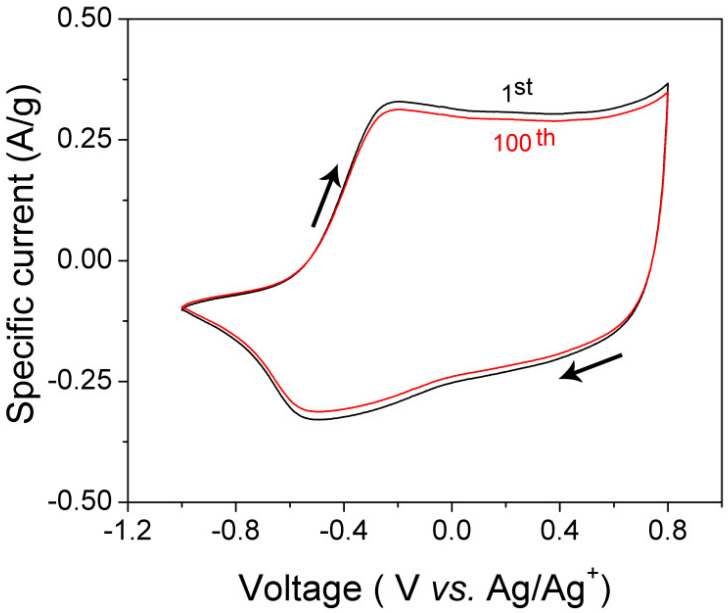

Figure 2.4. Cyclic voltammogram of PEDOT:PSS-CHI fibres before and after 100 cycles in PBS. The CV was performed in PBS (pH ~ 7.4) between -1.0 V and +0.8 V at a scan rate of 50 mV/s (B). Arrows indicate the direction of potential scan.

2.3.4 Electropolymerisation of Ppy.Cipro layer on PEDOT:PSS-CHI fibres

The drug selected was ciprofloxacin hydrochloride (Cipro) (Figure 2.5), a synthetic antibiotic of the fluoroquinolone drug class that covers a broad range of bacteria (Gram negative and Gram positive) [28].

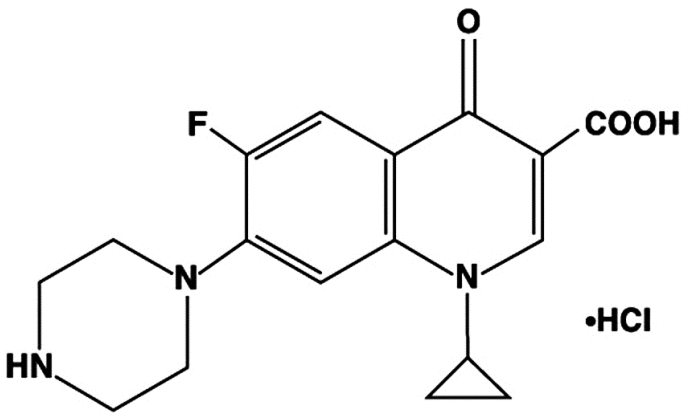

Figure 2.5. Chemical structure of ciprofloxacin hydrochloride.

There are several possible methods to incorporate drugs into the fibres. One way is to mix the drug with the PEDOT:PSS spinning solution. The other way is to add the drug via electropolymerisation of another layer of conducting polymer on the surface of fibres. The first method is facile, however the drug can be discharged inside the coagulation bath during wet-spinning resulting in negligible drug loading. However, the second method, which has been used to incorporate different molecules such as dyes or biological molecules such as drugs, growth factors, enzymes into the conducting polymer backbone [19, 29], does not lose the drug during the fabrication process. Therefore, ciprofloxacin incorporation using the polymerisation method was investigated. Polypyrrole (Ppy) is one of the conducting polymers which has been utilised for different biomedical applications including drug delivery. Vapour phase, chemical and electropolymerisation are different methods for Ppy synthesis, which have been introduced in Chapter 1 in detail. Electropolymerisation is a common synthesis procedure that has been used for more than a decade. Depending on the parameters selected for polymerisation, such as monomer and dopant concentrations, current density and time of polymerisation, the quality of the Ppy layer can be varied

from thin and bulky to thick and uniform layer. The polymerisation conditions applied in this work are based on previous research performed by Thompson *et al.* in our group [19].

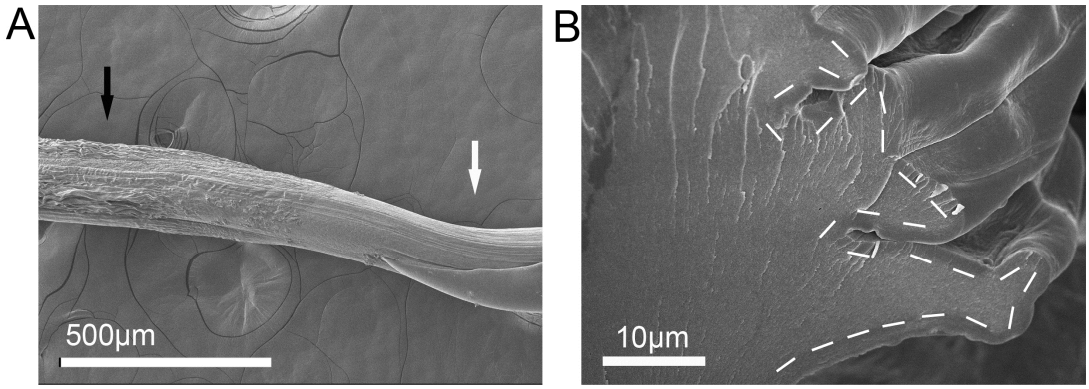

Figure 2.6. A) SEM images of PEDOT:PSS-CHI fibre after electropolymerisation of the Ppy.Cipro second layer (arrows show polymerised (black) and uncoated (white) ends). B) Cross-section of Ppy.Cipro end (the white dashed line is included to aid the reader in observing the Ppy.Cipro layer). The current density used to polymerise the Ppy.Cipro layer was 2 mA/cm^2 and the polymerisation time was 10 min.

The electropolymerisation was performed in a 3-electrode cell using PEDOT:PSS-CHI fibres as working electrode. By applying electric forces from an external potential source, pyrrole monomer was radicalised and initiated dimer and oligomer synthesis [29]. Over time, the oligomer chains grow longer and eventually polymer is synthesised. The difference in physical morphology of PEDOT:PSS-CHI fibre with and without Ppy.Cipro layer is clear in Figure 2.6-A. The black arrow indicates the end of the fibre which was exposed to the polymerisation solution, while the white arrow indicates another end of the fibre which was not immersed in the polymerisation solution. Figure 2.6-B illustrates the cross-section of PEDOT:PSS-

CHI-Ppy.Cipro that clearly shows the layer of Ppy.Cipro on the PEDOT:PSS-CHI fibre. Additionally, the presence of the Ppy layer on the fibres was confirmed by Raman spectra in the following sections.

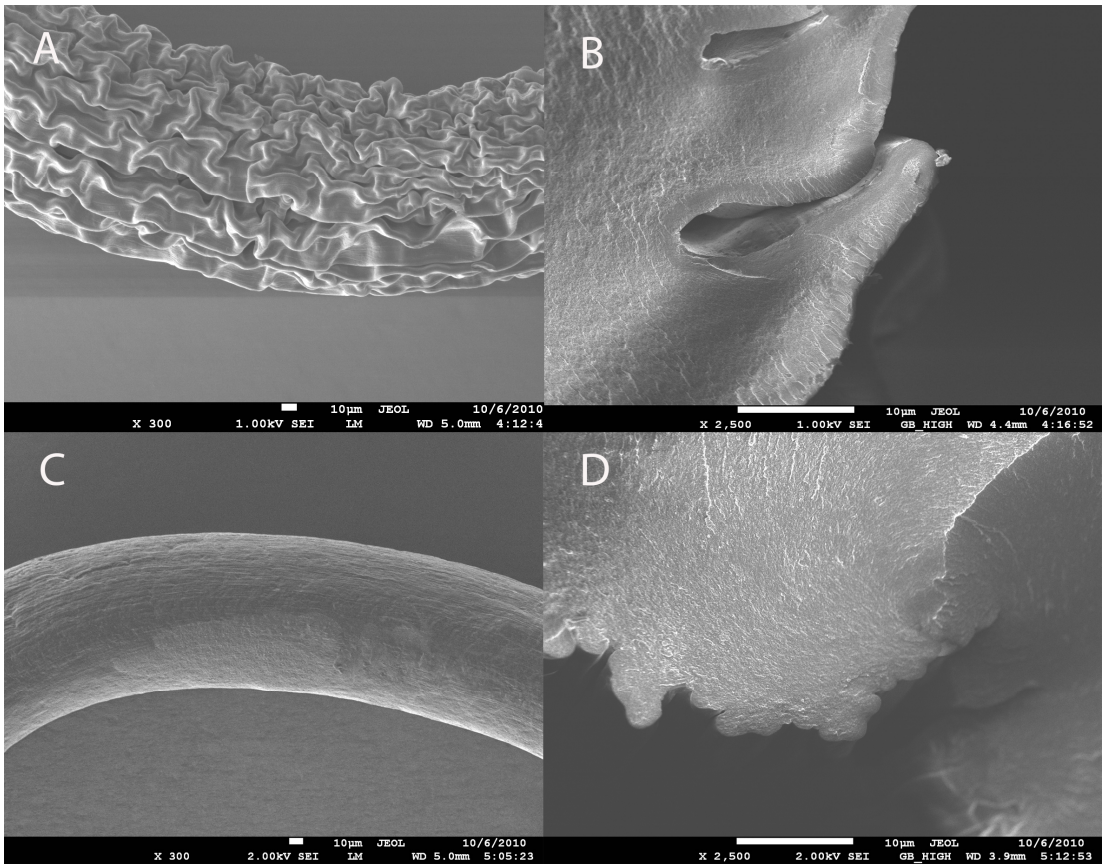

Figure 2.7. SEM images of PEDOT:PSS-CHI-Ppy.cipro prepared at different times of polymerisation. A and B) polymerisation time: 20 min, current density: 2.0 mA/cm^2. C and D) polymerisation time: 30 sec, current density: 2.0 mA/cm^2. B and D images are the cross-sections of A and C images respectively.

It was demonstrated that as current density and time of polymerisation increases, the thickness of Ppy.Cipro layer rises (Figure 2.7). This can be useful in alteration of drug loading in Ppy.Cipro layer. The polymerisation potentials (~ +0.2 to +0.5) observed were lower than potentials (+0.9 to +1.2) commonly observed for Ppy;

showing a safer region against overoxidation of polymer and synthesis of non-conducting layer eventually. Table 2.3 shows thicknesses of Ppy.Cipro layers and the oxidation potentials of polymerisation, obtained using SEM images and EDAQ data respectively, as functions of current density and polymerisation time. As the current density decreased the oxidation potential decreased and the thickness of the Ppy.Cipro decreased in a given polymerisation duration. It was also possible to increase the thickness of the Ppy.Cipro layer by increasing the polymerisation duration. However, the current density of 2.0 mA/cm^2 and polymerisation time of 10 min were used in this study and provided sufficient thickness of the polymer layer.

Table 2.3. Oxidation potential and thickness of Ppy.Cipro layer as a function of polymerisation conditions. The thickness was determined using SEM images.

Current density (mA/cm^2)	Polymerisation time (min)	Thickness of Ppy.Cipro layer (μm)	Oxidation potential (V)
2.0	20	1.9± 0.1	0.45
2.0	10	1.3± 0.3	0.45
2.0	0.5	NA	0.45
0.5	20	1.4± 0.1	0.33
0.5	10	0.5± 0.1	0.28
0.5	0.5	NA	0.28

2.3.5 Physical and electrochemical characterisations of PEDOT:PSS-CHI-Ppy.Cipro fibres

In order to confirm the presence of Ppy.Cipro on the surface of PEDOT:PSS-CHI fibres, Raman spectroscopy of fibres was carried out. The Raman characteristics of

PEDOT:PSS-CHI fibres with/out Ppy.Cipro layer were studied (Figure 2.8). For the PEDOT:PSS-CHI fibre, peaks were observed at 1530 1/cm (C=C stretching), 1426 1/cm (C=C stretching), 1366 1/cm (C-C stretching) and 1257 1/cm (C=C stretching) with these assignments based on reports by others [23]. The spectra of the PEDOT:PSS-CHI-Ppy.Cipro fibre and Ppy.Cipro film (control) presented strong sharp peaks in 1580 1/cm (C=C stretching), a double peak at 1320 and 1380 1/cm (ring stretching) and peaks at 927 and 1240 1/cm (C-H out of plane bending) indicative of the oxidised form of Ppy [29].

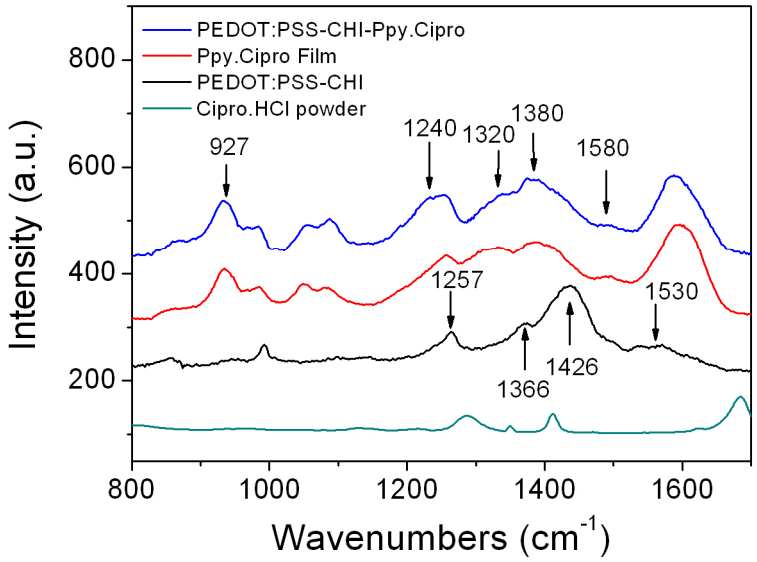

Figure 2.8. Raman spectra of Ppy.Cipro grown on PEDOT:PSS-CHI fibre.

Transformation of the Raman vibration properties from PEDOT:PSS to Ppy after electropolymerisation of the second layer confirms formation of the Ppy layer on the fibre substrate. However, changes in Raman spectra depend on the thickness of the Ppy layer and time of polymerisation since, after polymerisation of longer than 10 min, the Ppy.Cipro layer was thick enough to avoid penetration of the Raman laser into the PEDOT:PSS-CHI layer.

The electrochemical properties of the fibres are crucial when, the aim of the fibres fabrication is for application in the control of drug release via electrical stimulation. Electrochemical testing by CV of the PEDOT:PSS-CHI fibres (Figure 2.9-A) showed oxidation and reduction peaks at -0.3 V and -0.5 V, respectively. Upon Ppy.Cipro polymerisation, the oxidation and reduction peaks shifted to +0.2V (oxidation) and -0.1V (reduction) when a thick Ppy.Cipro layer was achieved (i.e. thickness of Ppy.Cipro: 1.3± 0.3 μm and polymerisation time: 10 min). This redox behaviour was similar to that of a Ppy.Cipro film grown on gold mylar in PBS [19], suggesting these redox peaks were due to the Ppy.Cipro polymer. The redox values are at potentials higher than the oxidation state of the PEDOT:PSS fibre core (-0.2V). This provides the possibility to switch between oxidised and reduced states for the Ppy.Cipro layer whilst, the PEDOT:PSS layer remains in its oxidised state (conducting state). This is very important as the PEDOT:PSS core can act as a conduit for charge delivery during different redox states of the drug loaded Ppy.Cipro outer layer.

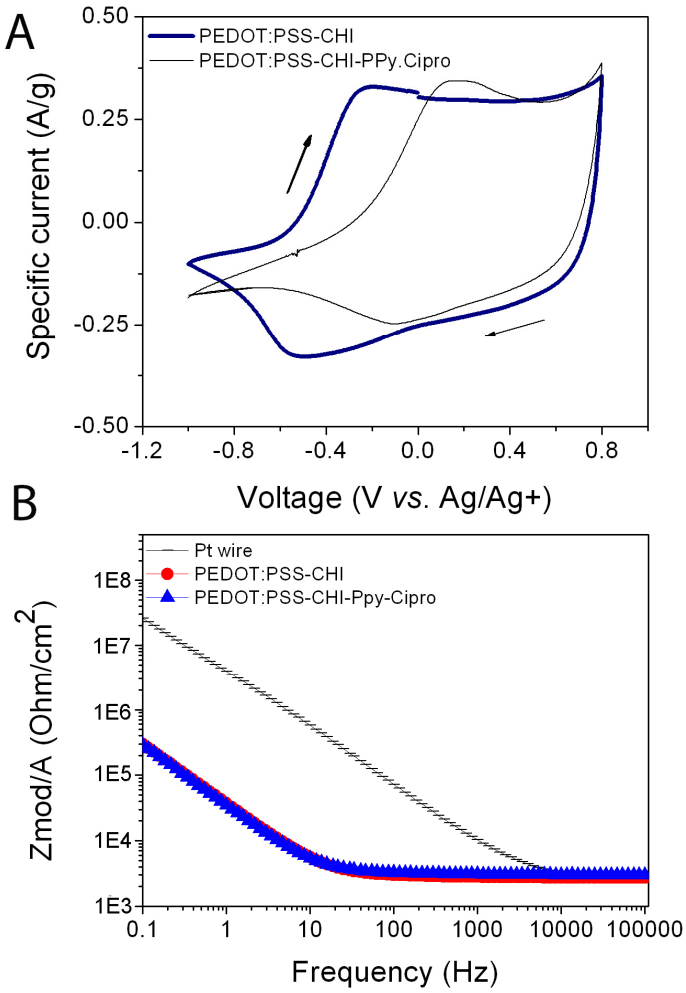

Figure 2.9. A) Cyclic voltammogram of PEDOT:PSS-CHI fibre in PBS (pH ≃ 7.4) scanned between -1.0 V and +0.8 V at a scan rate of 25 mV/s before and after electropolymerisation of Ppy.Cipro layer (current density: 2.0 mA/cm^2 and polymerisation time: 10 min). Arrows indicate the direction of potential scan. B) Electrochemical impedance spectroscopy of wet-spun fibres in comparison to a Pt wire in PBS.

Figure 2.9-B shows lower impedance of the PEDOT:PSS-CHI-Ppy.Cipro (~2.8 kΩ/cm^2) at 1.0 kHz (relevant frequency of biological activities [1, 17]) in comparison to platinum wire (~ 10.3 kΩ/cm^2). This improved impedance resulted

from facilitated penetration of ions over a much higher electroactive surface area compared to the Pt wire (as a common metal to use in neuroprosthetic electrode [1]) due to the gel-like nature of the hybrid fibre. Moreover, the impedance of fibres did not change after polymerisation of Ppy.Cipro.

The mechanical properties of PEDOT:PSS-CHI-Ppy.Cipro fibres were enhanced compared to their as-spun counterparts. Modulus, strength and breaking strain of PEDOT:PSS-CHI-Ppy.Cipro fibres, obtained from stress–strain curves, were calculated to be 2.9 ± 0.2 GPa, 128 ± 11 MPa, 30.5 ± 4%, respectively (Figure 2.10). The as-dried EG-treated PEDOT:PSS-CHI fibres displayed modulus, strength and breaking strain of 2.0 ± 0.3 GPa, 99 ± 7 MPa, 20.6 ± 1.2%, respectively.

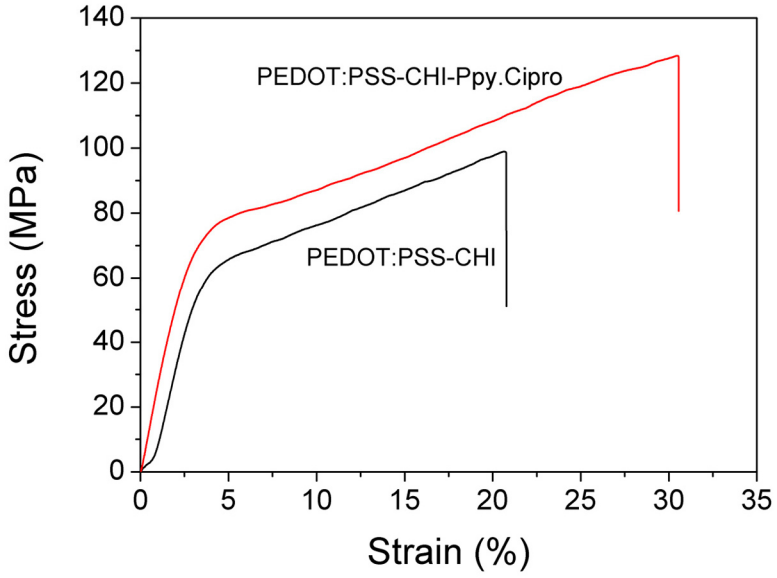

Figure 2.10. Stress–strain curves of PEDOT:PSS-CHI and PEDOT:PSS-CHI-Ppy.Cipro fibres.

3.3.3 Release profiles of ciprofloxacin hydrochloride

The release of Cipro from the Ppy.Cipro layer was performed under passive and electrical stimulation conditions in PBS (pH ≃ 7.4) at 37 ^{o}C in a 3-electrode cell. A

1.0 cm length of PEDOT:PSS-CHI-Ppy.Cipro fibre was placed in PBS with samples taken at various time intervals. Electrically stimulated release was performed under potentials that induced an oxidised (+0.3 V *vs* Ag/AgCl) and reduced (-0.26 V *vs* Ag/AgCl) state in the Ppy.Cipro layer. These potentials were chosen from the PEDOT:PSS-CHI-Ppy.Cipro CV shown in Figure 2.9-A.

The release measurements of Cipro have been carried out using UV.Vis spectroscopy and the calibration curve of Cipro was calculated on the basis on the UV.Vis spectra shown in Figure 2.11-A. As Figure 2.11-B demonstrates, there is no peak observed for the fibre components in the window of 200-300 nm, where the Cipro peak occurs.

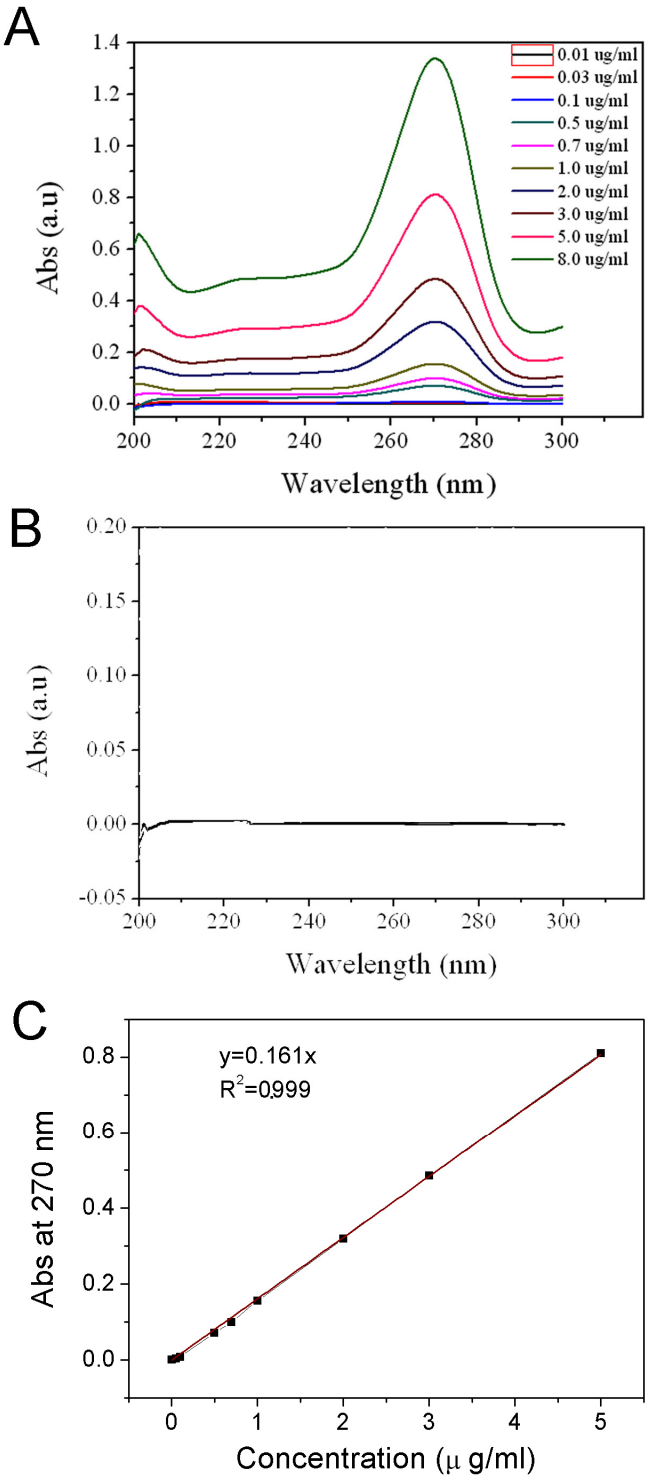

Figure 2.11. A) UV.Vis spectra of Cipro in PBS with different concentrations of Cipro, B) spectrum of fibre residual (dispersed fibre in PBS), C) calibration curve of Cipro at different concentrations.

The passive release of Cipro showed short-term release for the first 8.0 hr (Figure 2.13-B) followed by a plateau up to 72 hr (Figure 2.13-A). These results suggest that under passive conditions, Cipro release is dominated by diffusion of near-surface trapped Cipro. According to the Raman data (Figure 2.8) and the high electrical conductivity of the fibres, the Ppy.Cipro layer is in its conducting state; therefore Ppy tends to retain its dopant to balance the charge along the polymer backbone to maintain neutrality. As the interaction between dopant and polymer comes from electrostatic forces, passive Cipro release is predominantly the result of drug that is near the surface or loosely trapped within the layer.

The stimulated release profiles of Cipro from the Ppy.Cipro layer of the PEDOT:PSS-CHI-Ppy.Cipro fibre are shown in Figure 2.12-A. When the PEDOT:PSS-CHI-Ppy.Cipro fibre is electrically stimulated with constant potential, so that the Ppy.Cipro layer is in the oxidised state, the release profile is very similar to the passive release. The main difference is that in the oxidised state, the amount of Cipro release has decreased. When a reducing potential is applied to the PEDOT:PSS-CHI-Ppy.Cipro fibre, longer term sustained release up to 72 hr is observed with approximately two times higher concentration of released drug compared to the passive mode. The standard deviation of release amount is higher in reduced state compare to oxidised and passive states possibly due to the higher amount of drug which was released. However, the difference between Cipro amounts still is significant.

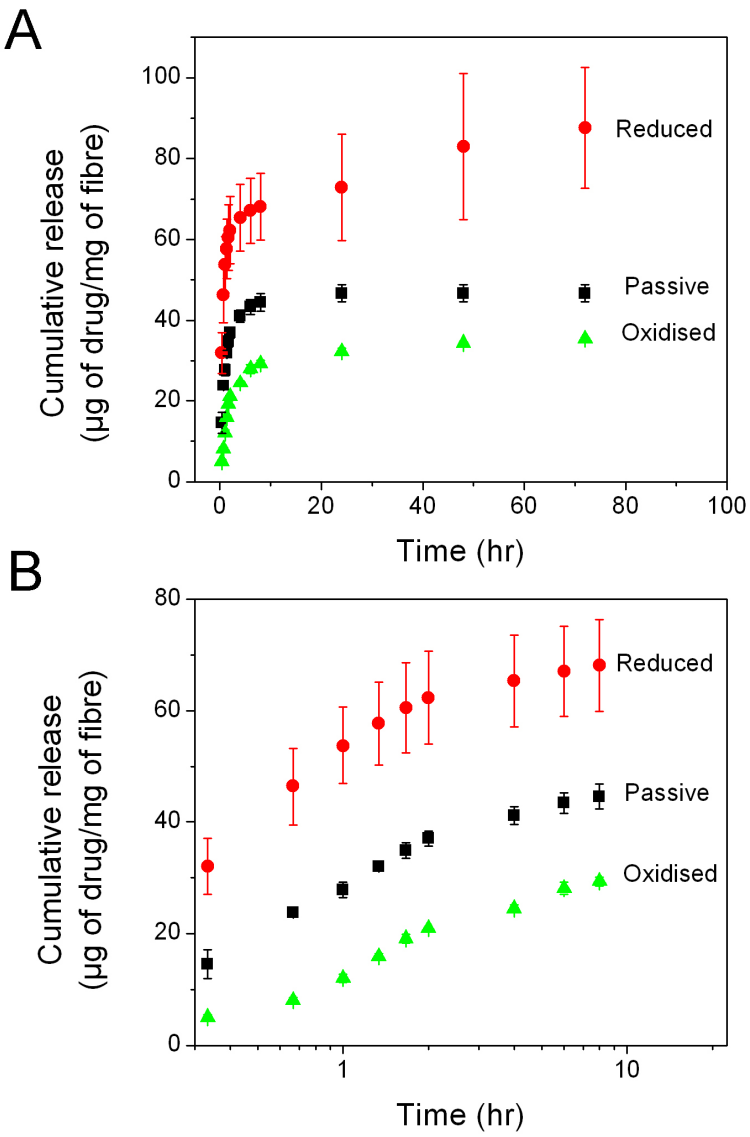

Figure 2.12. A) Cumulative release profile of Cipro in PBS from PEDOT:PSS-CHI-Ppy.Cipro fibres in different conducting states up to 72 hr. B) cumulative release profile of Cipro in PBS from first 20 min till 8.0 hr. The release experiments were carried out in PBS (pH ≃ 7.4) at 37 ^{o}C. Error bars indicate the standard error of the mean (n = 3).

During reduction of Ppy.Cipro, an excess negative charge is placed along the polymer backbone. Therefore, in order to balance this charge the polymer can either

release its negatively charged Cl^- dopant or incorporate cations from the media it is residing in. We have previously shown that Cl^- ions are very mobile and are readily expelled upon Ppy electrochemical reduction [30]. As the dopant is expelled, so is the drug that was physically entrapped during synthesis as reported before for NT-3 delivery [18]. It has previously been shown that the dopant plays an important role in determining the extent of release of the entrapped drug [31]. In the oxidised state around 20 % less Cipro is released in comparison to passive conditions over 72 hr. When the Ppy.Cipro is further oxidised, the polymer possesses a positive charge and therefore the Cl^- dopant is retained within the Ppy.Cipro layer. It is likely that the positive charge is balanced by uptake of negative ions from the PBS solution. However, it is clear that upon oxidation Cipro release is observed, albeit not to the same degree as when in the passive or reduced state. In addition, release experiments have also been carried out by switching the potential between the reduced and oxidised states of Ppy.Cipro, demonstrating the capability to tune the release profile of the conducting polymer fibres (Figure 2.13).

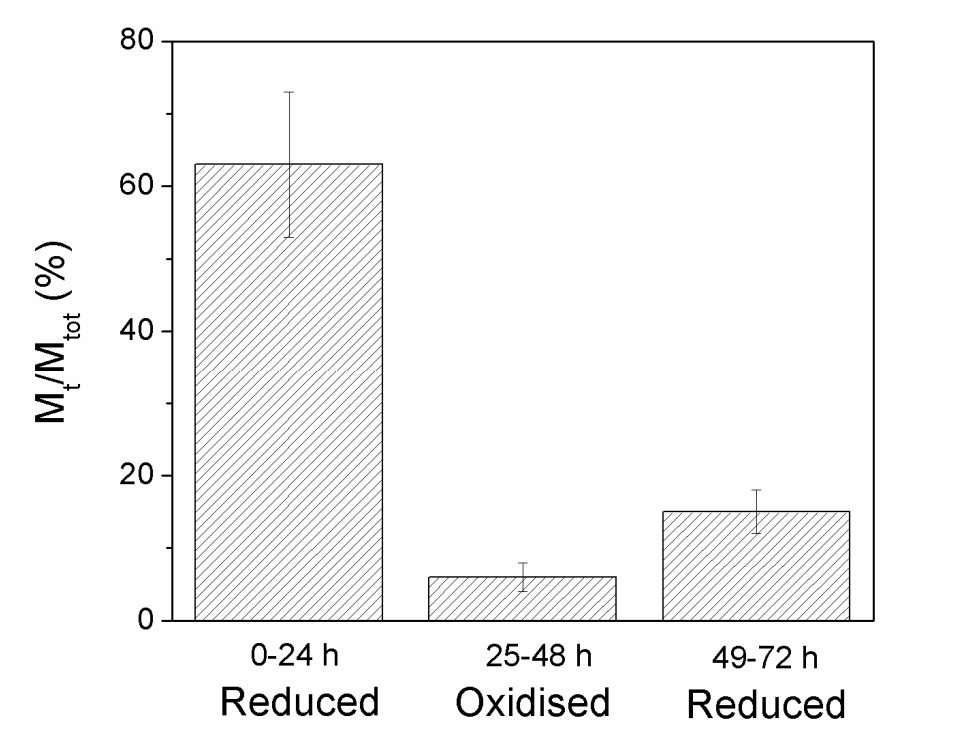

Figure 2.13. Percentage of drug amount (M_t) released relative to drug loading (M_{tot}) from fibres. The switchable drug release experiments were carried out in PBS (pH ≃ 7.4) at 37 ^oC. Error bars indicate the standard error of the mean (n = 3).

The control of release demonstrated here, based on charge application, highlights the versatility of our fibres for drug delivery systems for drugs with ionic charge on their structures. The mechanism for Cipro release is proposed to involve electrostatic interactions as the application of an electrical stimulation protocol varied the amount of Cipro release. However, both the ionic and hydrophobic properties of polypyrrole have been shown to vary upon application of electrical stimulus. The expansion and contraction (actuation) [29] of polypyrrole is also a well-documented property of polypyrrole upon oxidation and reduction, and these processes may be involved in the release of Cipro. As all of these properties change simultaneously it is not

possible to separate them to determine which process is the dominant factor driving this release.

2.3.6 *In vitro* antibacterial efficacy

The previous section clearly demonstrates that it is possible to incorporate and release Cipro from the fibres in a controlled manner. However, it is important to evaluate whether the Cipro maintains its antibacterial properties during the fabrication process. The formation of a zone of inhibition (ZOI) within a lawn of bacteria was used to evaluate the efficacy of released Ciprofloxacin. A ZOI represents inhibition of the growth of an organism within a designated zone corresponding to the presence of an active substance. In this study, the ZOI of Cipro was determined for representative Gram-positive and Gram-negative bacteria. Firstly, the drug loaded and control fibres were applied to lawns of each bacterial strain (Figure 2.14).

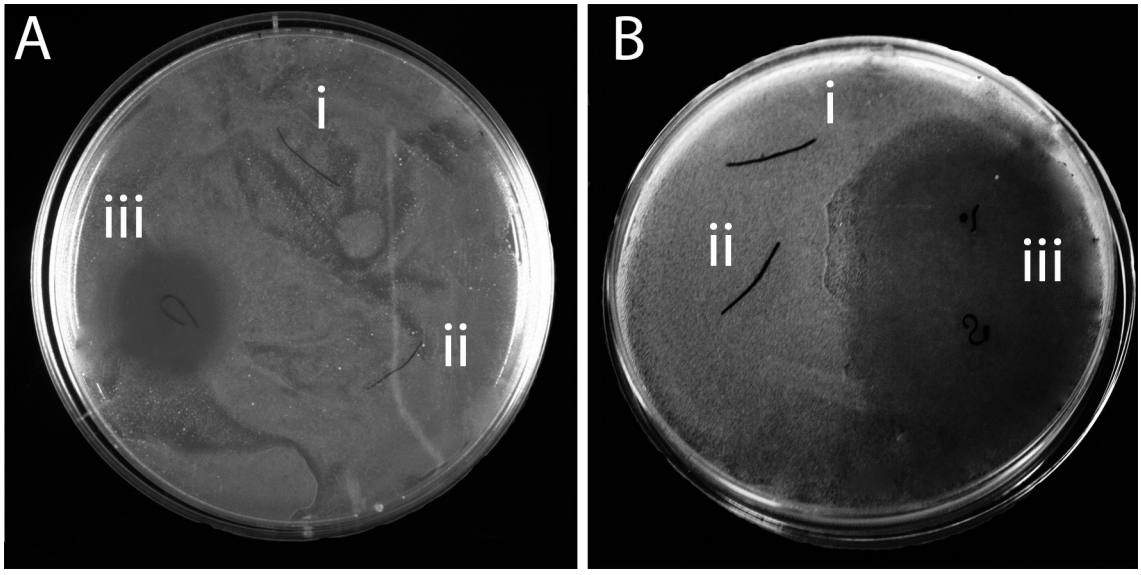

Figure 2.14. Zone of inhibition (ZOI) of three different fibres against A) *S. pyogenes*, B) *E.coli.* (i: PEDOT:PSS-CHI-Ppy.Cl), (ii: PEDOT:PSS-CHI) & (iii: PEDOT:PSS-CHI-Ppy.Cipro). Each sample was repeated 3 times.

A ZOI was observed surrounding the drug loaded fibres (Figure 2.14) placed on the lawns of each bacterial strain, but not surrounding the underlying PEDOT:PSS fibre, nor PEDOT:PSS-CHI-Ppy.Cl fibres. These results confirm that the inhibition of bacterial growth was solely due to the presence of ciprofloxacin in these fibres. The absence of a ZOI surrounding the control fibres (PEDOT:PSS-CHI and PEDOT:PSS-CHI-Ppy.Cl) shows that the components of these fibres do not display any antibacterial effect. The inhibition of bacterial growth indicates that the associated processing steps required to prepare these fibres do not adversely affect the bioactivity of the ciprofloxacin under passive release conditions. Moreover, the amount of drug loaded and subsequently released from the fibre under passive conditions was sufficient to diffuse through the agar media to affect bacterial growth. Secondly, the effect of the method of Cipro release from the fibres on its efficacy was investigated (Figure 2.15). Cipro-containing media collected after 72 hr of cumulative release was loaded onto bacterial lawns via paper discs. The release medium obtained following application of electrical stimulation, at both oxidising and reducing potential, resulted in maintained antibacterial activity, which indicates that electrical stimulation did not disrupt drug biological activity.

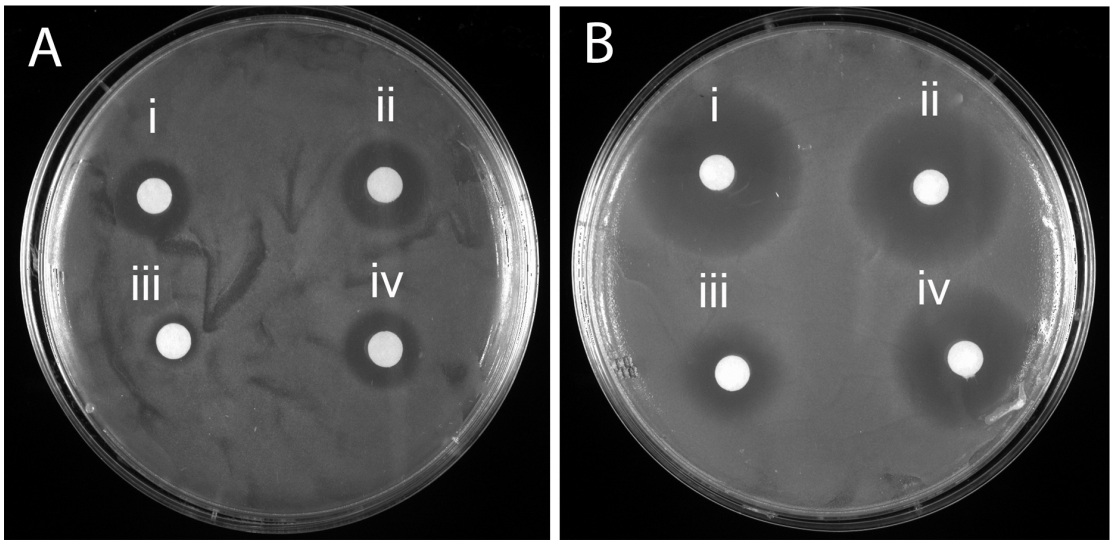

Figure 2.15. Zone of inhibition (ZOI) of three different drug release media after 72 hr cumulative release against A) *E. coli* and B) *S. pyogenes* strain. (i: 1.0 µg Cipro), (ii: drug release in reduced state), (iii: drug release in oxidised state), (iv: drug release in passive state). Each sample was repeated 3 times.

This study importantly confirms that Cipro maintains its bioactivity against both Gram-positive and Gram-negative bacteria during loading via electrochemical polymerisation and the subsequent electrically stimulated release. Moreover, zones of inhibition (ZOI) obtained using 72 hr cumulative release samples against *E. coli* and *S. pyogenes* correlated well with the trend of cumulative release profiles in passive, reduced and oxidised states of the fibres (Table 2.4). However, the zone of inhibition is not significantly different in reduced compared to passive state. This may be attributed to the fact that the amount of Cipro used on all paper discs was higher than the minimum effective Cipro dose that was required to kill the bacteria, therefore, causing a drug saturation effect in the culture.

Table 2.4. Zone of inhibition resulting from the application of volumes of release medium obtained under different conditions onto lawns of bacteria via paper discs. Averages of three independent experiments are shown with standard errors.

Samples	**M_t/M_{tot} (%)[a]**	**Zone of Inhibition (mm)**	
		E. coli	***S. pyogenes***
Reduced	88.0 ±14.0	26.6±0.9	14.3±0.3
Passive	47.1±1.2	27.3±0.3	14.0±1.0
Oxidised	36.5±0.5	22.7±2.8	12.0±1.2
1.0 µg	NA	31.3±0.6	15.0±0 0

[a.] The percentage of Cipro released was determined from the release profiles presented in Figure 2.13.

2.3.7 Cell growth studies

In order to utilise the fibres in biomedical applications, an understanding of their biocompatibility is critical due to the fact that toxicity of some materials is one of the obstacles in their applications to biological systems.

Previous studies have shown that a concentration less than 150 µg/ml ciprofloxacin hydrochloride had no adverse effect on proliferation and differentiation of a variety of cell types including primary cultures of astrocytes and primary fibroblast cell lines [32, 33]. The cytotoxicity of our fibres was tested in the presence of B35 neuroblastoma cells, chosen as a neural cell model due to the intended application of these fibres as neural recording/stimulation electrodes with controlled drug release. The presence of metabolically active cells in the presence of drug-loaded fibres was examined using Calcein AM, whereby the production of a green fluorescent product indicates living, viable cells. The acetomethoxy derivate of calcein (calcein AM) is a

common indicator in biology for cell viability tests since it can be transported through the cellular membrane into live cells. An acetomethoxy group conceals the part of the molecule that chelates Ca^{2+}, Mg^{2+}, Zn^{2+} and other ions. After transport into the cells, intracellular esterases eliminate the acetomethoxy group; the molecule gets trapped inside and gives out strong green fluorescence. As dead cells do not have active esterases, only live cells are labelled. In our experiments, a counter stain (propidium iodide) was also used to indicate the presence of membrane-compromised cells, indicated by red fluorescence. Following 72 hr incubation, the cells surrounding the fibres were observed to show green fluorescence indicating them to be metabolically active with minimal presence of membrane compromised cells (Figure 2.16-A, B and C). These results together indicate the cytocompatibility of our fibres.

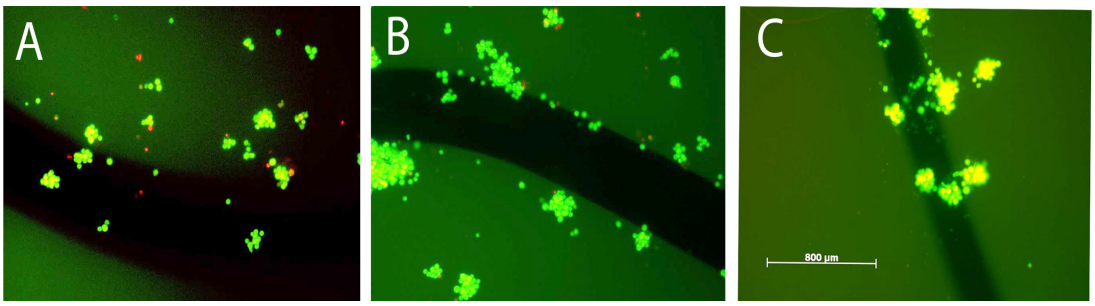

Figure 2.16. B35 neural cells cultured on A) PEDOT:PSS-CHI, B) PEDOT:PSS-CHI-Ppy.Cl, and C) PEDOT:PSS-CHI-Ppy.Cipro fibres over a period of 72 hr (scale bar 800 µm). Calcein AM/PI staining renders metabolically active and membrane compromised cells bright fluorescent green and red respectively.

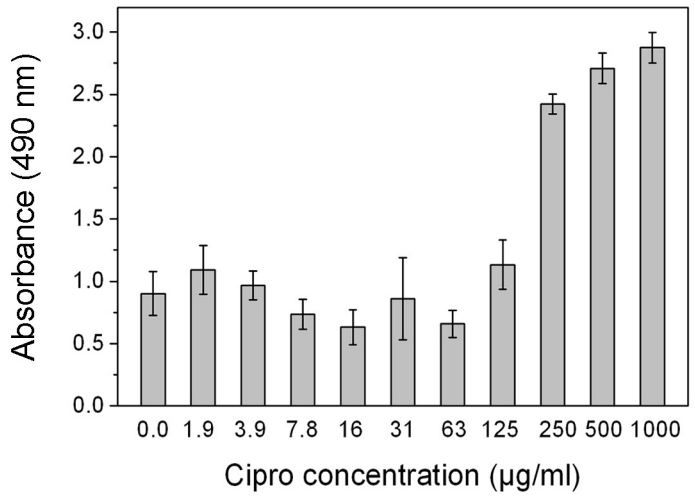

Figure 2.17. LDH release cytotoxicity assay on the effects of a dilution series of Cipro against B35 cells after 48 hr incubation. Error bars indicate the standard error of the mean (n = 3).

In order to test the possible toxicity of ciprofloxacin on cells growth, a Lactate Dehydrogenase (LDH) release assay was performed in the presence of a dilution series of Cipro and assessing LDH released into the media as a marker of dead cells. The results showed Cipro concentrations ≤ 125 µg/ml demonstrated no significant toxicity against B35 neuroblastoma cells. In addition, Cipro concentrations ≥ 250 µg/ml showed toxicity against B35 neuroblastoma cells (Figure 2.17). The results proved that the dosage of Cipro released from fibres is not high enough to cause cell mortality.

2.4 Conclusion

This chapter demonstrates a facile approach to produce new conducting polymer-based fibre that can be utilised as a micro-electrode for drug delivery applications. The controlled release of ciprofloxacin hydrochloride was achieved by electrical stimulation of a second conducting polymer layer. The antibacterial efficacy of the incorporated and released ciprofloxacin was confirmed against Gram-positive and Gram-negative bacteria indicating the stability of the antibiotic properties of the drug during both processing and the release method employed. In addition, cell culture studies on the fibres showed B35 neuroblastoma cells were not adversely affected by the presence of the Cipro loaded fibres, nor any released products from the fibres.

2.5 References

[1] Abidian MR, Martin DC. "*Multifunctional Nanobiomaterials for Neural Interfaces*". Adv Funct Mater. 2009;**19**(4):573-85.

[2] Abidian MR, Martin DC. "*Experimental and theoretical characterization of implantable neural microelectrodes modified with conducting polymer nanotubes*". Biomaterials. 2008;**29**(9):1273-83.

[3] Kotov NA, Winter JO, Clements IP, Jan E, Timko BP, Campidelli S, Pathak S, Mazzatenta A, Lieber CM, Prato M, Bellamkonda RV, Silva GA, Kam NWS, Patolsky F, Ballerini L. "*Nanomaterials for neural interfaces*". Adv Mater. 2009;**21**(40):3970-4004.

[4] Biran R, Martin DC, Tresco PA. "*Neuronal cell loss accompanies the brain tissue response to chronically implanted silicon microelectrode arrays*". Exp Neurol. 2005;**195**(1):115-26.

[5] Moulton SE, Higgins MJ, Kapsa RMI, Wallace GG. "*Organic Bionics: A New Dimension in Neural Communications*". Advanced Functional Materials. 2012:n/a-n/a.

[6] Kim D-H, Martin DC. "*Sustained release of dexamethasone from hydrophilic matrices using PLGA nanoparticles for neural drug delivery*". Biomaterials. 2006;**27**(15):3031-7.

[7] Buxton GA, Clarke N. "*Drug diffusion from polymer core-shell nanoparticles*". Soft Matter. 2007;**3**(12):1513-7.

[8] Kharlampieva E, Kozlovskaya V, Tyutina J, Sukhishvili SA. "*Hydrogen-Bonded Multilayers of Thermoresponsive Polymers*". Macromolecules. 2005;**38**(25):10523-31.

[9] Oh KS, Han SK, Choi YW, Lee JH, Lee JY, Yuk SH. "*Hydrogen-bonded polymer gel and its application as a temperature-sensitive drug delivery system*". Biomaterials. 2004;**25**(12):2393-8.

[10] Serizawa T, Matsukuma D, Akashi M. "*Loading and Release of Charged Dyes Using Ultrathin Hydrogels*". Langmuir. 2005;**21**(17):7739-42.

[11] Stevenson G, Moulton SE, Innis PC, Wallace GG. "*Polyterthiophene as an electrostimulated controlled drug release material of therapeutic levels of dexamethasone*". Synthetic Metals. 2010;**160**(9-10):1107-14.

[12] Wadhwa R, Lagenaur CF, Cui XT. "*Electrochemically controlled release of dexamethasone from conducting polymer polypyrrole coated electrode*". J Control Release. 2006;**110**(3):531-41.

[13] Auguste DT, Armes SP, Brzezinska KR, Deming TJ, Kohn J, Prud'homme RK. "*pH triggered release of protective poly(ethylene glycol)-b-polycation copolymers from liposomes*". Biomaterials. 2006;**27**(12):2599-608.

[14] Amidi M, Pellikaan HC, de Boer AH, Crommelin DJA, Hennink WE, Jiskoot W. "*Preparation and physicochemical characterization of supercritically dried insulin-loaded microparticles for pulmonary delivery*". Eur J Pharm. 2008;**68**(2):191-200.

[15] Recksiedler CL, Deore BA, Freund MS. "*A Novel Layer-by-Layer Approach for the Fabrication of Conducting Polymer/RNA Multilayer Films for Controlled Release*". *Langmuir*. 2006;**22**(6):2811-5.

[16] Lin Y, Wallace GG. "*Factors influencing electrochemical release of 2,6-anthraquinone disulphonic acid from polypyrrole*". J Control Release. 1994;**30**(2):137-42.

[17] Abidian MR, Kim DH, Martin DC. "*Conducting-Polymer Nanotubes for Controlled Drug Release*". Adv Mater. 2006;**18**(4):405-9.
[18] Thompson BC, Chen J, Moulton SE, Wallace GG. "*Nanostructured aligned CNT platforms enhance the controlled release of a neurotrophic protein from polypyrrole*". Nanoscale. 2010;**2**(4):499-501.
[19] Thompson BC, Moulton SE, Ding J, Richardson R, Cameron A, O'Leary S, Wallace GG, Clark GM. "*Optimising the incorporation and release of a neurotrophic factor using conducting polypyrrole*". J Control Release. 2006;**116**(3):285-94.
[20] Thompson BC, Richardson RT, Moulton SE, Evans AJ, O'Leary S, Clark GM, Wallace GG. "*Conducting polymers, dual neurotrophins and pulsed electrical stimulation -- Dramatic effects on neurite outgrowth*". J Control Release. 2010;**141**(2):161-7.
[21] Sirivisoot S, Pareta R, Webster TJ. "*Electrically controlled drug release from nanostructured polypyrrole coated on titanium*". Nanotechnology. 2011;**22**(8):085-101.
[22] G.Wallace G, Moulton S, Kapsa RMI, MichaelHiggins. Organic Bionics. Weinheim: Wiley-VCH Verlag GmbH & Co. KGaA
2012.
[23] Jalili R, Razal JM, Innis PC, Wallace GG. "*One-Step Wet-Spinning Process of Poly(3,4-ethylenedioxy-thiophene):Poly(styrenesulfonate) Fibers and the Origin of Higher Electrical Conductivity*". Advanced Functional Materials. 2011;**21** (17):363-3370.
[24] Foroughi J, Spinks GM, Wallace GG, Whitten PG. "*Production of polypyrrole fibres by wet spinning*". Synthetic Metals. 2008;**158**(3–4):104-7.
[25] Okuzaki H, Harashina Y, Yan H. "*Highly conductive PEDOT/PSS microfibers fabricated by wet-spinning and dip-treatment in ethylene glycol*". Eur Polym J. 2009;**45**(1):256-61.
[26] Sadki S, Schottland P, Brodie N, Sabouraud G. "*The mechanisms of pyrrole electropolymerization*". Chemical Society Reviews. 2000;**29**(5):283-93.
[27] Granero AJ, Razal JM, Wallace GG, in het Panhuis M. "*Spinning Carbon Nanotube-Gel Fibers Using Polyelectrolyte Complexation*". Adv Funct Mater. 2008;**18**(23):3759-64.
[28] Nelson JM, Chiller TM, Powers JH, Angulo FJ. "*Fluoroquinolone-Resistant Campylobacter Species and the Withdrawal of Fluoroquinolones from Use in Poultry: A Public Health Success Story*". Clin Infect Dis. 2007;**44**(7):977-80.
[29] Svirskis D, Travas-Sejdic J, Rodgers A, Garg S. "*Electrochemically controlled drug delivery based on intrinsically conducting polymers*". J Control Release. 2010;**146**(1):6-15.
[30] Lewis TW, Moulton SE, Spinks GM, Wallace GG. "*Optimisation of a polypyrrole based actuator*". Synt Met. 1997;**85**(1-3):1419-20.
[31] Richardson RT, Thompson B, Moulton S, Newbold C, Lum MG, Cameron A, Wallace G, Kapsa R, Clark G, O'Leary S. "*The effect of polypyrrole with incorporated neurotrophin-3 on the promotion of neurite outgrowth from auditory neurons*". Biomaterials. 2007;**28**(3):513-23.
[32] Gürbay A, Garrel C, Osman M, Richard M-J, Favier A, Hincal F. "*Cytotoxicity in ciprofloxacin-treated human fibroblast cells and protection by vitamin E*". Hum Exp Toxicol. 2002;**21**(12):635-41.

[33] Gürbay A, Gonthier B, Barret L, Favier A, Hincal F. "*Cytotoxic effect of ciprofloxacin in primary culture of rat astrocytes and protection by Vitamin E*". Toxicology. 2007;**229**(1-2):54-61.

3 COMBINED WET-SPINNING AND ELECTROSPINNING: NEW FABRICATION METHOD TO ENHANCE CYTO-COMPATIBILITY OF CONDUCTING FIBRES

3.1 Introduction

One of the main challenges in tissue engineering is to design and fabricate an appropriate artificial 3D extra cellular matrix (AECM) compatible with the *in vivo* environment to provide additional control over cell behaviour [1]. The composition and mechanical properties of AECM are some of elements that determine their performance [2]. AECM fabricated from submicron dimension materials provides a better biomimetic structure due to the interaction of cells with nanostructured surfaces [2]. To this end, significant control over cellular behaviour including adhesion, proliferation, migration, and differentiation has been achieved using electrospun fibres [3].

Electrospinning is a well-established and versatile technique used to produce submicron fibres. A vast range of polymers including, conducting and natural polymers have been used [2, 4-7]. The diameter of electrospun fibres is typically in the sub-micron and nanometer size range and this can facilitate cellular interactions [2, 3, 8]. Moreover, a scaffold made from aligned electrospun fibres, as opposed to non-aligned electrospun fibres, provides a more attractive substrate since cell adhesion, alignment and proliferation can be improved by the geometry and arrangement of the electrospun fibres [9, 10]. This positive effect is more pronounced when the AECM is designed to aid in regeneration of a specific tissue type such as nerves, tendon or muscle, where the cells must be aligned parallel to each other to form the final tissue [2, 9, 10]. Besides mimicking the AECM, the migration and extension of cells can be driven by the orientation of electrospun fibres in a 3D scaffold. Aligned poly(l-lactic acid) (PLA) nanofibres successfully directed neurites sprouting from neonatal mouse cerebellum (C17.2 NSCs) with 100 μm long axons [11]. Alignment in electrospun fibres also facilitates the healing process of

scars by directing the migratory routes of cells in specific directions [8]. For example, electrospun layers of poly caprolactone (PCL) and collagen fibres were fabricated and normal human dermal fibroblast (NHDF) cells were injected between the layers to generate a layer-by-layer cell assembly. The cells remained within the different layers and were shown to form dermal-like tissues or bilayer skin tissues after 1 week of culturing [12].

Methods that are used to control the alignment of electrospun fibres can be mainly classified into three groups based on the nature of the forces utilised to control the collection of the electrospun fibres. These forces are mechanical, electrostatic, and magnetic [6, 13-15]. In the case of mechanical force, a high speed-rotating spool is usually used to collect aligned electrospun fibres. In this method, the rotating speed of the spool controls the degree of alignment of the unidirectional non-woven sheath. Since electrostatic charges are carried by the electrospinning jet, manipulation of the electric/magnetic field can apply effective forces to the electrospun fibres just before their collection to control the alignment [6, 7, 13-15]. These methods, whilst useful, cannot produce continuous and unlimited lengths of aligned/unidirectional electrospun fibres. Another challenge associated with aligned electrospun fibres is to preserve the porosity of the final structure made from electrospun fibres [15].

Artificial ECM fabricated from conducting polymers can offer intriguing platforms for tissue regeneration due to the ability to enhance cellular growth via electrical stimulation as well as to control the release of incorporated biological molecules [16]. Topographical design and cyctocompatibility of the conducting AECM are critical factors that determine cell attachment to the AECM and the ability to transfer

the electrical signals to the cells [17]. Therefore, integration of conducting polymers into a cytocompatible electrospun scaffold is a great step toward utilising them in regenerative medicine.

In this chapter, we introduce a novel and facile method to integrate unidirectional electrospun PLGA fibres with a micron dimension PEDOT:PSS-CHI wet-spun fibre. The fibres showed a porous structure with suitable electrochemical and mechanical properties. Modulated drug release was achieved and introduction of porous PLGA improved the cell attachment. The structure simultaneously takes advantage of the high conductivity of PEDOT:PSS and the enhanced interactions between cells and the sub-micron structure environment provided by unidirectional aligned cytocompatible polymer electrospun fibres. The interaction of B35 neuroblastoma cells on the fibres were studied using fluorescent staining and cryo-SEM techniques. The antibiotic Ciprofloxacin hydrochloride (Cipro) was also incorporated into the fibre to provide antibacterial properties. The release of the Cipro from these fibre structures was also investigated.

3.2 Experimental

3.2.1 Materials

Poly(3,4-ethylenedioxythiophene) poly(styrene sulfonate) (PEDOT:PSS) pellets were obtained from Agfa (Orgacon dry, Lot A6 0000 AC). Ethanol (75 %), dimethyl sulfoxide (DMSO) and paraformaldehyde (PFA) were purchased from Sigma. Details of PEDOT:PSS, chitosan (CHI) and ciprofloxacin hydrochloride (Cipro) properties have been discussed in Chapter 2. PLGA (75:25) was purchased from Purac (Singapore). B35 neuroblastoma cells line was gifted by Dr. Anita Quigley at St. Vincent Hospital in Melbourne. Dulbecco's modified Eagle's medium (DMEM), fetal bovine serum (FBS), penicillin/streptomycin (Pen/strep) were purchased from Invitrogen. Anti-beta III tubulin primary antibody was obtained from Covance, Alexa fluo546 anti mouse secondary antibody and 4',6-diamidino-2-phenylindole (DAPI) were obtained from Invitrogen (Melbourne, Australia).

3.2.2 Combined wet-spinning and electrospinning method

A spinning solution of 25 mg/ml of PEDOT:PSS was prepared by dispersing required amounts of PEDOT:PSS pellets in water followed by homogenising at 10000 rpm for 10 min similar to the procedure described in Chapter 2. The PEDOT:PSS dispersion was loaded into a 5.0 ml syringe with a detachable needle (20 gauge) as the spinneret. The feed ratio applied for wet-spinning was 15 ml/hr using a syringe pump (KDS-Scientific 100). A concentration of 1.0 wt. % chitosan (CHI) was dissolved in 2.0 wt. % acetic acid and was used as the coagulation bath. The wet-spinning procedure described in Chapter 2 was used to form the PEDOT:PSS-CHI fibres. 15 wt./v % poly lactic-co-glycolic acid (PLGA) (75:25)

was prepared in a mixture of dichloromethane and dimethylformamide (DCM:DMF) (50:50). A feed rate of 1 ml/hr and applied potential of 15 kV was used to electrospin smooth, bead-free electrospun fibres. The composite wet-spun-electrospun fibres were prepared by electrospinning PLGA onto the PEDOT:PSS-CHI fibres as they passed through the ethanol bath.

3.2.3 Electrochemical properties of fibres

The electrochemical properties of fibres was investigated via cyclic voltammetry (CV) in phosphate buffered saline (PBS) pH ~ 7.4 in a 3-electrode cell, using a platinum mesh counter electrode, an Ag/AgCl reference electrode and a PEDOT:PSS-CHI-PLGA fibre as the working electrode with the set-up described in detail in Chapter 2.

3.2.4 Mechanical properties characterisation of fibres

The mechanical properties of the fibres were evaluated by a Shimadzu tensile tester (EZ-S) at a strain rate of 0.5 %/min. In order to hold the fibres, they were mounted on aperture cards (1.0 cm length of window) then fixed using commercial superglue and allowed to air dry.

3.2.5 Size distribution and imaging of fibres

The morphology of fibres was characterised by field scanning electron microscopy (FESEM) (JEOL JSM-7500FA). Fibre specimens for cross-section images were prepared by immersing in liquid nitrogen for 2.0 min followed by fracturing. The

size distribution of electro-spun fibres was determined by evaluating the diameter of fibres (250 measurments) using SEM images and Image-J software.

3.2.6 Ciprofloxacin hydrochloride release measurement

The release of Cipro from electrospun PLGA was measured using UV.Vis spectroscopy by determining the absorption of Cipro at its λmax (270 nm) in PBS. The UV–Vis spectra of Cipro in PBS solutions containing Cipro at varying concentrations (0.1-5.0 μg/ml) were recorded between 200 nm and 300 nm using a Shimadzu UV 1601 spectrophotometer in order to construct an absorbance/concentration calibration curve for sample analysis.

3.2.7 Cell culture and seeding

In order to culture cells, a B35 neuroblastoma cell line was sub-cultured on tissue culture plate (TCP) with Dulbecco's modified Eagle's medium DMEM medium supplemented with 10 % (v/v) fetal bovine serum (FBS) to passage (8-9) to use in the experiments. Cell passaging was carried out at a splitting ratio of 1:5 when the culture reached 70–80% confluence. To seed cells onto the fibres, cells were trypsinised, centrifuged, and re-suspended in DMEM supplemented with 10 % FBS and 1 % Pen/Strep at a final concentration of 1×10^5 cells/ml. The fibres were placed onto glass slides in an aligned pattern followed by glueing four-well chambers on the glass slide (Figure 3.1). The surface of fibres was sterilised by rinsing with 70 % v/v ethanol. After drying of fibres in a biosafety cabinet, cells were seeded at a density of 5,000 cells/cm^2 for proliferation studies. Cells were placed in an incubator at 37 °C in a humidified 5% CO_2 environment for 48 hr prior to staining and imaging.

In addition, cells were seeded in a density of 10,000 cells/cm^2 on fibres and differentiated by replacement of growth media with differentiation media containing DMEM, 1.0 % horse serum and 1 mM cAMP, and incubated for 72 hr with feeding after 48 hr. The schematic set up of fibres under four-well chambers is shown below.

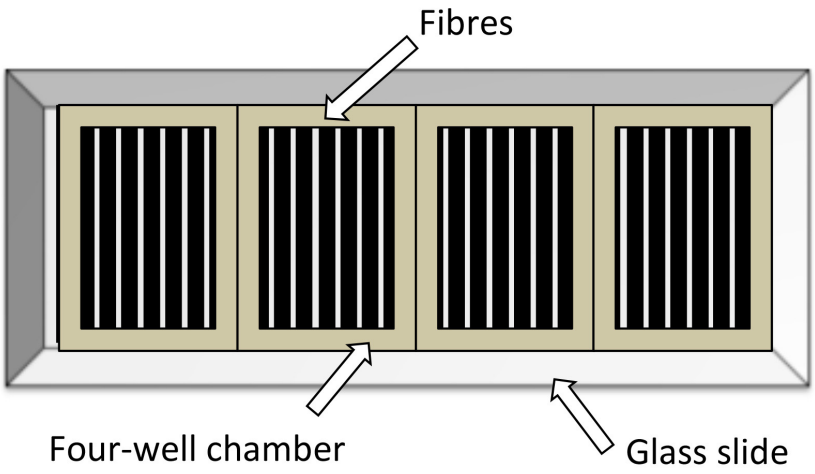

Figure 3.1. Schematic of the cell culture set up.

3.2.8 Fluorescent staining and imaging of cells

Calcein AM assay

A stock solution of 1.0 mM Calcein AM (Invitrogen) in DMSO was prepared. A concentration of 5.0 μM in cell growth media was added to cells followed by incubation for 15 min in cell culture environment (37 ^{o}C, 5% CO_2). Images were captured using an AxioImager fluorescent microscope (Zeiss) with AxioVision software. Live cells stain bright fluorescent green.

Beta III tubulin immunostaining

In order to perform beta III tubulin staining, the B35 cells were first washed in PBS. Cells were then fixed using 3.7 % paraformaldehyde (PFA) for 10 min followed by rinsing with PBS. Cells were then permeabilised with a mixture of methanol:acetone (50:50) on ice for 5.0 min followed by washing the cells with PBS. Then, cells were blocked using 10 % donkey serum in PBS for 1.0 hr at room temperature. Cells were then incubated with primary antibody diluted 1 in 1000 in blocking solution overnight at 4 °C followed by washing with PBS twice. Cells were then incubated with secondary antibody diluted 1 in 1000 in blocking solution at 37°C for 1 hour followed by three PBS washes for 20 min each. Following this, cell nuclei were stained with DAPI (1 in 1000 in PBS) for 5 min at room temperature and the media was replaced with PBS for imaging.

Cryo-SEM imaging of cells on the fibres

Cells were fixed by 3.7 % paraformaldehyde (PFA) for 10 min at room temperature. Then, they were washed and kept in PBS for imaging using a JSM-6490LV SEM.

3.3 Results and discussion

3.3.1 Introduction of a novel method of combined wet-spinning and electrospinning

Fabrication of appropriate biomaterials structures that accommodate living cells is one of the key issues in the biofabrication field. In addition to the cytocompatibility of materials, the architecture and topography are important due to the fact that cells need to attach to the structure in order to follow its geometry. The PEDOT:PSS-CHI and PEDOT:PSS-CHI-Ppy.Cipro fibres, described in Chapter 2, showed good ability to control the release of drugs using electrical stimulation, however they exhibited poor cell attachment. This chapter discusses the development of a novel and facile fabrication technique, the physical and electrochemical characterisation of the composite fibres produced, and the *in vitro* cytocompatibility of the fibres to develop a better conducting polymer fibre for cell attachment.

Figure 3.2 presents a schematic of the method used to spin continuous electrospun wet-spun fibres. In this method, 25 mg/ml PEDOT:PSS dispersion in water was injected into a chitosan (1.0 wt. %) coagulation bath to form a continuous fibre. The subsequent washing bath contained ethanol similar to the method employed in Figure 2.1. At the same time, PLGA fibres were electrospun on the top of the ethanol washing bath. When the electrospun PLGA fibres accumulated on the surface of the ethanol washing bath, they gradually sink into the ethanol. These electrospun fibres were collected by the wet-spun PEDOT:PSS-CHI fibre as it emerged from the washing bath. The PEDOT:PSS-CHI fibres covered with the electrospun PLGA were then collected on the take-up spool.

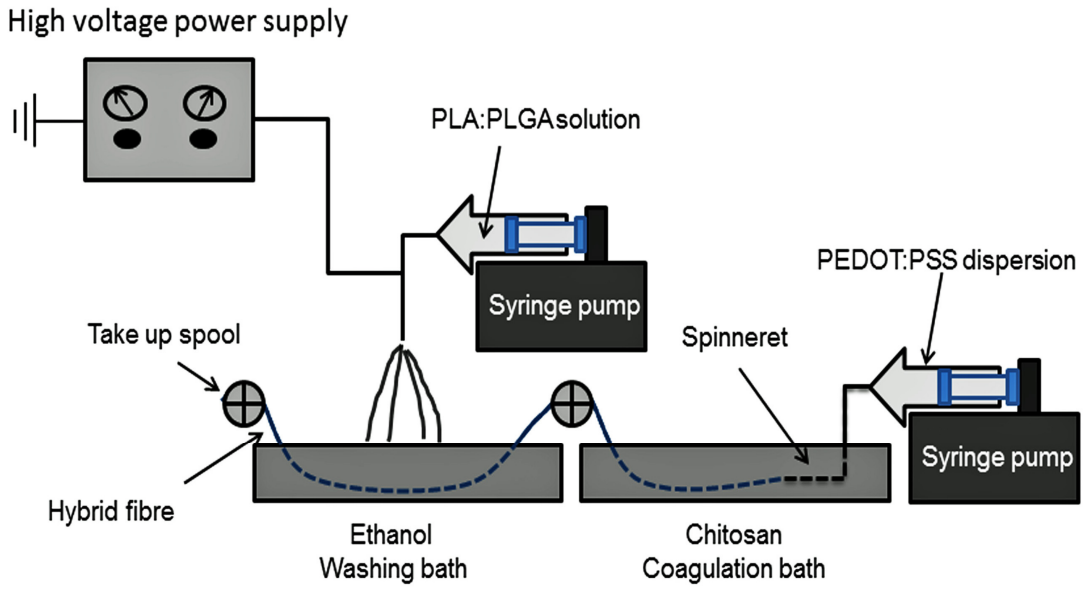

Figure 3.2. Schematic of combined wet-spinning and electrospinning method

In order to investigate the morphology of fibres, scanning electron microscopy (SEM) imaging was performed. Figure 3.3 shows SEM images of the fibres and cross-sections of the resulting PEDOT:PSS-CHI-PLGA fibres. As can be seen, the thickness of the electrospun layer around the PEDOT.PSS-CHI core is relatively constant (30 ± 5.0 μm, for a feed rate of 1.0 ml/hr) indicating uniform coverage of the electrospun layer around the wet-spun fibre.

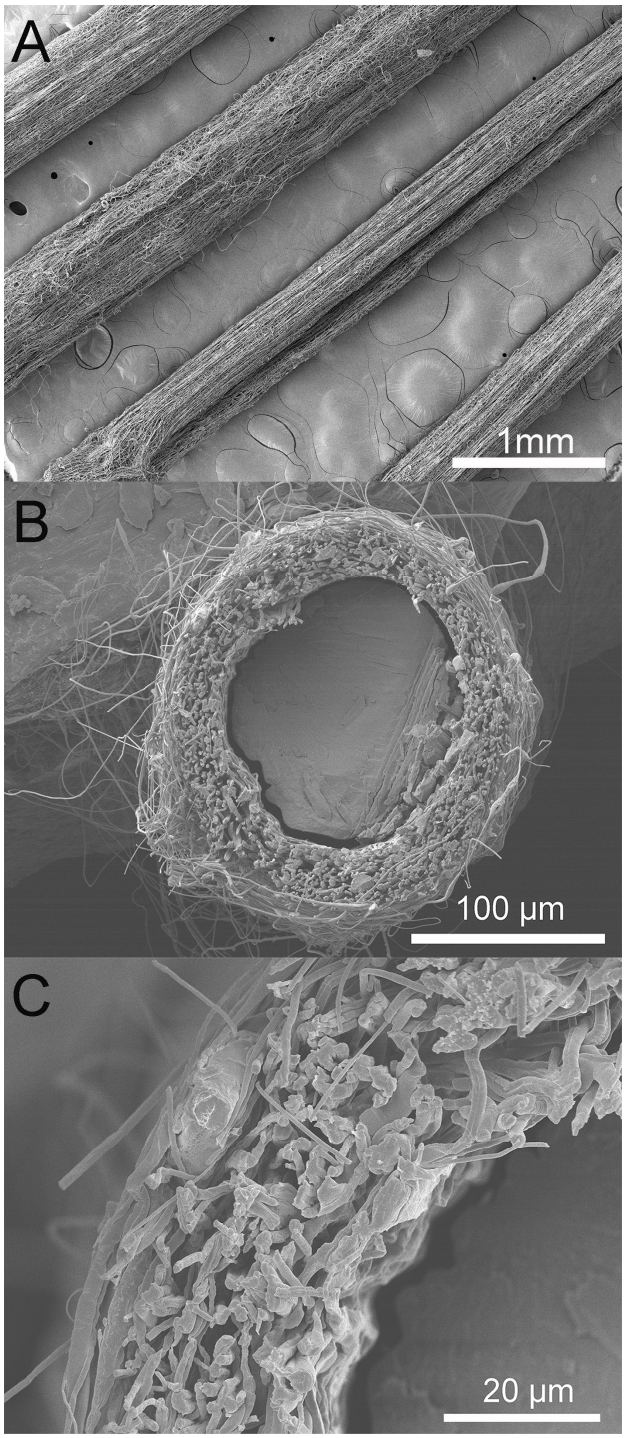

Figure 3.3. Scanning electron microscopy (SEM) images PEDOT:PSS-CHI-PLGA fibre, A) SEM of the fibres in parallel configuration, B) SEM images of cross-section of fibres: the middle area shows the cross section of PEDOT:PSS-CHI wet-spun fibre and the edge shows the PLGA electrospun sheath. C) The cross-section of the fibre at higher magnification.

The SEM images represent a coherent coating of electrospun PLGA fibres wrapped around the wet-spun fibres. There is no evidence of this coating peeling away from the PEDOT:PSS-CHI fibres with preparation for SEM imaging. SEM images also confirmed the alignment of electrospun fibres as well as the uniform diameter of the fibres along the fibres' axis (Figure 3.4). Using this method, as evidenced by SEM images, the porosity of the final core-shell structure is preserved. This porous structure most likely occurs when the PLGA electrospun fibres are collected from the ethanol bath; the ethanol evaporates quickly so that PLGA solidifies and retains its porous structure. The morphology of PEDOT:PSS-CHI-PLGA fibres at different magnifications (Figure 3.4) shows that PLGA electrospun sheaths covered the surface of PEDOT:PSS-CHI fibres.

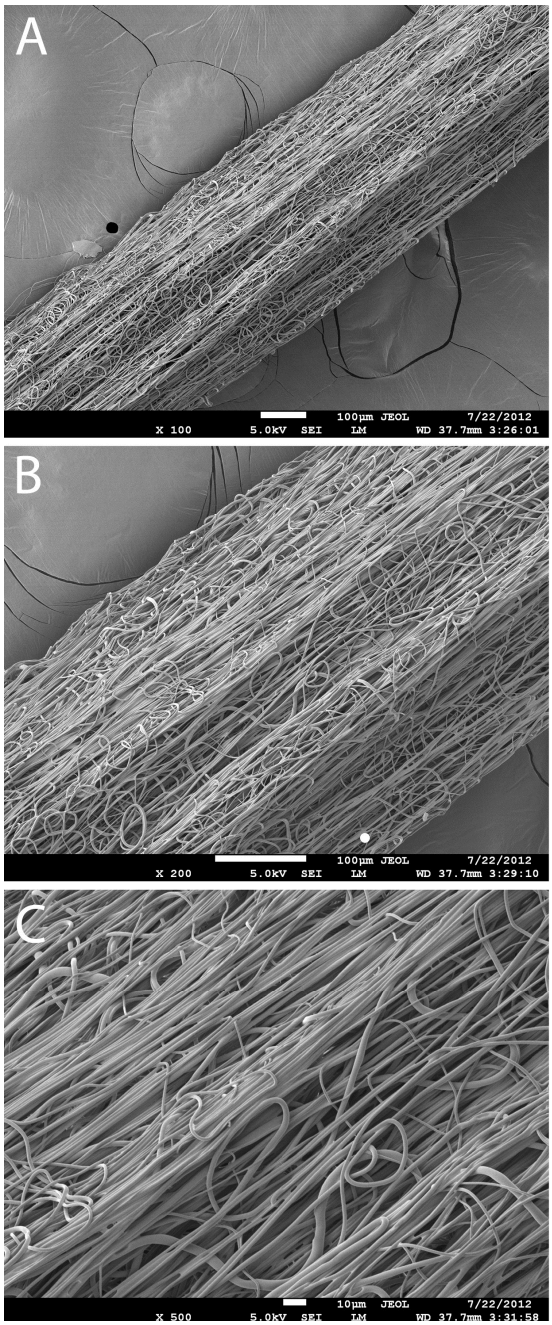

Figure 3.4. Scanning electron microscopy images of PEDOT:PSS-CHI-PLGA fibres at different magnifications. A) PEDOT:PSS-CHI-PLGA fibre at 100X magnification, B) the same fibre at 200X, C) PLGA electrospun sheath at 500X. The scale bar represents 100 µm in each image.

The diameter of electrospun fibres in the outer layer was determined from SEM images (Figure 3.5-A). Using Image-J software, the size distribution of the PLGA electrospun sheath is presented in Figure 3.5-B. The mean diameter of the electrospun fibres is found to be 1.64 ± 0.6 μm.

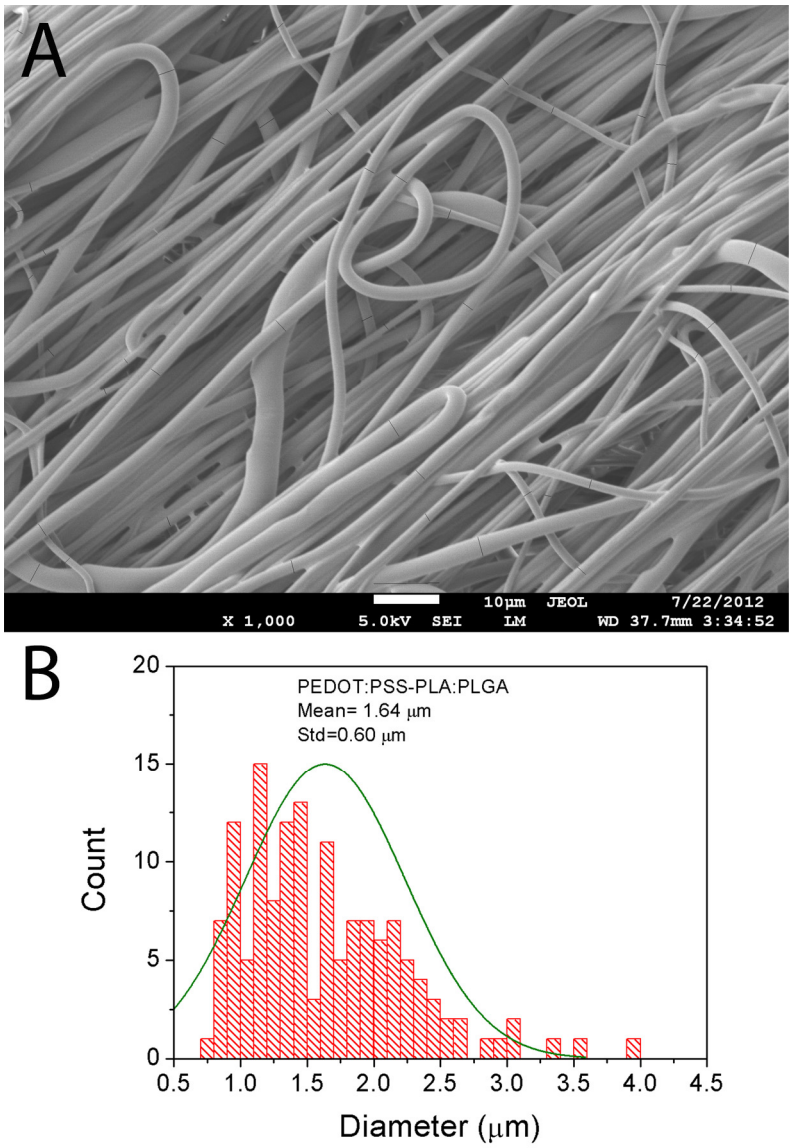

Figure 3.5. A) Scanning electron microscopy (SEM) image of PLGA fibres in the electrospun sheath. B) Size distribution of fibres in the electrospun sheath shown in A.

3.3.2 The effect of feed rate of PLGA solution

The feed rate of the electrospinning solution was varied from 0.5 to 2.0 ml/hr to evaluate the effect on the thickness of the electrospun layer. Figure 3.6 presents SEM images of PEDOT:PSS-CHI-PLGA fibres produced using various feed rates. Increasing the feed rate resulted in thicker fibres collected on the top of wet-spun PEDOT:PSS-CHI fibres. Fibres with feed rates of 0.5, 1, 1.5 and 2 ml/hr, produced sheath thicknesses of 39±6, 57±8, 70±8 and 80±5μm, respectively. The diameter of PEDOT:PSS-CHI core fibres was constant (111± 5μm) since the wet-spinning parameters such as feed rate, spinneret diameter and collecting speed were kept constant during the spinning process.

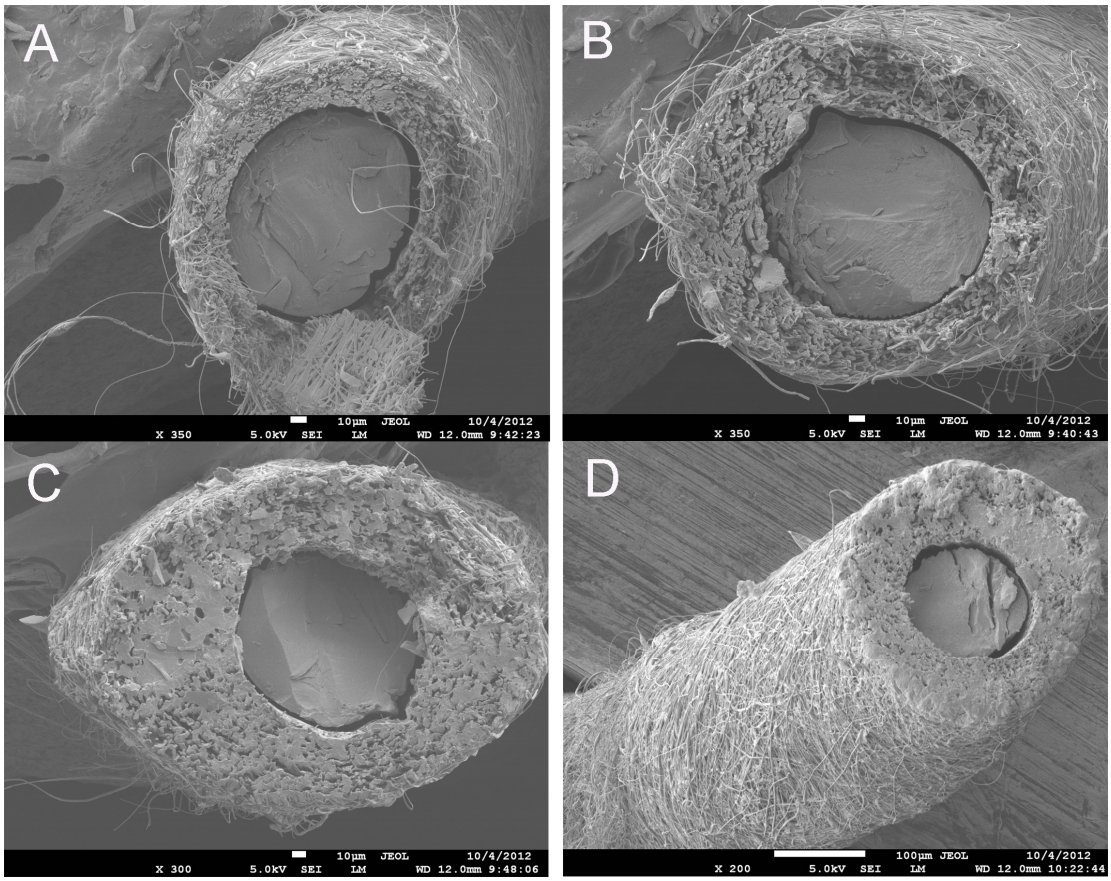

Figure 3.6. Scanning electron microscopy images of cross-sections of the PEDOT:PSS-CHI-PLGA fibres with respect to electrospinning feed rate. A) 0.5 ml/hr, B) 1 ml/hr, C) 1.5 ml/hr, D) 2 ml/hr. The scale bars in images A, B and C represent 10 µm, whereas in image D the scale bar represents 100 µm.

3.3.3 Electrochemical properties of fibres

Cyclic voltammograms (CV) of a PEDOT:PSS-CHI fibre and the PEDOT:PSS-CHI-PLGA fibre are shown in Figure 3.7. The main features of the CV are as follows: upon oxidation a peak is observed at ~ +0.2 V, which is followed by a second small oxidation peak at 0.4 V. Upon reduction the CV exhibits two broad reduction peaks observed at 0.4 V and -0.1 V. Similar redox responses for both fibres confirmed the minimum disruption of the access of ions after the addition of the PLGA electrospun

sheath. The results showthat PEDOT:PSS-CHI fibres are electro-active and have the capability to switch between reduced and oxidised states [18].

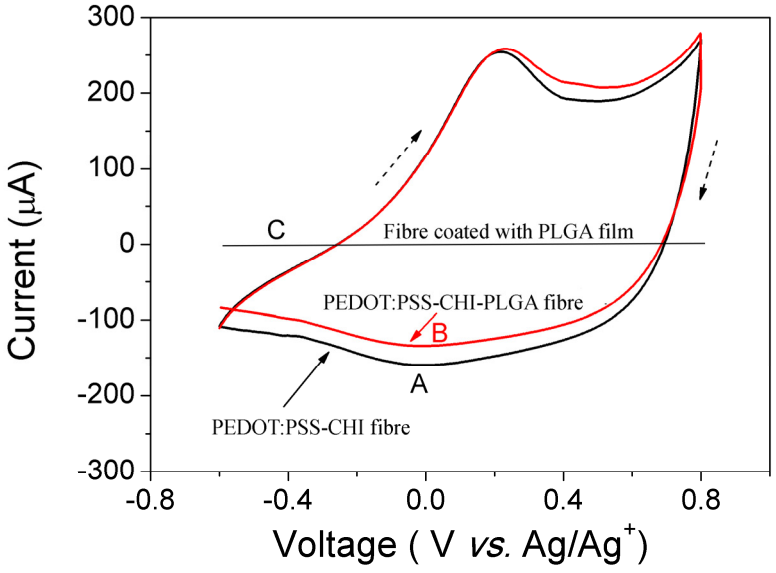

Figure 3.7. Cyclic voltammogram of A) PEDOT:PSS-CHI fibre, B) PEDOT:PSS-CHI-PLGA fibre, and C) PEDOT:PSS-CHI fibre coated with PLGA film in PBS (pH ≃ 7.4) scanned between E_i = -0.6 V and E_f = +0.8 V at a scan rate of 25 mV/s. The feed rate of electrospinning was 1 ml/hr. Dashed arrows indicate the direction of the potential scan.

Cyclic voltammetry performed on the PEDOT:PSS-CHIT-PLGA fibre, where a feed rate of greater than 1 ml/hr was used to form the PLGA electrospun sheath, resulted in the loss of electroactivity (the sheath was too thick for PBS to penetrate). This is presumably due to the thick layer of PLGA, that forms at these high feed rates (as indicated in Figure 3.6), preventing the PBS electrolyte from diffusing to the PEDOT:PSS core. PLGA fibres spun at a feed rate of 1 ml/hr or less provided suitable thicknesses through which ions could diffuse to the PEDOT:PSS, resulting in measurable electroactivity of the fibre (Figure 3.7). In order to preserve the

electrochemical property of the fibres, the electrospinning feed rate was kept at 1 ml/hr for subsequent experiments. It is worth mentioning that when the PEDOT:PSS-CHI fibres were completely coated by a layer of PLGA (by dip-coating the fibres into a PLGA solution of the same concentration used for electrospinning) it was not possible to record any electrochemical response (Figure 3.7). This non-porous coating of PLGA would not permit the diffusion of PBS ions into the inner conducting PEDOT:PSS-CHI core.

3.3.4 Mechanical properties of the fibres

The mechanical properties of PEDOT:PSS-CHI-PLGA fibres were evaluated by tensile tests and the resultant stress-strain curves. The total diameter of the fibres was measured including the compact PEDOT:PSS-CHI and the porous PLGA electrospun layer.

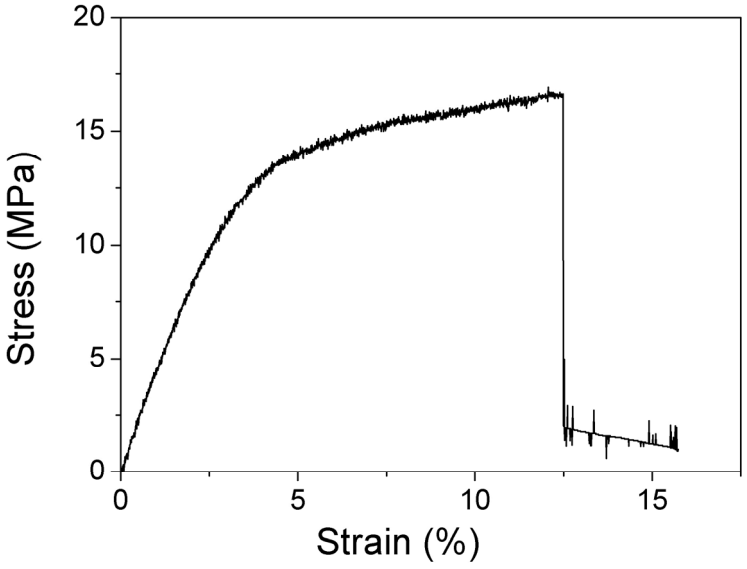

Figure 3.8. Stress-strain curve obtained from a PEDOT:PSS-CHI-PLGA fibre.

The as-dried PEDOT:PSS-CHI-PLGA fibre revealed modulus and ultimate stress of 420 MPa and 16.5 KPa, respectively. The lower calculated ultimate stress and modulus of the fibres compared to the neat PEDOT:PSS-CHI fibres (Chapter 2. Figure 2.11) are due to the larger diameter of the fibre which includes the porous PLGA electrospun sheath.

The fibres were easily handled, which made it possible for them to be utilised in cell culture studies. Unlike other wet-spun fibres (i.e PEDOT:PSS fibres), the novel composite fibres produced here did not swell in cell culture medium, possibly due to the presence of the PLGA electrospun sheath.

3.3.5 Release of ciprofloxacin hydrochloride from fibres

The multi-functionality of the PEDOT:PSS-CHI-PLGA fibres was established by incorporation of an antibacterial drug (ciprofloxacin hydrochloride) into the structure during electrospinning. Ciprofloxacin hydrochloride was combined into the electrospinning solution to be loaded in the fibre. The drug is released by degradation of the PLGA electrospun layer as well as by diffusion of the drug from the PLGA fibres [19]. Figure 3.9 presents the release profile into PBS over 28 days. A burst release within the first few days was observed followed by sustained release for the following 27 days. The burst release is most likely due to discharging of Cipro from the surface of the electrospun sheath into the PBS media [19]. Moreover, release from the PEDOT:PSS-CHI-PLGA fibres without Cipro loading did not show any

peak at 270 nm (λmax for Cipro) which confirms that no non-drug products released from the PEDOT:PSS-CHI interfered with the drug detection.

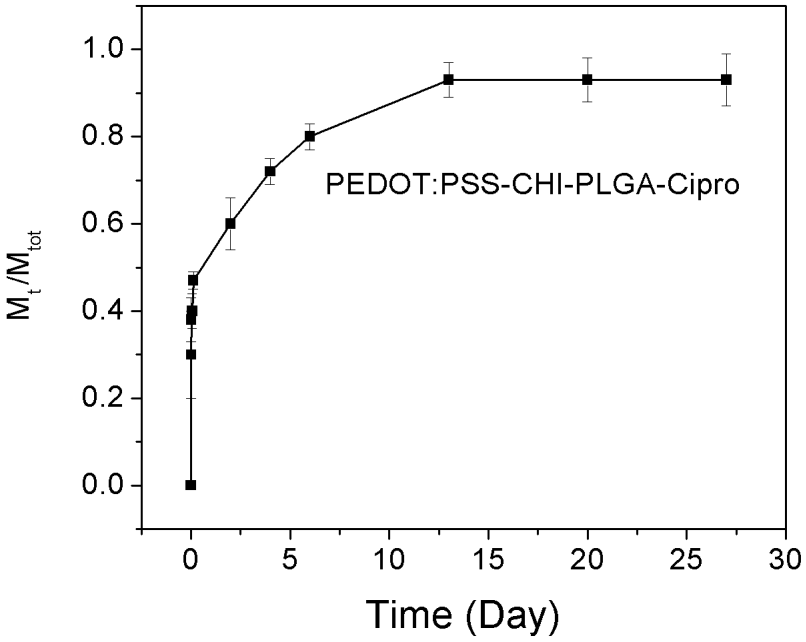

Figure 3.9. Cumulative release profile of Cipro from PEDOT:PSS-CHI-PLGA fibres in PBS medium.

3.3.6 Cytocompatibility of the fibres

The micro-dimensional fibres (PEDOT:PSS-CHI) made by wet-spinning can provide electrochemical activity, while the sub-micron dimensional electrospun fibres were expected to improve cell attachment to the multifunctional structure. In order to investigate the cytocompatibility of the fibres, B35 neural cells were seeded on PEDOT:PSS-CHI-PLGA fibres laid in a parallel configuration on the surface of a glass slide. B35 cell adhesion onto the fibres was investigated in order to evaluate the suitability of the fibre to be used in neural tissue regeneration. The cells were

cultured on tissue culture plastic (TCP) as control, fluorescently stained for β-tubulin (neural marker) and imaged using optical microscopy. Images in Figure 3.10 illustrate the B35 neural cells cultured on TCP for 2-4 days and immunostained for β-III tubulin.

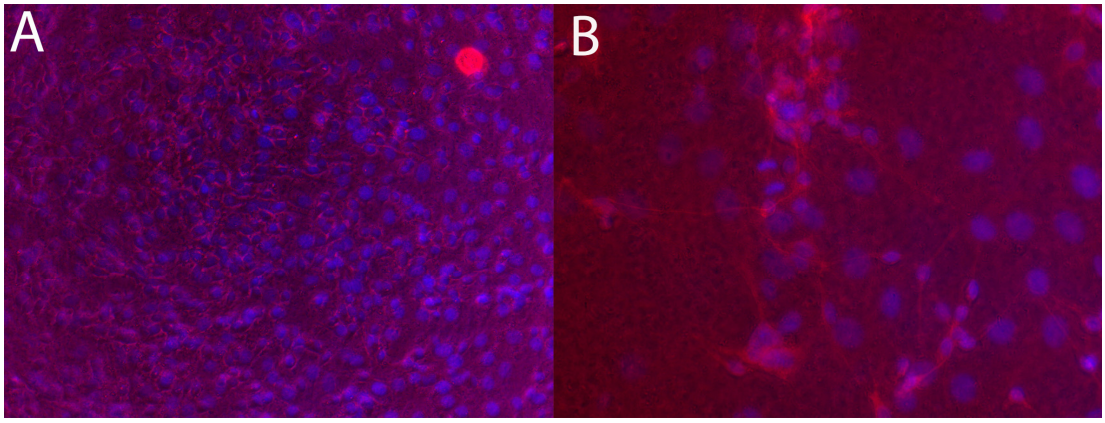

Figure 3.10. Beta III tubulin staining imaging of B35 neural cells on TCP. A) In growth media after 2 days. B) In differentiation media after 4 days.

Figure 3.11 represents the results of beta III tubulin staining performed on B35 cells on the fibres. Cells attached to PEDOT:PSS-CHI-PLGA fibres (Figure 3.11A-C) and moved into the electrospun sheath. For DAPI images, the blue spots represent nuclei of cells which penetrated into layers of the electrospun sheath, however, the beta III tubulin images (Figure 3.11B-F) did not show the cytoskeleton of cells well. This is due to PLGA fluorescing at the same wavelength that is required for detection of beta III tubulin (red areas on fibres without cells).

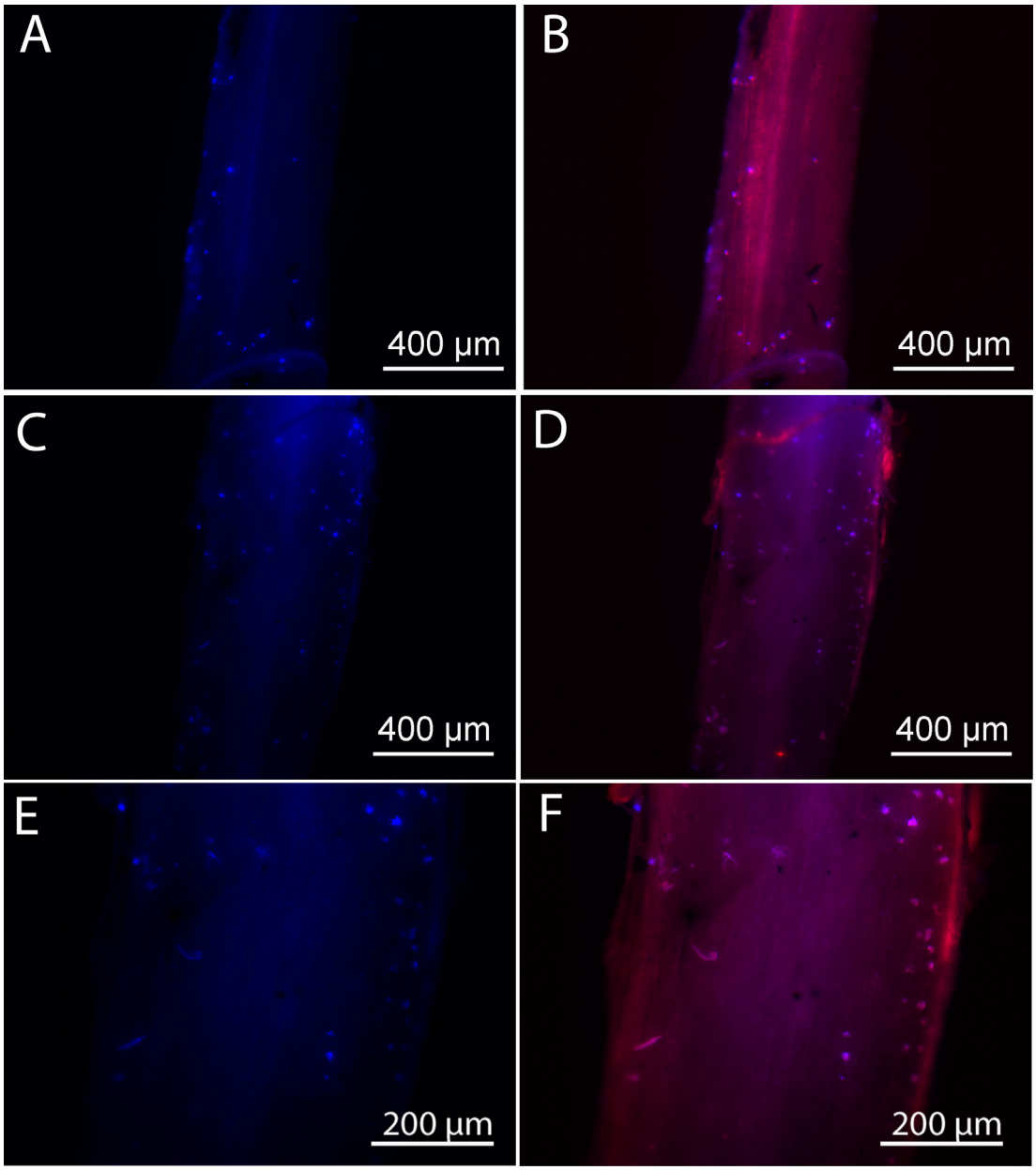

Figure 3.11. Beta III tubulin staining imaging of B35 neural cells on fibres. A, C and E) DAPI staining after 2 days in growth media. (Blue spots represent nuclei of cells) B, D and F) Purple spots represent nuclei and cytoskeleton of cells together (merged images).

Since, in the case of beta III tubulin staining, there was a problem with autofluorescence of PLGA in the red channel, calcein AM staining was performed in order to illustrate the viability of the cells. Figure 3.12 (A-F) revealed live cells in the surface of electrospun fibres and pore bridging (connection of cells between two electrospun fibres) with no evidence of dead cells on the surface of fibres, whereas Calcein AM staining of B35 cells on PEDOT:PSS-CHI fibres (developed in Chapter 2) resulted in poor cell attachment to the fibres (Figure 3.12-H) and their agglomeration on the surface of fibres (Figure 3.12 G) with some dead cells detected. In addition, the higher specific surface area of the PLGA electrospun sheath provided improved cell attachment compared to the PEDOT:PSS-CHI wet-spun fibre. When cells spread and fill the spaces between the individual electrospun fibres, they are in direct contact with other cells forming cell-connected tissue-like structures (Figure 3.12 B and D). These results are similar to that of other researchers working with electrospun silk for tissue engineering [20]. The balance between fabricating a suitable ECM for cells and the challenges of this from an engineering point of view highlights the difficulties of building an optimised tissue-engineering scaffold.

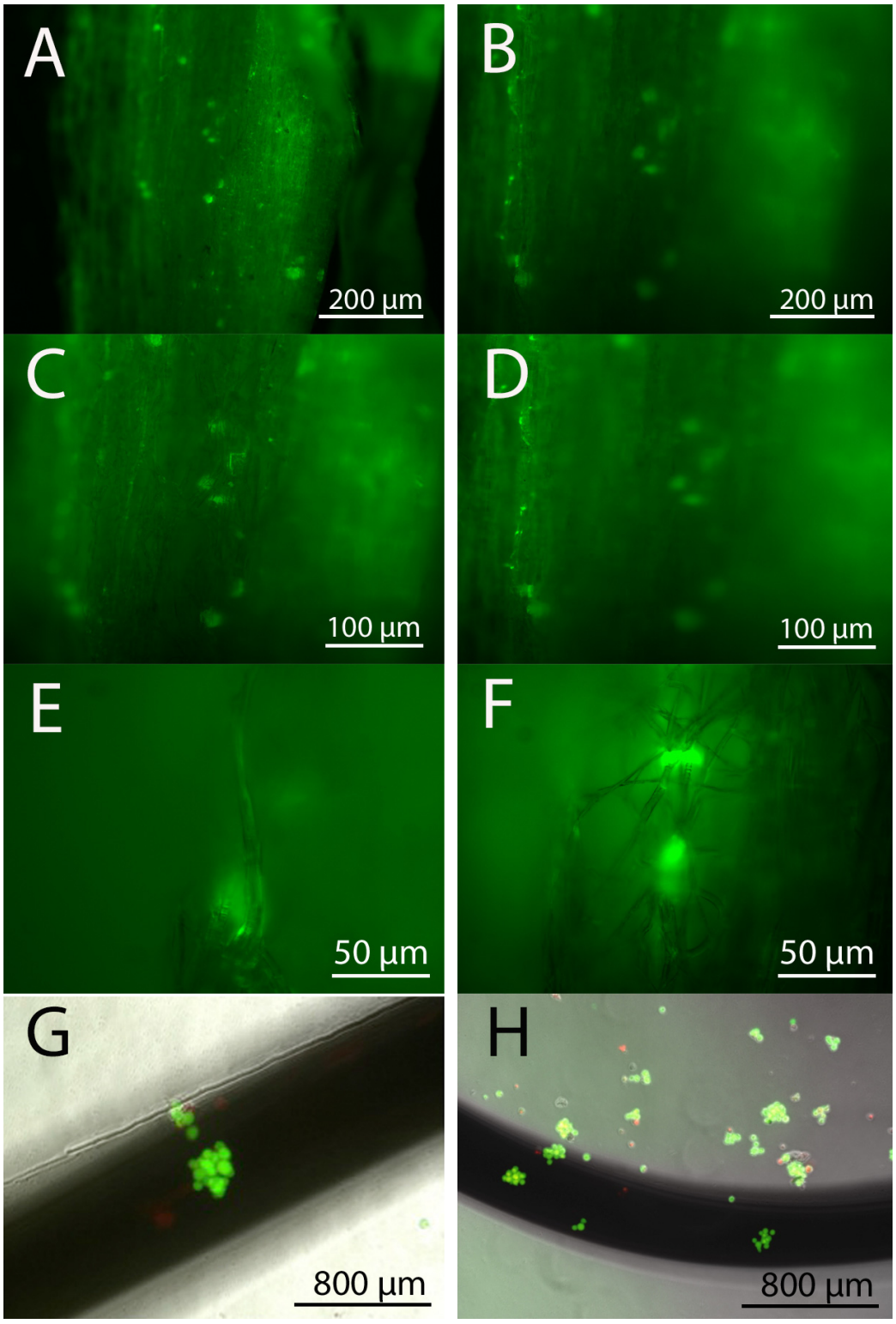

Figure 3.12. Calcein AM images of B35 cells on PEDOT:PSS-CHI-PLGA fibres. (A, B, C and D) at low magnification (10X), (E and F) at high magnification (50X). (G and H) PEDOT:PSS-CHI fibres with cells.

As the cells spread into the electro-spun layers, they followed the direction of the long micro-dimensional fibres. Cryo-SEM images of fibres (Figure 3.13) show cells differentiating on the fibres with the electrospun sheath hosting axons and guiding their direction. In images A, C and E, cells proliferated on the surface and migrated into the layers, however in images B, D and F, cells started to differentiate. Some directed axons of cells can be observed in Figure 3.13 B-F and are marked using black arrows. It is worth noting that since the majority of cells migrated into the electro-spun sheaths, it was hard to quantify the lengths of axons. These results showed that the PLGA electrospun sheaths on the surface of the fibres facilitate cells attachment by providing a cytocompatible platform, while the porosity of the electrospun layer would be expected to provide benefits for the transport of nutrients.

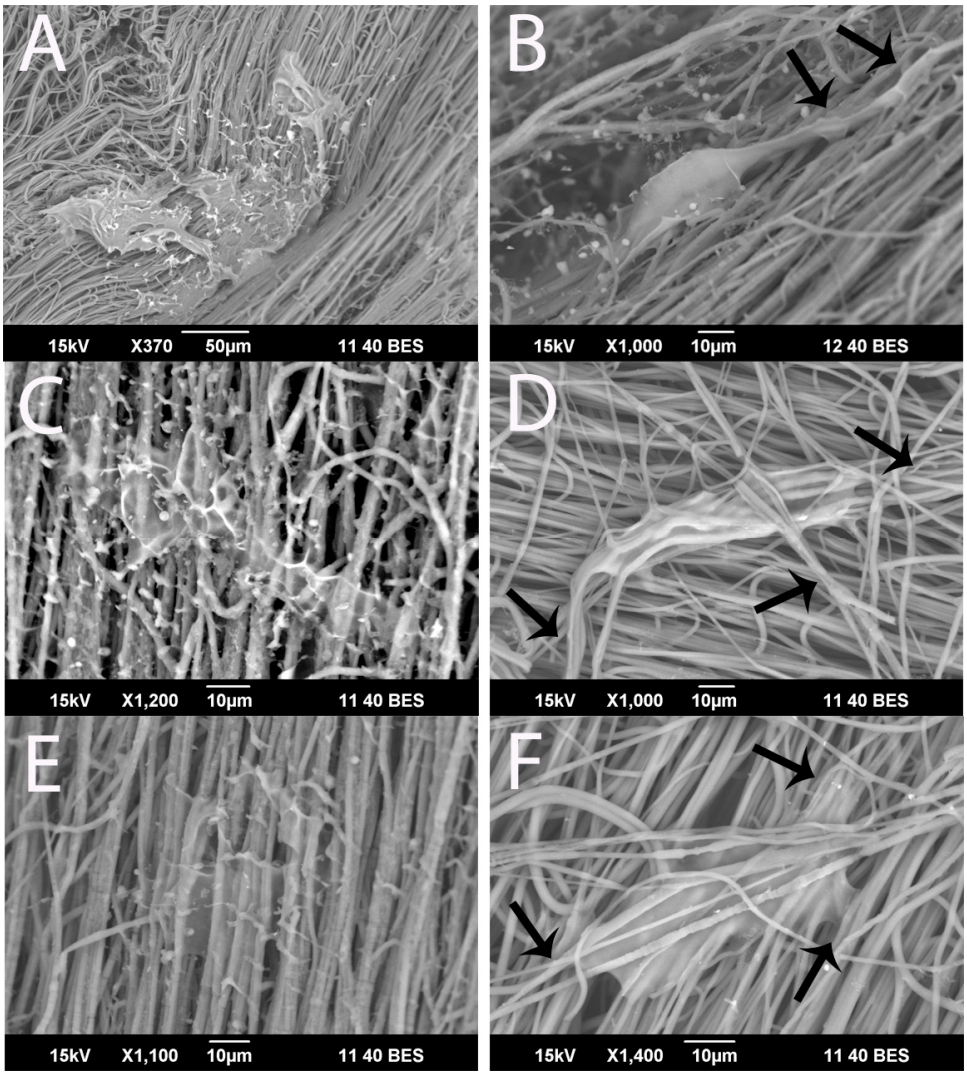

Figure 3.13. Cryo-SEM images of B35 neural cells on PEDOT:PSS-CHI-PLGA fibres at different magnifications. (A, C and E) B35 cells in growth media after 2 days. (B, D and F) cryo-SEM images of the differentiated B35 cells for three days on fibres (the black arrows show the direction of axons on the electro-spun sheaths).

3.4 Conclusion

This chapter describes the development of a novel and facile fabrication technique, which is the combining of electrospinning and wet-spinning simultaneously. The method discribed here is not limited to PEDOT:PSS and PLGA but has the capability to be applied to other spinable polymers. This technique has the capability to produce conducting biomaterials with the potential to release an antibiotic drug (ciprofloxacin) within 28 days in PBS. The physical characterisation of the fibres viewed in cross-section revealed a solid PEDOT:PSS-CHI wet-spun fibre covered by a porous PLGA electrospun sheath without peeling off the electrospun from wet-spun fibres. The electrochemical characterisation of the fibres demonstrated the electroactive behavior of the PEDOT:PSS-CHI core in PBS, which was not adversely affected by covering of the fibres with the PLGA electrospun sheath. The *in vitro* cytocompatibility tests of the fibres for the B35 neuroblastoma cells line including fluorescent staining and Cryo-SEM imaging techniques demonstrate the cytocompatibility of PEDOT:PSS-CHI-PLGA fibres due to the fact that B35 cells attached to the surface of the fibres and migrated into the electropsun sheaths, as well as their differentiation on/into PLGA electropsun sheaths. All the mentioned properties above suggest the potential of PEDOT:PSS-CHI-PLGA fibres for utilisation in biomedical fields.

3.5 References

[1] Khademhosseini Ali, Vacanti Joseph P., Langer Robert. "*Progress in Tissue Engineering*". Scientific American.**300**:64 - 71

[2] Liu W, Thomopoulos S, Xia Y. "*Electrospun Nanofibers for Regenerative Medicine*". Advanced Healthcare Materials. 2012;**1**(1):10-25.

[3] Dvir T, Timko BP, Kohane DS, Langer R. "*Nanotechnological strategies for engineering complex tissues*". Nat Nano. 2011;**6**(1):13-22.

[4] Luu YK, Kim K, Hsiao BS, Chu B, Hadjiargyrou M. "*Development of a nanostructured DNA delivery scaffold via electrospinning of PLGA and PLA–PEG block copolymers*". Journal of Controlled Release. 2003;**89**(2):341-53.

[5] Moradzadegan A, Ranaei-Siadat S-O, Ebrahim-Habibi A, Barshan-Tashnizi M, Jalili R, Torabi S-F, Khajeh K. "*Immobilization of acetylcholinesterase in nanofibrous PVA/BSA membranes by electrospinning*". Engineering in Life Sciences. 2010;**10**(1):57-64.

[6] Esrafilzadeh D, Morshed M, Tavanai H. "*An investigation on the stabilization of special polyacrylonitrile nanofibers as carbon or activated carbon nanofiber precursor*". Synthetic Metals. 2009;**159**(3–4):267-72.

[7] Matthews JA, Wnek GE, Simpson DG, Bowlin GL. "*Electrospinning of Collagen Nanofibers*". Biomacromolecules. 2002;**3**(2):232-8.

[8] Nisbet DR, Forsythe JS, Shen W, Finkelstein DI, Horne MK. "*A Review of the Cellular Response on Electrospun Nanofibers for Tissue Engineering*". Journal of Biomaterials Applications. 2009;**24**(1):7-29.

[9] Yin Z, Chen X, Chen JL, Shen WL, Hieu Nguyen TM, Gao L, Ouyang HW. "*The regulation of tendon stem cell differentiation by the alignment of nanofibers*". Biomaterials. 2010;**31**(8):2163-75.

[10] Zong X, Bien H, Chung C-Y, Yin L, Fang D, Hsiao BS, Chu B, Entcheva E. "*Electrospun fine-textured scaffolds for heart tissue constructs*". Biomaterials. 2005;**26**(26):5330-8.

[11] Yang F, Murugan R, Wang S, Ramakrishna S. "*Electrospinning of nano/micro scale poly(l-lactic acid) aligned fibers and their potential in neural tissue engineering*". Biomaterials. 2005;**26**(15):2603-10.

[12] Yang X, Shah JD, Wang H. "*Nanofiber Enabled Layer-by-Layer Approach Toward Three-Dimensional Tissue Formation*". Tissue Engineering Part A. 2009;**15**(4):945-56.

[13] Jalili R, Morshed M, Ravandi SAH. "*Fundamental parameters affecting electrospinning of PAN nanofibers as uniaxially aligned fibers*". Journal of Applied Polymer Science. 2006;**101**(6):4350-7.

[14] Esrafilzadeh D, Jalili R, Morshed M. "*Crystalline order and mechanical properties of as-electrospun and post-treated bundles of uniaxially aligned polyacrylonitrile nanofiber*". Journal of Applied Polymer Science. 2008;**110**(5):3014-22.

[15] Barnes CP, Sell SA, Boland ED, Simpson DG, Bowlin GL. "*Nanofiber technology: Designing the next generation of tissue engineering scaffolds*". Advanced Drug Delivery Reviews. 2007;**59**(14):1413-33.

[16] Quigley AF, Razal JM, Kita M, Jalili R, Gelmi A, Penington A, Ovalle-Robles R, Baughman RH, Clark GM, Wallace GG, Kapsa RMI. "*Electrical Stimulation of Myoblast Proliferation and Differentiation on Aligned Nanostructured Conductive Polymer Platforms*". Advanced Healthcare Materials. 2012;**1**(6):801-8.

[17] Razal JM, Kita M, Quigley AF, Kennedy E, Moulton SE, Kapsa RMI, Clark GM, Wallace GG. "*Wet-Spun Biodegradable Fibers on Conducting Platforms: Novel Architectures for Muscle Regeneration*". Adv Funct Mater. 2009;**19**(21):3381-8.
[18] Ouyang J, Xu Q, Chu C-W, Yang Y, Li G, Shinar J. "*On the mechanism of conductivity enhancement in poly(3,4-ethylenedioxythiophene):poly(styrene sulfonate) film through solvent treatment*". Polymer. 2004;**45**(25):8443-50.
[19] Viry L, Moulton SE, Romeo T, Suhr C, Mawad D, Cook M, Wallace GG. "*Emulsion-coaxial electrospinning: designing novel architectures for sustained release of highly soluble low molecular weight drugs*". Journal of Materials Chemistry. 2012;**22**(22):11347-53.
[20] Unger RE, Wolf M, Peters K, Motta A, Migliaresi C, James Kirkpatrick C. "*Growth of human cells on a non-woven silk fibroin net: a potential for use in tissue engineering*". Biomaterials. 2004;**25**(6):1069-75.

4 WET-SPINNING OF MULTIFUNCTIONAL PLGA-GRAPHENE FIBRES

4.1. Introduction

Synthesis and fabrication of conducting biomaterials in 3-dimensional (3D) architectures are likely to be an integral part of the field of regenerative medicine. Biocompatibility and degradation in conjunction with cellular affinity to the 3D structures are some of key features to consider in developing appropriate structures. Moreover, biocompatible 3D structures fabricated from conducting polymers can offer very interesting platforms for cells due to their capability to modify cellular growth via electrical stimuli as well as controlling the release of biological molecules [1, 2].

A range of organic conductors such as carbon nanotubes and conducting polymers have been utilised to induce or enhance electrical conductivity in biomaterials [3-5]. The debatable toxicity issue of carbon nanotubes, due to the inclusion of metal catalysts as well as their aspect ratio, limits their application in biomedical fields [6]. Conducting polymers also suffer from the fact that their electrochemical stability is relatively low in aqueous solution [7, 8]. On the other hand, graphene, a novel 2D conductor, presents high conductivity, electrochemical stability as well as *in vitro* biocompatibility [9].

Pristine graphene is a tightly packed two-dimensional honeycomb crystal lattice of sp^2 bonded carbon which is only a single atom thick [10]. Graphene has received increasing scientific attention as a result of its high surface area [11], outstanding electronic conductivity [12, 13], mechanical properties [14], biocompatibility [11] and stable electrochemical performance even in physiological electrolyte [11]. However, there are challenges that need to be addressed to take full advantage of

these excellent properties of pristine graphene. Given the lack of a cost-effective reliable bottom-up approach for the large-scale production of graphene, attention has turned to top-down routes that might be able to deliver low-cost, high quality graphene sheets (*refer to chapter 1 for more detail*) [15].

Among the various methods introduced for the preparation of graphene [15-24], liquid-phase exfoliation of graphite using solvent or surfactants (*refer to chapter 1 for more detail*), revealed promising results. This method has several advantages compared to others (i.e. graphene oxide route) such as production of graphene in a liquid phase without any additional oxidation steps and easy processing of the final products [25]. Processing in a solution not only permits the fabrication of paper-like structures and/or thin films but also, facilitates the introduction of graphene into polymer hosts, simplifying the fabrication of composites [26-28]. As such, solvent- or surfactant-exfoliated graphene has the potential to be employed in composites; this method is of interest in both research and industry [27-30]. For instance, the blending of graphene with chitosan and subsequent production of films can be achieved by dispersing a few layers of surfactant-exfoliated graphene sheets in chitosan solution followed by a solution-casting method [9]. The elastic modulus of graphene composite was up to 200% higher than chitosan film alone. The graphene-chitosan films showed biocompatibility (adhesion and proliferation) for the fibroblast cell line L929 [9]. Zhao *et al. also* reported on increasing the mechanical strength of poly (vinyl alcohol) (PVA) using graphene nanosheets with a 150% improvement of tensile strength and a nearly 10-fold increase of Young's modulus at a graphene loading of 1.8 vol % compared to PVA only films [31].

Poly lactic-co-glycolic acid (PLGA) is a biocompatible, Food and Drug Administration (FDA) approved biodegradable polymer, which has been utilised extensively in biomedical applications such as scaffolds (*refer to chapter 1 for more detail*). Inducing electrical conductivity to PLGA through the addition of solvent exfoliated graphene can enhance its applications in the biomedical field. Moreover, PLGA-graphene composites in the form of fibres can act as mimetic structures to enhance cell growth and provide guidance with the appropriate topography of fibres. In addition, the capability of fibres to be knitted or braided holds promise for the fabrication of more complex 3D structures to act as tissue-culture scaffolds [32].

In this chapter, liquid phase exfoliated graphene is produced and characterised. Solvent exfoliated graphene is utilised to induce electrical conductivity in PLGA polymer structures. The wet-spinning method is employed to spin electrically conductive and robust composite fibres; followed by materials characterisation of the fibres. In addition, biocompatibility of the fibres is tested *in vitro* against skeletal muscle myoblast (C2C12) cells using fluorescent staining and cryo-scanning electron imaging techniques as well as biological assay.

4.2. Experimental

4.2.1. Materials

Dry expandable graphite flakes (3772) was provided by Asbury Graphite Mills USA. Cyclohexyl-pyrrolidone (CHP) and NMP were from Sigma Aldrich. PLGA (75:25) was purchased from Corbion purac (Singapore).

4.2.2. Solvent exfoliation of graphene

Dry expandable graphite flakes (3772, Asbury Graphite Mills USA) were expanded at 1050 °C for 15 seconds. 150 mg of resultant expanded graphite (EG) was added to 15 ml of CHP to make up a concentration of 10 mg/ml. EG was also dispersed in NMP and DMF (two of the most effective solvents for graphene [33]) for comparison using the same conditions as above. The dispersions were then sonicated in a bath sonicator (Branson B2500R-MTH) for between 2.0 to 96 hr. Aliquots were taken from the dispersions to measure the concentration of graphene as a function of sonication time. Centrifugation (Eppendorf centrifuge 5415D) was performed at 1000 rpm for 45 min. Two-thirds of the supernatant was taken and retained for further characterisations.

4.2.3. Preparation of the spinning solutions

A series of spinning solutions of PLGA in CHP (10 mg/ml to 50 mg/ml) was prepared by dissolving the required amount of PLGA in CHP and stirring overnight. Similarly for the composite formulations, various concentrations of PLGA (10 mg/ml to 50 mg/ml) were dissolved in the graphene/CHP dispersion (5 mg/ml). With this strategy different mass fractions of PLGA to graphene obtained in the spinning solution.

4.2.4. Fabrication methods

In order to evaluate mechanical and electrical properties of the produced graphene, free-standing papers were prepared before the composite production. Free-standing graphene papers were prepared by vacuum filtration onto porous hydrophobic PVDF membranes with 400 nm pore size (Millipore, Australia) followed by washing with ethanol, acetone and water, then oven drying at 70 °C overnight.

In order to prepare the wet-spinning solutions, different amounts of PLGA were added to the graphene dispersion in CHP (conc. 5.0 mg/ml) to achieve concentrations between 1.5 to 0.5 wt.% (Table 4.1). Wet-spinning was carried out at room temperature using isopropanol as a coagulation bath in a vertical set-up (Figure 4.1). In this arrangement, the PLGA-graphene spinning solutions were injected from the top (flow rates between 1.0 to 2.0 ml/hr) into a vertical glass column containing the coagulation bath. As the spinning solution exited the spinneret, the solidification process occurred gradually using a solvent/non-solvent strategy. During solidification, the fibre experiences gravitational force acting on it, resulting in the fibres being stretched during formation. Fibres were collected by winding onto a spool and washed several times using ethanol and water to remove remaining CHP, followed by vacuum oven drying overnight.

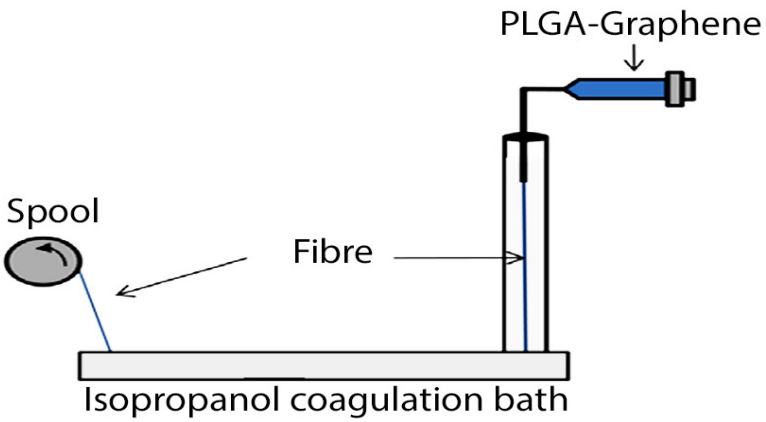

Figure 4.1. Schematic image of vertical wet-spinning set-up.

4.2.5. Characterisation of graphene dispersion

Absorbance measurements of EG in CHP dispersions were carried out using an UV.Vis spectrometer (Shimadzu, UV-3600 UV-VIS-NIR) at 660 nm and applying the Beer–Lambert law to measure the concentration of dispersed graphene [34, 35]. The extinction coefficient (α) was measured for a range of dispersions with known concentrations between 0.01 to 0.05 mg/ml. This resulted in a mean value of α = 3495 L/gm, which is very close to previously reported α = 3620 L/gm for a graphene dispersion in NMP [35]. This value was used for other experiments to determine the weight percentage of graphene in the dispersions using the Beer–Lambert law.

Samples for transmission electron microscopy (TEM) were prepared by depositing a few droplets of 50 µg/ml graphene dispersion on a holey carbon grid followed by vacuum oven drying at 70 °C overnight. These samples were examined using a JEOL JEM-2200FS TEM. The edges of each flake were observed carefully to count the number of layers per flake. Raman spectra were recorded on a Jobin Yvon Horiba

HR800 Raman microscope using a 632 nm laser line and a 300-line grating to achieve a resolution of ± 1.25 1/cm from 1000 1/cm to 3000 1/cm.

For conductivity measurements, 10 ml of diluted dispersion (0.1 mg/ml) was vacuumed filtered on a hydrophobic PVDF membrane then transferred onto a glass slide substrate. Then, samples were washed and oven dried (70 °C overnight) before electrical conductivity measurements. The electrical conductivity of these graphene papers was measured using a JANDEL resistivity system (Model RM2) with a linear four-point probe head.

4.2.6. Rheological characterisation of spinning solutions

Viscosity measurements of PLGA-graphene composite formulations in CHP were investigated in a rheometer (AR-G2 TA Instruments) with a conical shaped spindle (angle: 2°, diameter: 60 mm). Approximately 2.3 ml of solutions with different concentrations of PLGA and mass fraction of graphene were loaded into the rheometer. Viscosity was measured at shear rates between 0.01 to 100 using logarithmic steps (total 200 points). A solvent trap was employed to prevent CHP from evaporating during the test. No pre-stressing conditions were applied to avoid introducing any rearrangement in the system.

4.2.7. Mechanical characterisation of PLGA-graphene fibres

The mechanical properties of the fibres were evaluated by a Shimadzu tensile tester (EZ-S) at a strain rate of 0.5 %/min. The diameter of fibres was measured using an optical microscope. In order to hold the fibres, they were mounted on aperture cards (1.0 cm length window) then fixed using commercial superglue and allowed to air dry. Young's modulus (Y), tensile strength (σ) and breaking strain (ε) were calculated, and the mean and standard deviation reported (n=10).

4.2.8. Thermal gravimetric analysis (TGA) of PLGA-graphene fibres

In order to determine the ratio of graphene to PLGA in the composite fibres, the fibres with different graphene contents wet-spun and when dry were cut into smaller pieces. Small pieces of graphene paper and PLGA fibres were used as control. The applied heating rate of TGA was 1 °C/min in air from room temperature up to 700 ^{o}C.

4.2.9. Electrical conductivity characterisation

*C*onductivity of the fibres was measured using a linear four-point probe conductivity cell with uniform 2.3 mm spacing between probes. The fibres were connected to the electrodes using silver paint. A galvanostat current source (Princeton Applied research Model ED402), with currents in the range of 1, 10, 100 and 1000 μA, and digital multimeter (HP Agilent 34401A) were used to obtain the conductivity (under laboratory humidity and temperature conditions).

4.2.10. Cyclic voltammetry

A 3-electrode cell was used to characterise the electrochemical behavior of the PLGA-graphene fibres. A potentiostat (Princeton Applied research Model ED402) controlled by of EChem version 1.5 software were utilised for cyclic voltammetry. A three-electrode cell was used where the composite fibre was the working electrode, an Ag/AgCl was the reference electrode and a platinum mesh was the auxiliary electrode. All cyclic voltammetric tests were performed in 0.2M PBS (pH~7.4) at scan rates ranging from 10 mV/s to 100 mV/s.

4.2.11. *In vitro* cell characterisation

Skeletal muscle myoblast (C2C12) cell lines from ATCC (American Type Culture Collection) was selected due to availability in our laboratory and cultured in DMEM (Dulbecco's Modified Eagle's Medium, Invitrogen, Sydney, Australia) containing 4 mM L-glutamine (Sigma) and 10% Fetal Bovine Serum (FBS) from Thermo, Noble Park, Victoria. Primary myoblasts were cultured in Hams F10 (Sigma, Sydney, Australia) containing 20% (FBS), 2 mM L-glutamine, 2.5 ng/ml bFGF (Peprotech) and used for experimentation. Antibiotics (penicillin/streptomycin, P/S) were added to culture media for cell growth media on fibres at 1 % (v/v). Cells were cultured at 37 °C in a humidified, 5% CO_2 atmosphere and were subcultured twice weekly when they reached approximately 90 % confluence.

Calcein AM staining and cryo SEM imaging of cells on PLGA-graphene fibres

5 μM calcein AM in DMSO was added to cell growth media followed by incubation for 15 min in a cells culture environment (37 °C, 5 % CO_2) prior to imaging with a Leica microscope. (*For more details refer to previous chapters*). Additionally, specimens of cells growth on the fibres for cryo SEM imaging were prepared as mentioned in previous chapters.

Pico green cell number assay

Sterilised PLGA-graphene fibres were placed on glass slides in parallel followed by gluing 4-well chamber wells on top of them with silicon glue. Cells were seeded at 15×10^2 cells/cm^2 and allowed to grow for 72 hr at 37 °C in a humidified 5% CO_2 environment. After the incubation period, the growth medium was removed and cells washed 3 times with PBS to remove non-adherent cells. Remaining cells were lysed

by the addition 100 μL of 0.1% (w/v) Triton X-100 in Tris-EDTA buffer per well, followed by a freeze/thaw cycle (-80 °C/37 °C). Cell lysate was then collected and transferred to fresh 96 well plates along with cell number standards prepared by the same method. Lysate was then incubated with PicoGreen QuantIT reagent (Invitrogen) according to the manufacturer's instructions for 15 min, and the fluorescent signal was read utilising a FluoStar Omega with an excitation of 480 nm and an emission of 520 nm. The fluorescent signal obtained was converted to cell number based on cell number standards. Statistical differences were assessed using ANOVA t-test, with a 95% confidence level.

4.3. Results and discussion

4.3.1. Solvent exfoliation of graphite

Successful exfoliation of graphite using organic solvents depends on several parameters including the source of graphite, solvent used and processing conditions [27]. In the method used here, expanded graphite powder was mixed with an organic solvent such as NMP followed by sonication [35, 36]. In order to increase the quality of the dispersion (higher fraction of single layer graphene) and remove the non-exfoliated graphite, centrifugation was applied [35, 36]. Therefore, the correct choice of starting material (graphite), solvent used and sonication time are the parameters which were considered to obtain graphene dispersions with higher loading, good stability and enhanced electrical properties.

Thermal expansion of graphite

In order to increase the efficiency of the exfoliation process, the initial spacing between the graphite layers (in the graphite precursor) was increased by solid-state exfoliation of graphite (thermal expansion). The solid-state exfoliation of graphite has resulted in facilitating the production of graphene oxide [37]. Solid-state exfoliation of graphite was achieved by thermal expansion of graphite at an elevated temperature (1050 ^{o}C for 15 sec). At such a high temperature, solid-state exfoliation takes place due to a quick gasification and decomposition of the intercalated compounds such as sulfur groups, which builds up extremely high pressure between graphite layers that exceed the van der Waals forces holding the graphene sheets together [37]. As a result, expandable graphite flakes are transformed to a worm shape expanded graphite structure (Figure 4.2-B and C) with much higher spacing

between the edges of graphite layers as shown in the SEM image. These open edges can facilitate solvent diffusion and easier exfoliation.

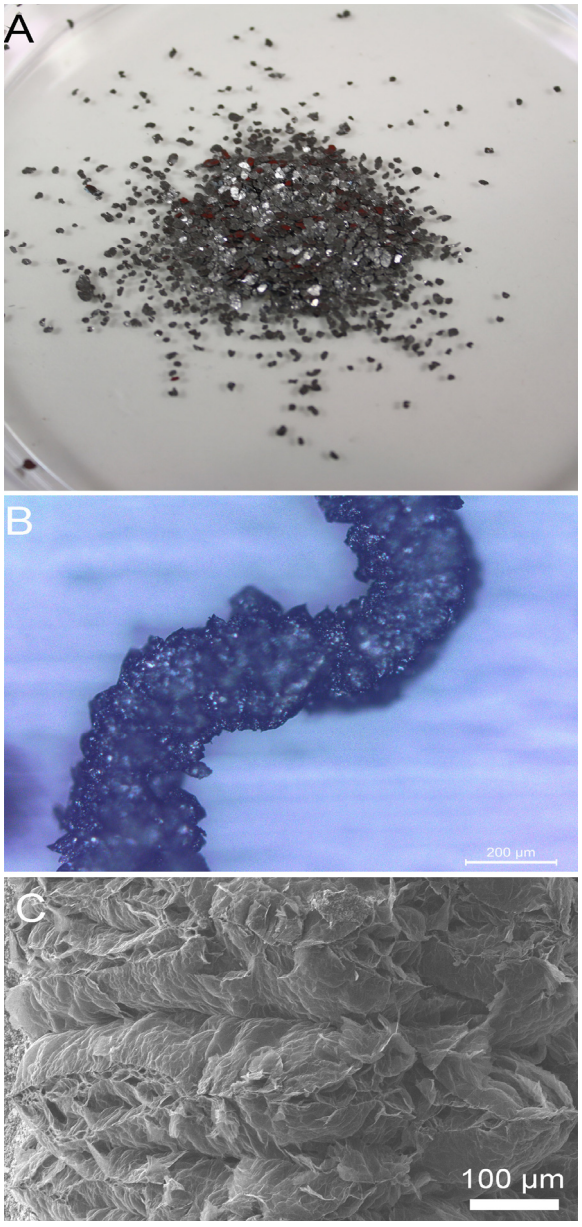

Figure 4.2. A) Image of graphite before thermal expansion. B) Optical microscopy image of a worm shape thermally expanded graphite. C) SEM micrograph of thermally expanded graphite at high resolution shows open edges, which can facilitate the diffusion of solvents during the solvent exfoliation process.

4.3.2. Liquid exfoliation of graphene: the effect of solvent

In order to exfoliate and disperse graphene in a solvent, there should be a strong interaction between the solvent and the edges of graphite [38]. It has been demonstrated that the most effective solvents to disperse graphene have a surface tension of ~ 40 mJ/m^2 [38, 39]. Amongst the different organic solvents which are reported to be effective for solvent exfoliation of graphene, NMP [35] and DMF [40] (with surface tensions of ~ 41.1 mJ/m^2 and 37.1 mJ/m^2, respectively) have been shown to be most effective [35, 40, 41]. Therefore, they were considered for liquid exfoliation of graphene in this thesis. In addition, cyclohexyl-pyrrolidone (CHP), which has a surface tension of 38.8 mJ/m^2 and is an effective solvent for SWNTs [42], was also considered for solvent exfoliation of graphene in this thesis for the first time.

Figure 4.3 shows expanded graphite (EG) dispersions in CHP, DMF and NMP after 8.0 hr bath sonication and left overnight. DMF could not disperse graphene at all and the graphite particles remained intact after the sonication. In the case of NMP, graphite turned to fine particles after sonication which entirely settles down at the bottom of the vial after overnight resting, thus leaving the supernatant liquid colourless.. On the other hand, the dispersion of EG in CHP was stable with only some small particles precipitated after overnight resting.

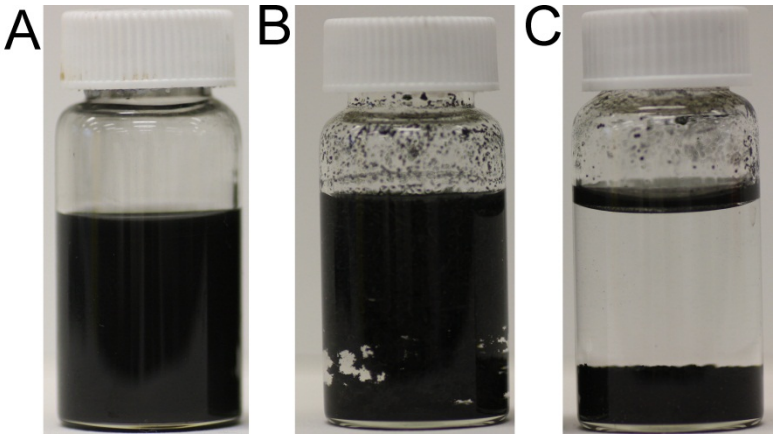

Figure 4.3. Expanded graphite (EG) dispersions in different solvents after 8.0 hr sonication and overnight resting. A) CHP, B) DMF, and C) NMP.

Optical microscopy was employed to evaluate the quality of the dispersed graphite (Figure 4.4). In the case of DMF, large graphite pieces were observed after the sonication process. In terms of NMP, graphite particles broke down to smaller sizes, but they were still large enough to be identified under the microscope. However, CHP contained much finer particles (Figure 4.4-C). The non-exfoliated graphite particles were removed by mild centrifugation (1000 rpm for 45 min), giving a homogeneous and clear dispersion. Therefore, no macroscopic particles/agglomerations could be observed in the final dispersion of graphene in CHP (Figure 4.4-D). It is worth noting that, no precipitation of particles was observed for the centrifuged sample, even after being left to stand for one month.

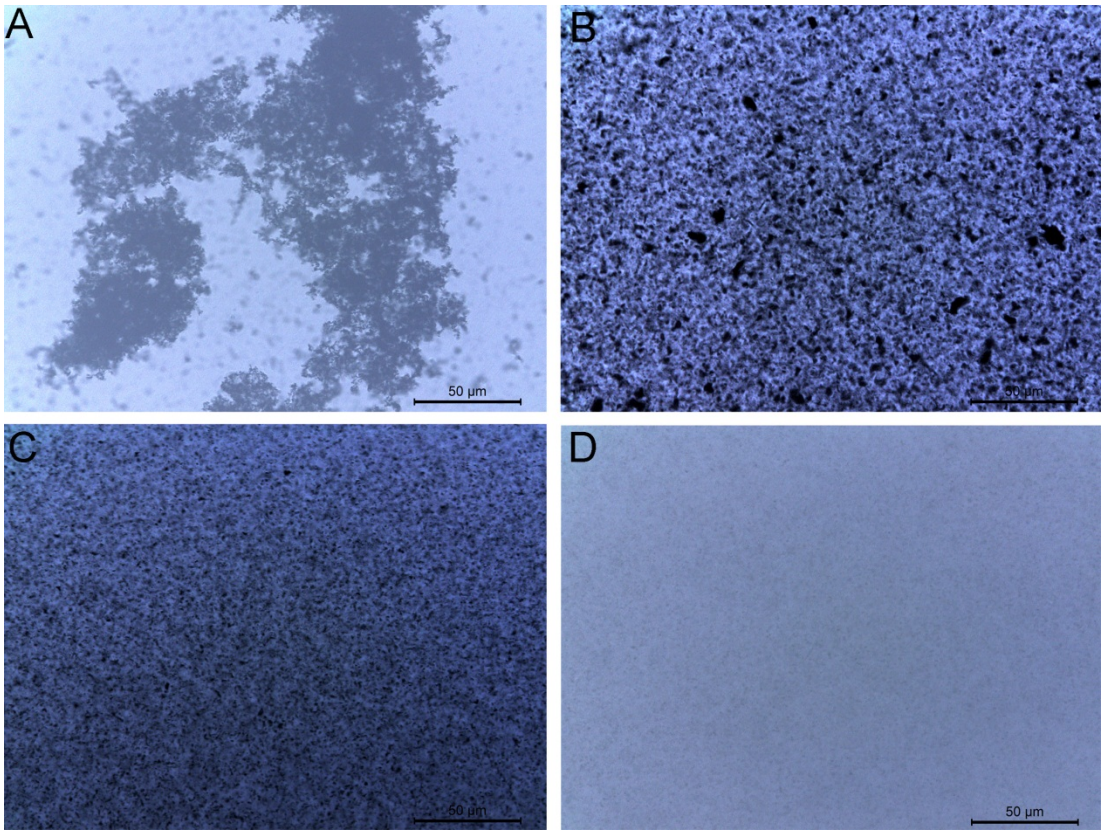

Figure 4.4. A-C) Optical microscopy images of dispersed graphene in various solvents, taken immediately after 95 hr sonication. A) DMF, B) NMP, C) CHP, and D) CHP dispersed graphene centrifuged at 1000 rpm for 45 min.

NMP and DMF have been reported to be very effective dispersants for graphene [27, 28, 33, 35], however, we found that they were ineffective for the dispersion of EG prepared as described. This discrepancy can be due to the difference between functional groups in natural graphite that do not exist in the case of EG. It should be noted that almost all of the available natural graphite contains a portion of impurities and defects, as indicated by the D band in their Raman spectra [15, 22]. Figure 4.5 compares the Raman spectra of expandable graphite before and after thermal expansion.

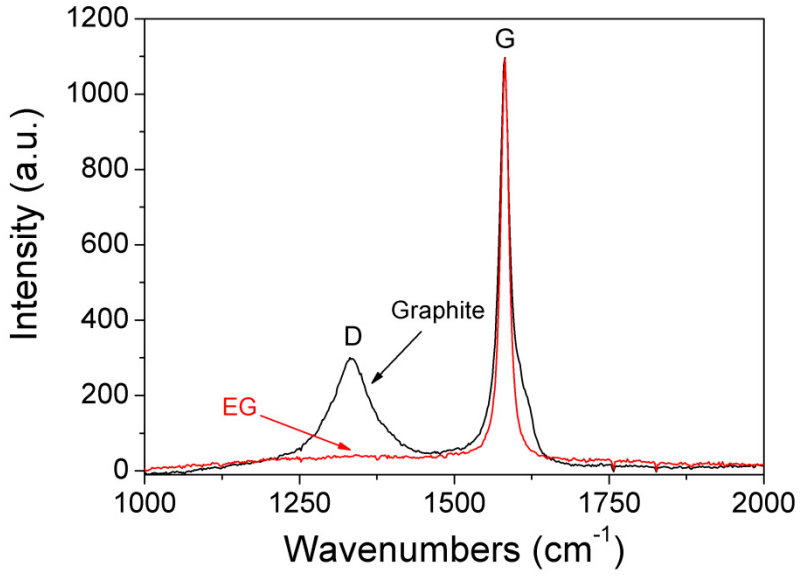

Figure 4.5. Raman spectra of graphite and expanded graphite (EG) recorded using 630 nm laser line. Spectra are normalised for the G band at ~1582 1/cm.

Raman spectra of graphite and EG are characterised by two sharp peaks between 1000 to 2000 1/cm as follows: the D band at 1325 1/cm and G band at 1582 1/cm. The G band corresponds to phonons at the Brillouin zone centre [43]. The D band is either due to breathing modes of sp^2 rings or carbon bonds of sp^3 nature (present at the edges or functional groups) [43, 44]. Graphite (before expansion) has a significant D band, which is commonly seen in natural graphite due to the presence of impurities and functionalities. In the case of expanded graphite, almost no defect-induced peak (D band) was observed as a result of thermal treatment at an elevated temperature (1050 ^{o}C). However, very low defect density in the expanded graphite (manifested itself through the absence of the D band) is preferable for the production of high conducting graphene dispersion, and the absence of functional groups resulted in NMP and DMF being non-effective for exfoliation.

Impurities and functionalities in natural graphite might cause some fluctuations in the surface energy of the graphite. NMP has been reported as the most effective solvent in terms of liquid exfoliation and stability of graphene dispersions [35]. This might be due to the fact that NMP can act as a good solvent for graphite containing some impurities and defects (presence of D band in Raman spectrum) [35]. On the other hand, low surface functionality and the defect-free nature of EG made NMP less effective than CHP. It worth noting that CHP is the best solvent for dispersing single-walled carbon nanotubes which are a kind of defect free/low defect graphite [39]. This finding suggests that CHP is a suitable solvent for dispersing defect free/low defect graphite either in the form of single-walled carbon nanotubes or thermally expanded graphite.

Transmission electron microscopy (TEM) was carried out to analyse the exfoliation state of the dispersed material in CHP. There are always some errors involved in the determination of the number of layers per flake, as the edges of flakes might not be very sharp. Careful examination of the edges of a graphene flake at high resolution showed that the dispersion contained some monolayer graphene (Figure 4.6) and some multilayers. Electron diffraction patterns also proved the presence of monolayers [41, 45]. The images in Figure 4.6 A and B are TEM images and electron diffraction patterns taken from what appears to be a graphene monolayer and in Figure 4.6 C and D as graphene multilayers.

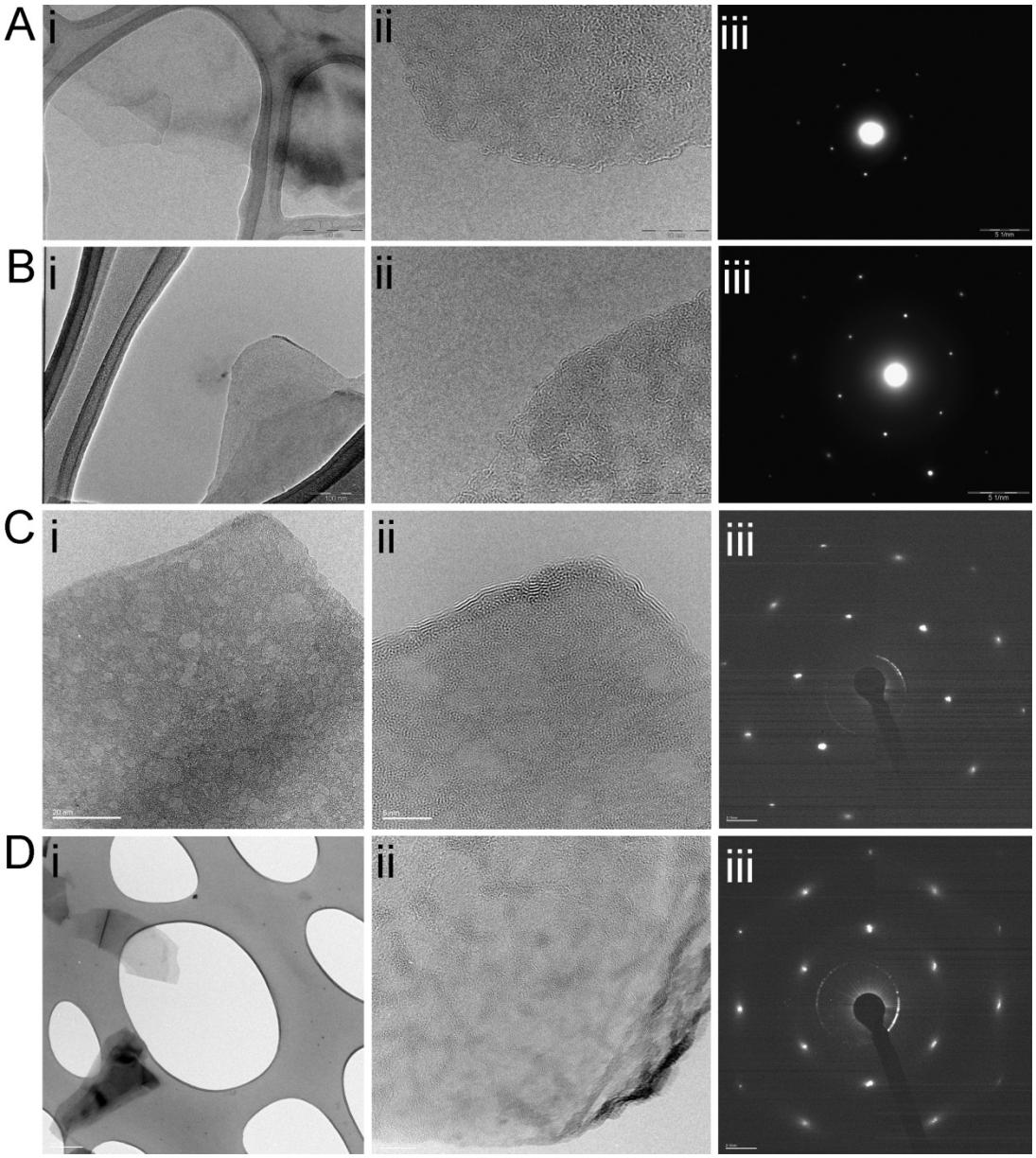

Figure 4.6. TEM micrographs of graphene flakes dispersed in CHP and the corresponding electron diffraction patterns. Images A and B (i and ii) appear to be monolayers whereas C and D (i and ii) are multilayer graphene. Images A and B (iii) illustrate the electron diffraction patterns of monolayers, and C and D (iii) images show the diffraction patterns of multilayer graphene.

4.3.3. Preparation of graphene paper

In order to demonstrate the processability of the solvent exfoliated graphene, the dispersion was used to prepare free-standing papers similar to those reported for carbon nanotubes [46, 47]. The ability to prepare graphene paper can be useful in many applications such as biomedical applications [7, 11, 48] and energy storage and conversion [49, 50]. Free-standing papers with thicknesses in the range of 5.0 μm to 100 μm were prepared through filtration of different amounts of graphene dispersions. The papers are robust and can be bent without breaking. Figure 4.7 shows an image of a free-standing graphene paper prepared by vacuum filtration of graphene in CHP (5.0 mg/ml) with a thickness of ~ 100 μm.

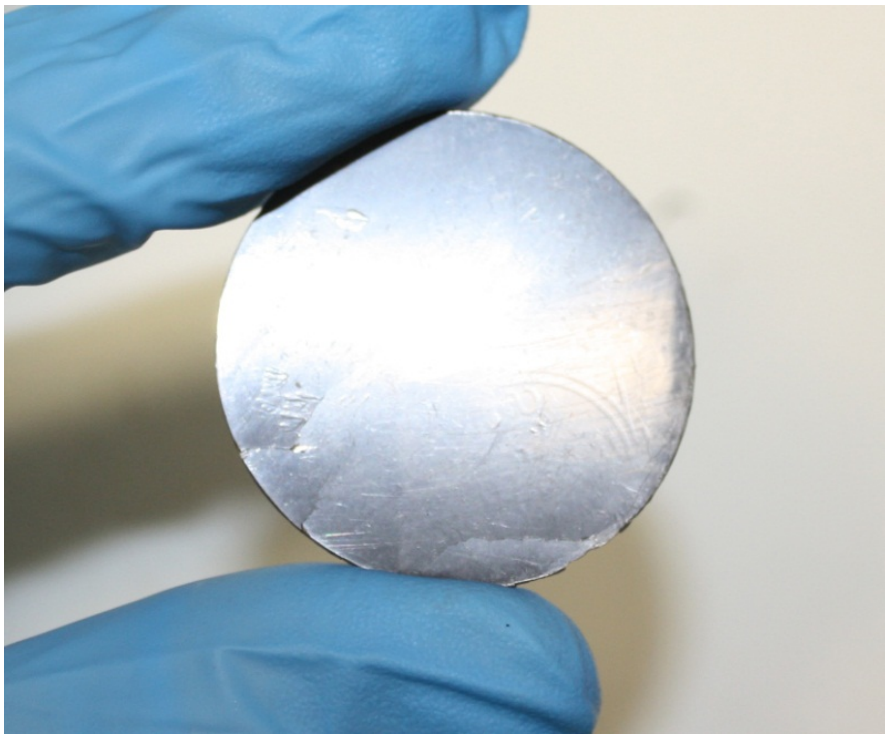

Figure 4.7. A photograph of a free-standing graphene paper (thickness of ~ 100 μm) prepared from a dispersion of graphene in CHP (95 hr sonication and centrifuged at 1000 rpm for 45 min).

SEM analysis in Figure 4.8 shows that a free-standing graphene film contains graphene flakes that are well-aligned in the plane of the film. It also displays a well-defined layered morphology (Figure 4.8-B). Although the porosity is fairly high, the graphene flakes building up the paper are reasonably well packed. SEM images (Figure 4.8-C) show that while the graphene needs to aggregate to form the paper, the flakes do not restack in a fully ordered assembly similar to graphite, and small multilayers have a tendency to restack arbitrarily on top of each other.

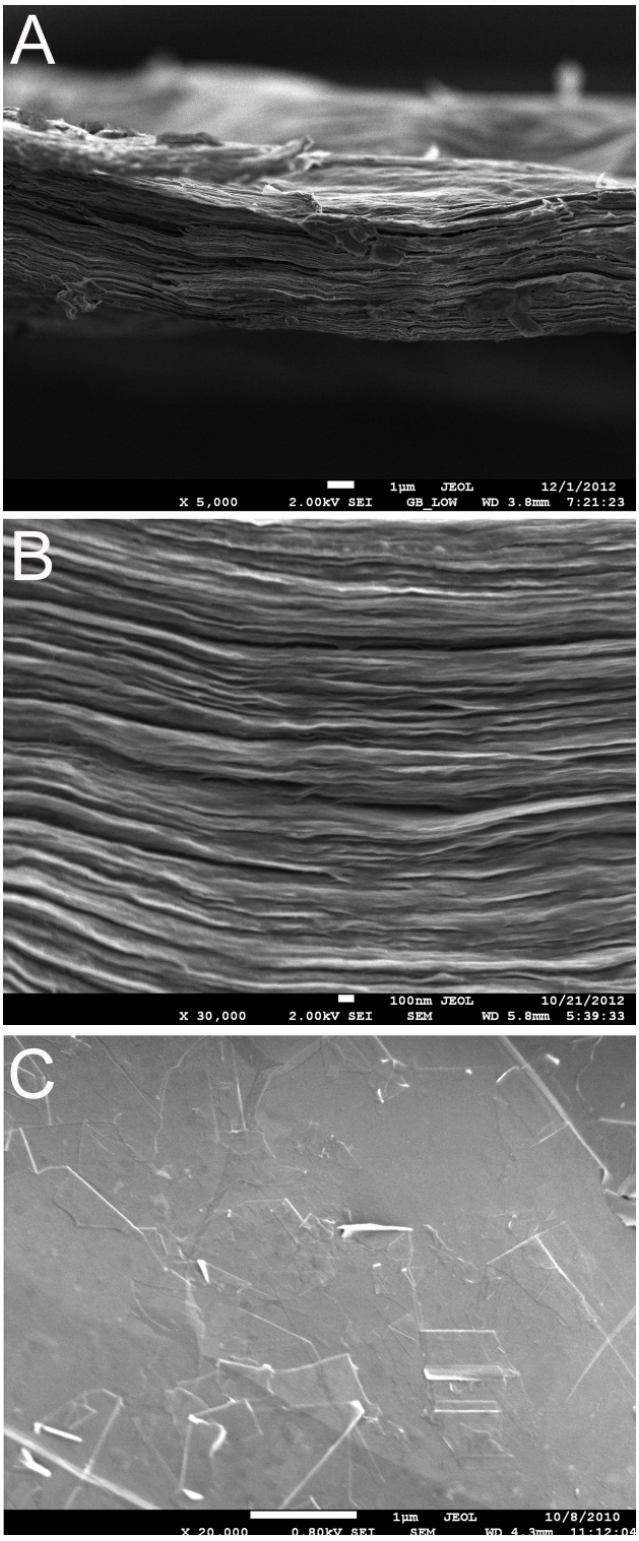

Figure 4.8. SEM micrograph of A) a cross-section of a free-standing graphene paper, B) a cross-section at higher magnification, and C) the surface of the free-standing paper. (graphene/CHP obtained after 95 hr sonication and centrifuged at 1000 rpm for 45 min).

The random stacking of graphene sheets in the free-standing paper is confirmed by the Raman spectra of the graphene paper. Figure 4.9 shows Raman spectra of expanded graphite and graphene paper. The graphene paper 2D peak is a single peak due to the turbostratic nature of disordered graphene layers, while in expanded graphite, the 2D peak consists of two peaks due to Bernal stacking of graphite [25]. Raman spectra of the papers show 2D bands previously reported for graphene flakes of three to five layers [25, 34, 44]. Prevention of the ordered restacking of the graphene flake preserved the electronic structure of the few layers graphene resulting in the observed Raman spectra.

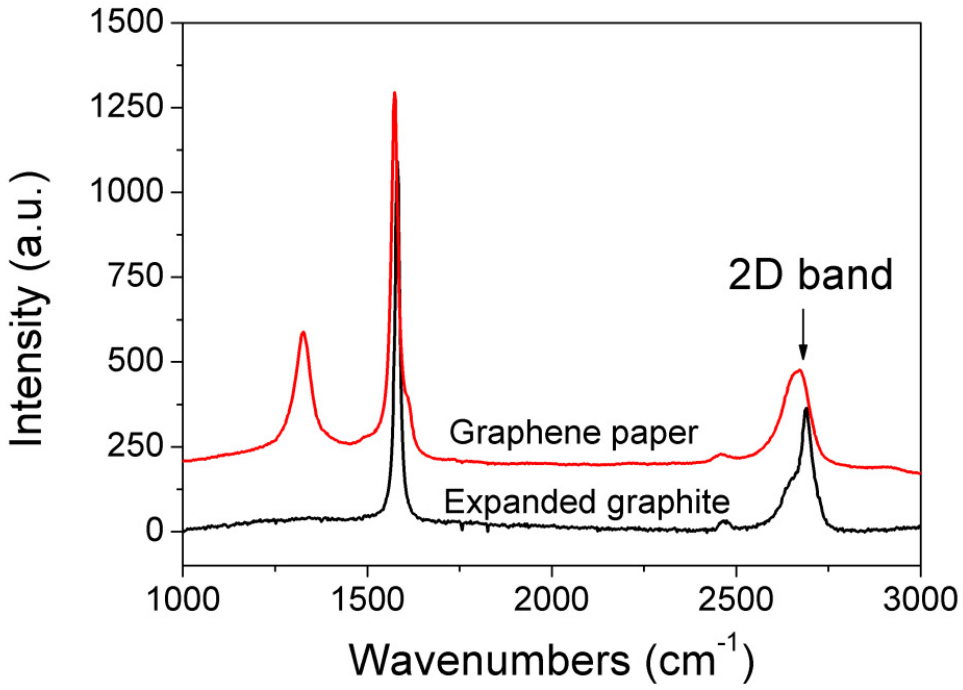

Figure 4.9. Raman spectra of the free-standing graphene paper and expanded graphite.

Free-standing graphene paper with 6.0 μm thickness had a conductivity of 310 ± 20 S/cm which is higher than the conductivity of free-standing graphene paper prepared by either surfactant exfoliated graphite (70 S/cm [34]) or NMP exfoliated graphite (180 S/cm [35]). This superior conductivity is due to the defect-free nature of the expanded graphite used as graphene precursor (discussed earlier) and makes these graphene dispersions an excellent choice for production of highly conducting composites.

4.3.4. Increasing the concentration of graphene

Solvent exfoliated graphene can be used in a range of applications including in the formation of composites. Preparing highly conducting graphene at a high concentration in solution is necessary to facilitate production of highly conducting composites with high loading of graphene [30, 51, 52].

The initial concentration of EG in CHP was limited to 10 mg/ml due to the fact that higher concentrations of EG (~300 times higher volume than graphite) could not be wetted by CHP. Therefore, 10 mg/ml of EG in CHP was selected for graphene preparation.

It was also found that by increasing the sonication time (up to 96 hr), more graphene was exfoliated and remained dispersed in CHP after centrifugation. The concentration of dispersed graphene measured by UV.Vis as a function of sonication time is plotted in Figure 4.10.

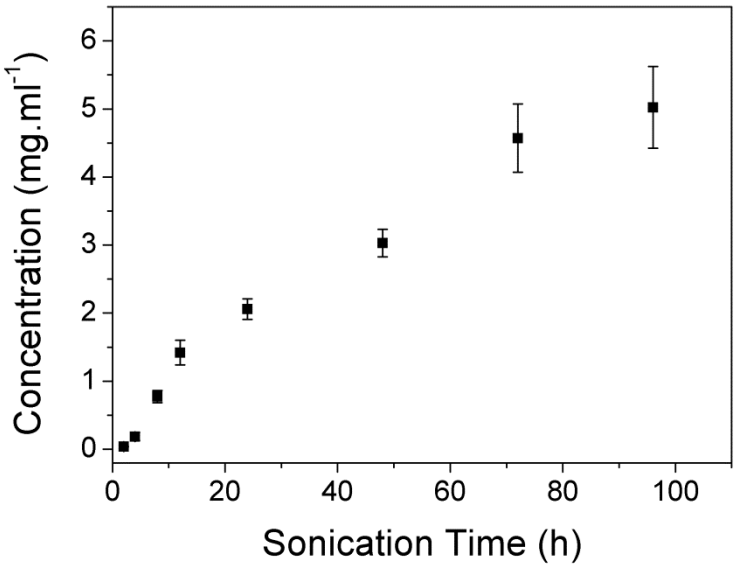

Figure 4.10. Graphene concentration as a function of sonication time. 10 mg/ml EG in CHP was dispersed using sonication followed by centrifugation at 1000 rpm for 45 min. The concentration refers to the graphene content in the resulting supernatant.

As sonication time was increased, more graphene was dispersed into the solvent up to the highest concentration at ~ 5.0 mg/ml (0.5 wt. %) after 96 hr sonication (yield of ~50%). This concentration is significantly higher than the previously reported values for graphene dispersed in NMP (1.2 mg/ml) obtained after even longer bath sonication times (460 hr) [35]. This concentration is also higher than most of the reported values for liquid phase exfoliation of graphene (see Table 1.1). As discussed earlier, solid-state exfoliation of graphite (thermal expansion) facilitates the solvent diffusion in between graphite layers to enhance the graphene exfoliation. This solid-state exfoliation was the key factor in achieving high concentrations of dispersed graphene at a much shorter sonication time.

4.3.5. Formulation of PLGA-graphene wet-spinning solutions

Since solvent exfoliation of graphene resulted in a stable dispersion with graphene concentration as high as 5 mg/ml, it is expected that the graphene formulation has the potential to be used as a filler in composite materials. Composite development can be facilitated by utilising the exfoliated graphene in liquid to give high concentration of mono-layer and few-layers graphene sheets (i.e., 5.0 mg/ml here). Apart from the high concentration of graphene, which can allow for a high mass fraction of graphene in a composite, the fact that graphene free-standing papers displayed high conductivity (~300 S/cm for the paper made from the highest concentration of graphene in CHP) holds promise for development of highly conducting composites. Therefore, the use of graphene as conducting filler for wet-spun conducting PLGA fibres was investigated.

The spinning solutions were prepared by dissolving the required amount of PLGA into the graphene stock dispersion (see experimental section 4.2.3). Using this method it was possible to systematically control the loading of graphene in the spinning formulation as well as achieving high volume fraction of graphene in the final fibres. Figure 4.11 compares optical microscopy images of the graphene dispersion with the PLGA-graphene composite. The addition of PLGA to the graphene dispersion did not cause any aggregation of graphene flakes (Figure 4.11-B). Optical microscopy images confirmed that there was no agglomeration of the graphene flakes after production of the composite formulation.

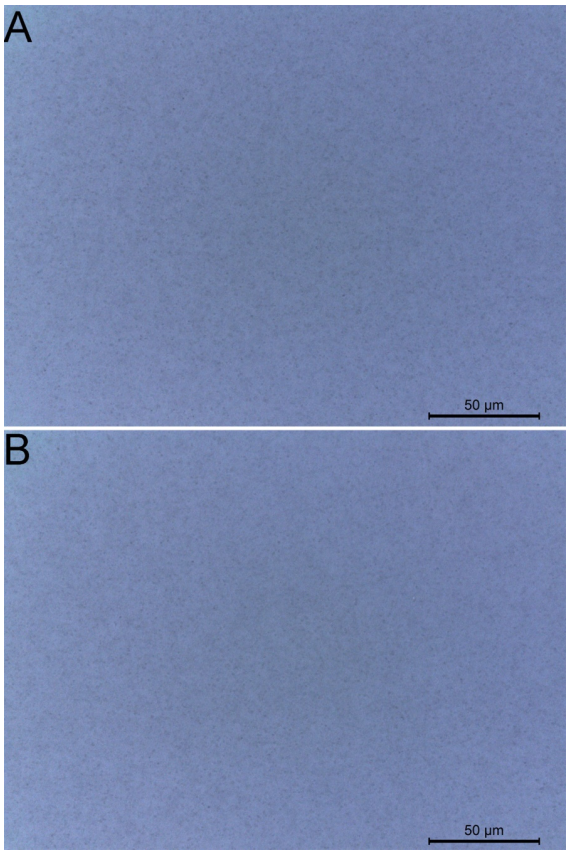

Figure 4.11. Optical microscopy images of: A) dispersed graphene in CHP (0.5 wt. %), B) PLGA-graphene composite in CHP (solution containing 1.5 wt. % PLGA and 0.5 wt. % graphene).

4.3.6. Wet-spinning of fibres containing the highest loading of graphene

One role of PLGA in solution is to increase the viscosity of the solution and consequently provide spinnability. Figure 4.12 compares the viscosity of PLGA and PLGA-graphene composite solutions as a function of solution concentration (from 1.0 wt% to 5.0 wt% of PLGA). As, the concentration of PLGA in CHP increases from 1.0 wt. % to 5.0 wt. %, the viscosity increases from 0.015 Pa s to 0.069 Pa s (Figure 4.12-A).

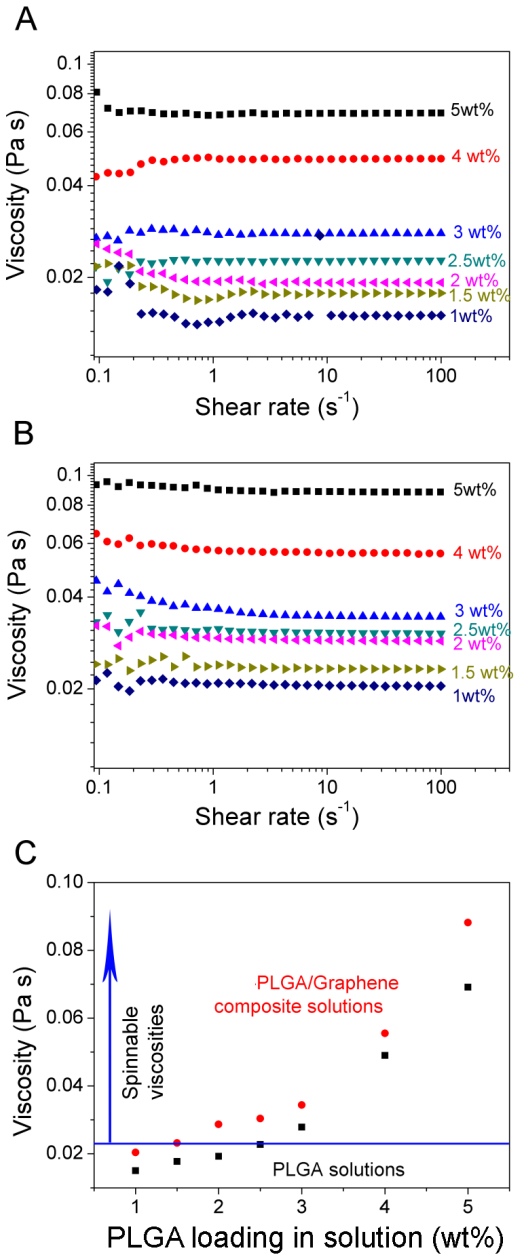

Figure 4.12. Viscosity *vs* shear rate of solutions as a function of PLGA concentration. The mass percentage of PLGA in each solution are indicated next to the corresponding graph in pictures A and B. A) PLGA-only solutions. B) Various concentrations of PLGA dissolved in 5.0 mg/ml graphene CHP stock dispersion (~ 0.5 wt. %). C) Comparison of the viscosity of PLGA and PLGA-graphene solutions as a function of PLGA loading in solution at 100 Pa s shear rate, since the curves levelled out at this shear rate.

All prepared solutions were tested for wet-spinning in order to measure the lowest viscosity (concentration) required for wet-spinning of PLGA solutions. The lowest concentration of PLGA in a spinning solution should result in the highest mass fraction of graphene in the final fibre. The results showed that the lowest viscosity of PLGA required for wet-spinning of continuous PLGA fibres was 0.023 Pa s, corresponding to a PLGA-only concentration of 2.5 wt. %. However, the addition of graphene to the spinning solutions resulted in an increase in the viscosity. Comparing the viscosities of wet-spinnable PLGA-only with PLGA-graphene solutions suggests that a minimum concentration of 1.5 wt. % of PLGA in the composite spinning solution is required. A concentration of 1.5 wt. % and above can provide viscosity of $\geq$ 0.023 Pa s which was found to be spinnable.

Figure 4.13 shows SEM micrographs of PLGA-graphene composite fibres with diameter of 105±6.0 μm obtained from wet-spinning of a solution containing 1.5 wt. % of PLGA and 0.5 wt. % of graphene (0.5 wt. % stock solution of graphene). The surface morphology of the PLGA-graphene composite fibres indicates a smooth surface topography; however, graphene flakes are visible on the cross section of the composite fibre. The observed layered structure, as in the cross-section, is due to the presence of graphene flakes. The image at higher magnification clearly shows homogeneous incorporation of graphene flakes in the composite fibre, confirming the compatibility of the composite formulation and the stability of the graphene even after the spinning process.

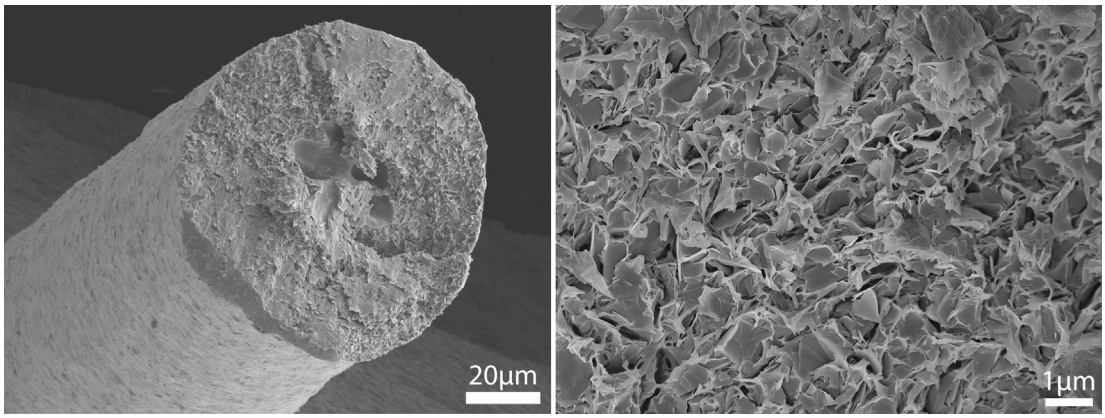

Figure 4.13. A) SEM micrographs of PLGA-graphene composite fibres obtained from wet-spinning of a spinning solution containing 1.5 wt. % PLGA and 0.5 wt. % graphene. B) The cross-sectional FE-SEM images of PLGA/graphene composite fibre confirmed that the graphene flakes were well blended in the composite fibre.

4.3.7. Measuring the mass fraction of graphene from fibres

In order to measure the final mass fraction of graphene in the composite fibres, thermal gravimetric analysis (TGA) was employed. Figure 4.14 shows TGA graphs of dried PLGA-graphene fibres as a function of graphene loading. The measured loadings obtained from TGA are listed in Table 4.1 and compared with the estimated loadings (calculated from the initial spinning solution compositions). The results show a promising correlation between the estimated fractions of graphene in dried fibres with the values measured from TGA graphs.

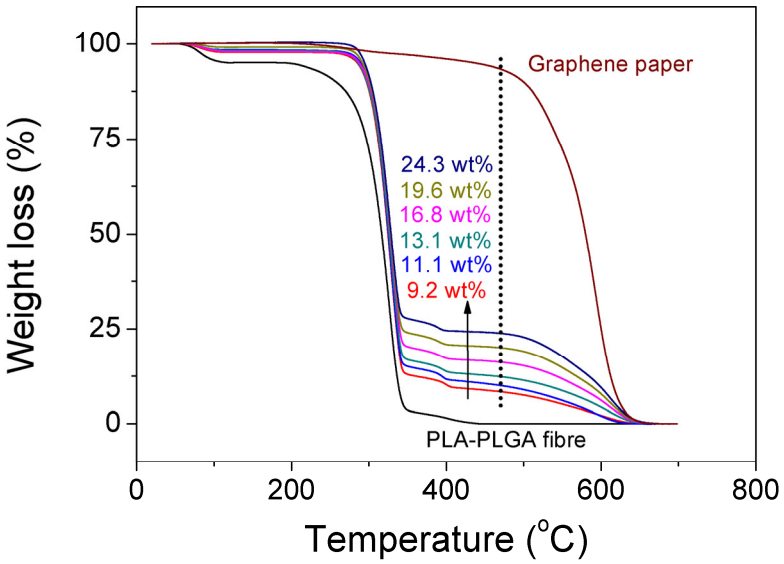

Figure 4.14. TGA graphs of PLGA fibres, graphene paper and PLGA-graphene fibres with different loading percentages of graphene. The measured percentage of graphene in each composite fibre was obtained from TGA traces at 480 °C as indicated on the graph by a dashed line.

Table 4.1. Comparisons between the measured graphene loadings obtained from TGA graphs with the estimated loadings of graphene calculated from the initial spinning solution compositions.

PLGA concentration in the spinning solution (wt. %)	Estimated loading of graphene in dried fibres (wt. %)*	Measured loading of graphene in dried fibres using TGA data (wt. %)#
1.5	25	24.3
2	20	19.6
2.5	16.6	16.8
3	14.3	13.1
4	11.1	11.1
5	9.1	9.2

* The estimated amount of graphene is based on the ratio of PLGA added to the stock solution of graphene (0.5 wt. %).

The measured values were obtained from the TGA traces in Figure 4.14.

4.3.8. Mechanical characterisation of PLGA-graphene fibres

The mechanical properties of PLGA-graphene fibres were evaluated using stress-strain curves (Figure 4.15). Increasing the loading of graphene resulted in significant enhancement in tensile modulus and ultimate stress of composite fibres. At the highest loading (24.3 wt. %) the Young's modulus and tensile strength increased significantly up to 13.6±1.3 GPa and 103 MPa, respectively (647 and 59 folds, respectively) (Table 4.2). The improvement in the mechanical properties can possibly be attributed to the strong interfacial interactions between graphene flakes and the polymer matrix due to the bonding between the functional groups on the edges of the graphene sheets and the hydroxyl groups of the PLGA polymer [53]. On the other hand, when graphene was introduced as filler the strain at break of the fibres dropped due to the loading effect of the graphene in the PLGA matrix [53].

Other similar work has reported 2 and 4 times improvement of the modulus and tensile strength of polyethylene terephthalate fibres respectively, after the addition of ~ 2 wt. % of NMP dispersed graphene [29]. Polyvinyl alcohol-graphene composite from NMP dispersed graphene has resulted in doubling of the modulus and strength of a composite film (loadings <0.4 vol% graphene) [30]. Higher improvement in the mechanical properties of PLGA-graphene fibres reported here is due to higher loading of graphene in the fibres, which were obtained from a high concentration of graphene/CHP dispersion.

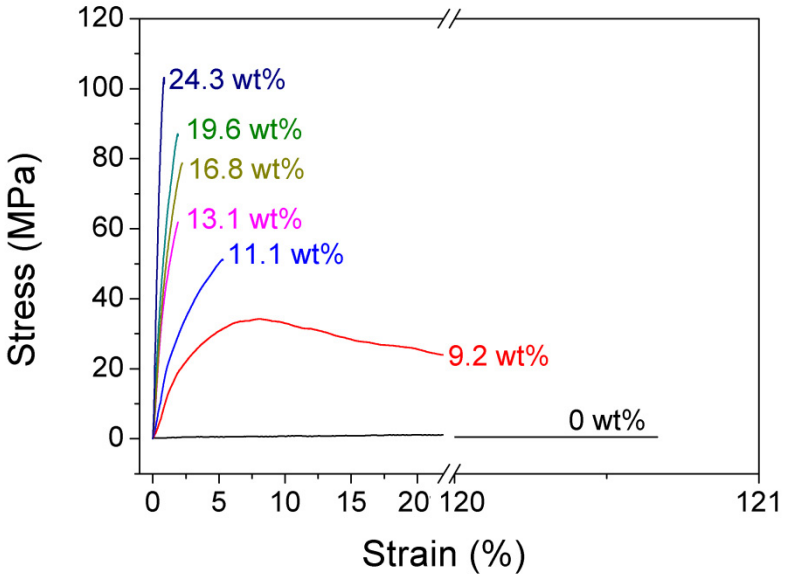

Figure 4.15. Stress-strain curves of PLGA-graphene fibres with different loading percentages of graphene. The numbers represent mass percentage of graphene in the final composite fibres (data obtained from TGA traces in Figure 4.14)

Table 4.2. Mechanical properties of PLGA and PLGA-graphene fibres with different loading percentages of graphene using stress-strain curves.

Graphene content (wt. %)	Young's modulus (GPa)	Ultimate stress (MPa)	Strain at break (%)
0	0.021±0.003	0.58±0.04	121±25
9.2	1.22±0.46	24.3±4	24±3
11.1	3.11±0.45	51.2±5	5.3±0.9
13.1	5.23±0.74	61.7±6	1.9±0.4
16.8	6.14±0.85	78.7±7	2.2±0.3
19.6	7.51±1.1	87.1±8	1.9±0.4
24.3	13.6±1.3	103±5	0.87±0.2

The mechanical properties data in the table are averages of 10 measurements.

4.3.9. Electrical conductivity of PLGA-graphene fibres

By adding graphene to the PLGA fibres (more than 11.1 wt. %), conductivity was induced in the composite system and enhanced by increasing the graphene **content**

(Figure 4.16). Beyond the percolation threshold (11.1 wt. %), the conductivity increased from ~30 S/m to 150 S/m by increasing the loading of the graphene up to 24.3 wt. %. In this system, which includes a non-conducting matrix and conducting filler, the non-conducting matrix limits the charge transfer between the graphene sheets. This is due to the fact that the insulator-coating on graphene results in enhanced contact resistance between the adjacent graphene sheets [54]. Therefore, much lower conductivity obtained from the composite fibres compared to the free-standing graphene paper. However, the conductivity (150 S/m) was more than 5 orders of magnitude higher than carbon nanofibres-PLGA composite nanofibres [55] and 6 orders of magnitude higher than multi-walled carbon nanotube-PLGA nanofibres [56]. Therefore, PLGA-graphene fibres with highest conductivity and graphene content were selected for further tests.

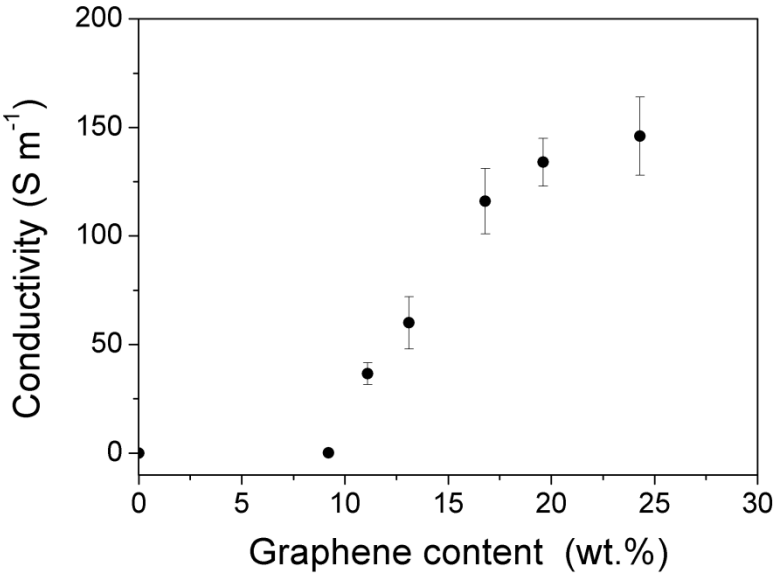

Figure 4.16. Conductivity of PLGA-graphene fibres as a function of graphene content.

4.3.10. Electrochemical characterisation of PLGA-graphene fibres

The cyclic voltammogram (CV) of PLGA-graphene fibres (24.3 wt. %) (Figure 4.17) demonstrates the effect of graphene nanosheets as organic conductors in inducing the electrochemical activity of the fibres. The CV of PLGA-graphene fibres in PBS, which has not been reported in literature so far, confirms the electroactive properties of fibres and shows promise for applying these fibres in biomedical applications.

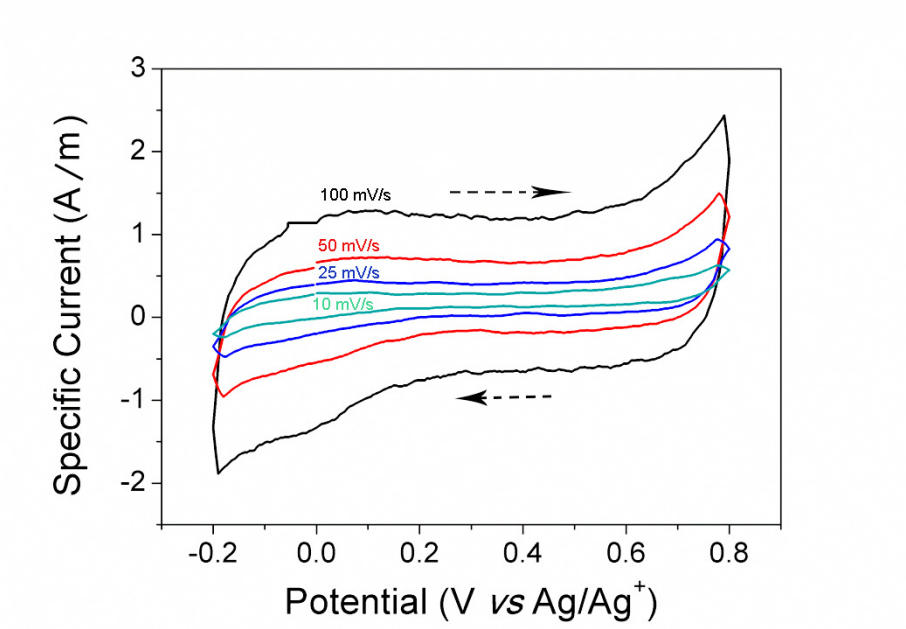

Figure 4.17. Cyclic voltammogram of PLGA-graphene fibres (24.3 wt. %) in PBS as a function of different scan rates (from 10 mV/s to 100 mV/s, E_i = -0.2 V and E_f = 0.8 V). Arrows show the direction of the potential scan.

4.3.11. *In vitro* biocompatibility characterisation of PLGA-graphene fibres

Calcein AM staining imaging of C2C12 on the fibres

In order to confirm the ability to utilise these fibres as biomaterials, the cytotoxicity of fibres was investigated using C2C12 muscle cells. A tissue culture plate was used as control in Calcein AM assay. Studies showed that pristine PLGA did not exhibit cytotoxicity against C2C12 myoblast cells [57, 58] .Figure 4.18 shows the results of calcein AM staining on C2C12 cells revealing metabolically active cells. The results show that cells attached to the fibres and spread along their length well.

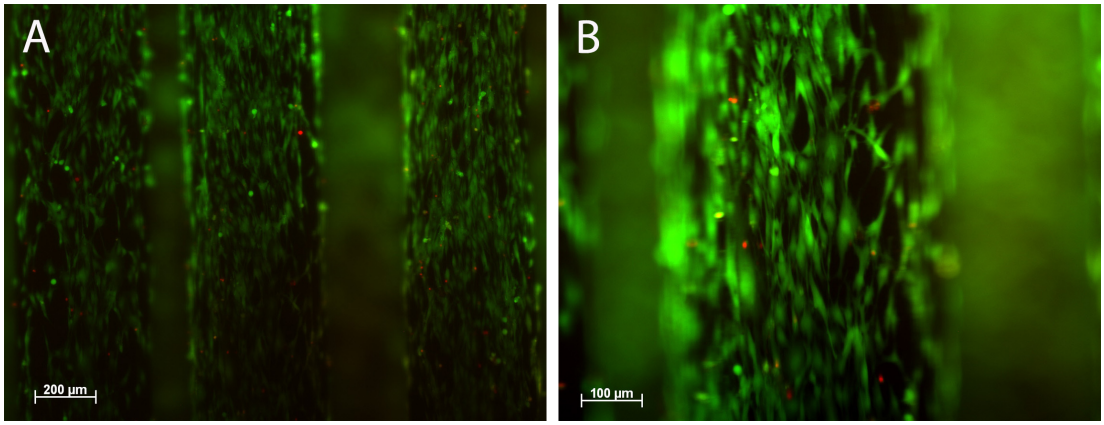

Figure 4.18. Calcein AM stained C2C12 cells on PLGA-graphene fibres (24.3 wt. % graphene loading) after 3 days, green spots represent live cells. A) 10X and B) 20X.

Cryo-SEM imaging of C2C12 cells on the fibres.

Cryo-SEM images of the fibres (Figure 4.19) also show C2C12 myoblast cell attachment and growth. The areas marked with white arrows in Figure 4.19-D show C2C12 myoblast cells attached on the fibres and spread according to the topology of the fibres. Figure 4.19-E illustrates the bridging between myoblast cells. Moreover, attachment and growth of C2C12 cells in direct contact with PLGA-graphene on

fibres (Figure 4.19-F) evaluate the cytotoxicity of PLGA-graphene fibres for C2C12 myoblast cells. Li *et al.* studied the toxicity of different biodegradable graphene derivatives with/out different coatings and showed that graphene oxide with/out coatings has higher toxicity risk compare to reduced graphene oxide [59]. They confirmed that graphene oxide had highest level of toxicity against three different cell lines, human liver cell line, HL-7702, human lung fibroblast cell line MRC-5, and human macrophage line U937, after they incubated for 72 hr on different graphene derivatives [59]. Yang et al. utilised ultra-small reduced graphene oxide with poly ethylene glycol functionalization in phototherapies of cancer [60].

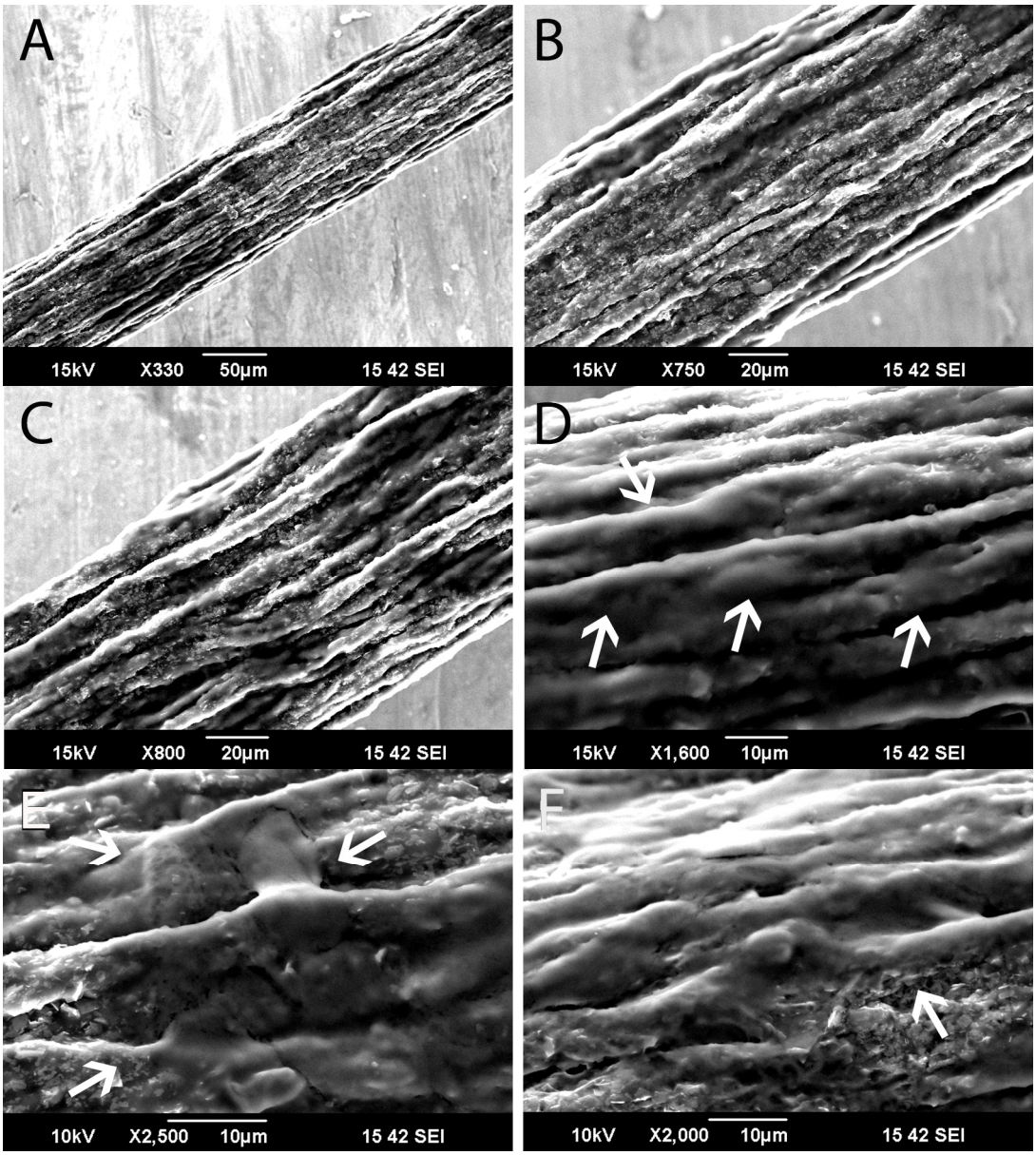

Figure 4.19. Cryo-SEM images of PLGA-graphene fibres with C2C12 myoblast cells on them at different magnifications. The white arrows in image D illustrate the attachment and spread of C2C12 cells on the fibre. The white arrows in image E shows cell-to-cell bridging on the PLGA-graphene fibre. The white arrows in image F represent the growth of cells on graphene nanosheets.

Viability test on C2C12 cells of fibres

C2C12 myoblast cells grown on the PLGA-graphene fibres and on glass slides (as a control) were subjected to a Pico green assay to characterise the viability of cells quantitatively. Figure 4.20 presents the number of viable cells on the fibres and glass slide within three days and shows the growth of cells increased ($p^* < 0.05$) over a 72 hr period on fibres however there was no significant difference in cell growth between fibres or glass slide after 72 hr. These results confirm the proliferation of C2C12 cells on fibres and glass slides. To conclude, the cells were keen to proliferate over 72 hr on PLGA-graphene fibres.

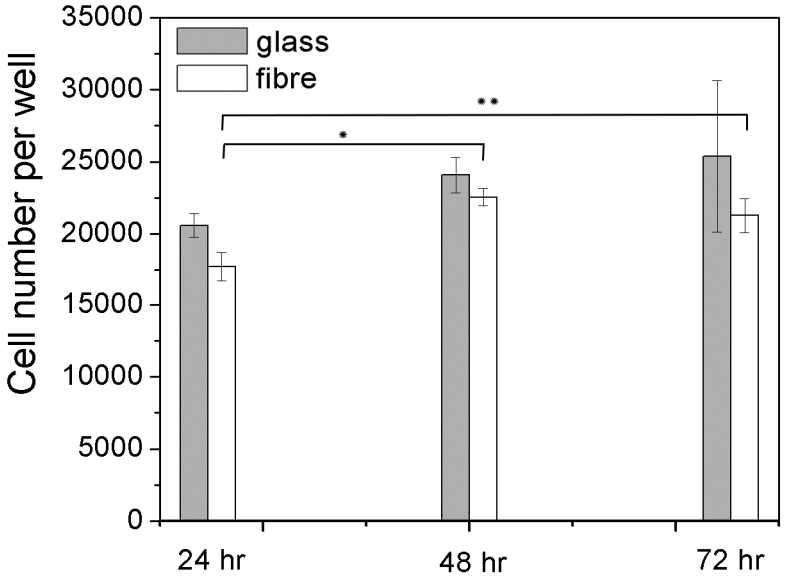

Figure 4.20. Pico green cell number assay on C2C12 myoblast cells on PLGA-graphene fibres and glass slide within 72 hr. The stars represent 95% significant confidence level in ANOVA t-test and the bars show selected groups for comparison.

4.4. Conclusion

It has been demonstrated that employing thermally expanded graphite instead of natural graphite as precursor for solvent exfoliation of graphene results in much lower sonication time and much higher graphene concentration, with a stable dispersion obtained. Thermal expansion removes most of the functional groups and results in improved maintenance of electronic properties of the final graphene sheets. This preservation of electronic properties was utilised to prepare PLGA-graphene fibres with high electrical conductivity and electrochemical activity. The PLGA-graphene fibres had a conductivity of ~30 S/m with 11.1 wt. % graphene loading and it increased to 150 S/m when the graphene content was 24.3 wt. %. The composite fibres possessed appropriate mechanical properties; with Young's modulus between 1.22±0.46 to 13.6±1.3 GPa depended on the loading of graphene. Additionally, the calcein AM fluorescent staining and Cryo-SEM images showed that C2C12 myoblast cells were metabolically active, attached to the surface of fibres and spread along it. The results of Pico green cell number assay also showed that cells were active and proliferated along the fibres during 72 hr.

4.5. References

[1] Quigley AF, Razal JM, Kita M, Jalili R, Gelmi A, Penington A, Ovalle-Robles R, Baughman RH, Clark GM, Wallace GG, Kapsa RMI. "*Electrical Stimulation of Myoblast Proliferation and Differentiation on Aligned Nanostructured Conductive Polymer Platforms*". Advanced Healthcare Materials. 2012;**1**(6):801-8.

[2] Esrafilzadeh D, Razal JM, Moulton SE, Stewart EM, Wallace GG. "*Multifunctional conducting fibres with electrically controlled release of ciprofloxacin*". Journal of Controlled Release. (0).

[3] Luo S-C. "*Conducting Polymers as Biointerfaces and Biomaterials: A Perspective for a Special Issue of Polymer Reviews*". Polymer Reviews. 2013;**53**(3):303-10.

[4] Razal JM, Gilmore KJ, Wallace GG. "*Carbon nanotube biofiber formation in a polymer-free coagulation bath*". Adv Funct Mater. 2008;**18**(1):61-6.

[5] Granero AJ, Razal JM, Wallace GG, in het Panhuis M. "*Conducting gel-fibres based on carrageenan, chitosan and carbon nanotubes*". Journal of Materials Chemistry. 2010;**20**(37):7953-6.

[6] Zong X, Bien H, Chung C-Y, Yin L, Fang D, Hsiao BS, Chu B, Entcheva E. "*Electrospun fine-textured scaffolds for heart tissue constructs*". Biomaterials. 2005;**26**(26):5330-8.

[7] Moulton SE, Higgins MJ, Kapsa RMI, Wallace GG. "*Organic Bionics: A New Dimension in Neural Communications*". Advanced Functional Materials. 2012:n/a-n/a.

[8] G.Wallace G, Moulton S, Kapsa RMI, MichaelHiggins. Organic Bionics. Weinheim: Wiley-VCH Verlag GmbH & Co. KGaA
2012.

[9] Fan H, Wang L, Zhao K, Li N, Shi Z, Ge Z, Jin Z. "*Fabrication, Mechanical Properties, and Biocompatibility of Graphene-Reinforced Chitosan Composites*". Biomacromolecules. 2010;**11**(9):2345-51.

[10] Geim AK, Novoselov KS. "*The rise of graphene*". Nat Mater. 2007;**6**(3):183-91.

[11] Chen H, Müller MB, Gilmore KJ, Wallace GG, Li D. "*Mechanically Strong, Electrically Conductive, and Biocompatible Graphene Paper*". Advanced Materials. 2008;**20**(18):3557-61.

[12] van den Brink J. "*Graphene: What lies between*". Nat Mater. 2010;**9**(4):291-2.

[13] Balog R, Jorgensen B, Nilsson L, Andersen M, Rienks E, Bianchi M, Fanetti M, Laegsgaard E, Baraldi A, Lizzit S, Sljivancanin Z, Besenbacher F, Hammer B, Pedersen TG, Hofmann P, Hornekaer L. "*Bandgap opening in graphene induced by patterned hydrogen adsorption*". Nat Mater. 2010;**9**(4):315-9.

[14] Lee C, Wei X, Kysar JW, Hone J. "*Measurement of the Elastic Properties and Intrinsic Strength of Monolayer Graphene*". Science. 2008;**321**(5887):385-8.

[15] Hernandez Y, Nicolosi V, Lotya M, Blighe FM, Sun Z, De S, McGovern IT, Holland B, Byrne M, Gun'Ko YK, Boland JJ, Niraj P, Duesberg G, Krishnamurthy S, Goodhue R, Hutchison J, Scardaci V, Ferrari AC, Coleman JN. "*High-yield production of graphene by liquid-phase exfoliation of graphite*". Nat Nano. 2008;**3**(9):563-8.

[16] Novoselov KS, Geim AK, Morozov SV, Jiang D, Zhang Y, Dubonos SV, Grigorieva IV, Firsov AA. "*Electric Field Effect in Atomically Thin Carbon Films*". Science. 2004;**306**(5696):666-9.
[17] Sutter PW, Flege J-I, Sutter EA. "*Epitaxial graphene on ruthenium*". Nat Mater. 2008;**7**(5):406-11.
[18] Kosynkin DV, Higginbotham AL, Sinitskii A, Lomeda JR, Dimiev A, Price BK, Tour JM. "*Longitudinal unzipping of carbon nanotubes to form graphene nanoribbons*". Nature. 2009;**458**(7240):872-6.
[19] Amini S, Garay J, Liu G, Balandin AA, Abbaschian R. "*Growth of large-area graphene films from metal-carbon melts*". Journal of Applied Physics. 2010;**108**(9):094321--7.
[20] Choucair M, Thordarson P, Stride JA. "*Gram-scale production of graphene based on solvothermal synthesis and sonication*". Nat Nano. 2009;**4**(1):30-3.
[21] Sun Z, Yan Z, Yao J, Beitler E, Zhu Y, Tour JM. "*Growth of graphene from solid carbon sources*". Nature. 2010;**468**(7323):549-52.
[22] Nuvoli D, Valentini L, Alzari V, Scognamillo S, Bon SB, Piccinini M, Illescas J, Mariani A. "*High concentration few-layer graphene sheets obtained by liquid phase exfoliation of graphite in ionic liquid*". Journal of Materials Chemistry. 2011;**21**(10):3428-31.
[23] Lotya M, Hernandez Y, King PJ, Smith RJ, Nicolosi V, Karlsson LS, Blighe FM, De S, Wang Z, McGovern IT, Duesberg GS, Coleman JN. "*Liquid Phase Production of Graphene by Exfoliation of Graphite in Surfactant/Water Solutions*". Journal of the American Chemical Society. 2009;**131**(10):3611-20.
[24] Cui X, Zhang C, Hao R, Hou Y. "*Liquid-phase exfoliation, functionalization and applications of graphene*". Nanoscale. 2011;**3**(5):2118-26.
[25] Behabtu N, Lomeda JR, Green MJ, Higginbotham AL, Sinitskii A, Kosynkin DV, Tsentalovich D, Parra-Vasquez ANG, Schmidt J, Kesselman E, Cohen Y, Talmon Y, Tour JM, Pasquali M. "*Spontaneous high-concentration dispersions and liquid crystals of graphene*". Nat Nano. 2010;**5**(6):406-11.
[26] Stankovich S, Dikin DA, Dommett GHB, Kohlhaas KM, Zimney EJ, Stach EA, Piner RD, Nguyen ST, Ruoff RS. "*Graphene-based composite materials*". Nature. 2006;**442**(7100):282-6.
[27] Hernandez Y, Nicolosi V, Lotya M, Blighe FM, Sun Z, De S, McGovern IT, Holland B, Byrne M, Gun'Ko YK, Boland JJ, Niraj P, Duesberg G, Krishnamurthy S, Goodhue R, Hutchison J, Scardaci V, Ferrari AC, Coleman JN. "*High-yield production of graphene by liquid-phase exfoliation of graphite*". Nat Nanotechnol. 2008;**3**(9):563-8.
[28] Coleman JN. "*Liquid Exfoliation of Defect-Free Graphene*". Accounts of Chemical Research. 2012.
[29] Khan U, Young K, O'Neill A, Coleman JN. "*High strength composite fibres from polyester filled with nanotubes and graphene*". Journal of Materials Chemistry. 2012;**22**(25):12907-14.
[30] May P, Khan U, O'Neill A, Coleman JN. "*Approaching the theoretical limit for reinforcing polymers with graphene*". Journal of Materials Chemistry. 2012;**22**(4):1278-82.
[31] Zhao X, Zhang Q, Chen D, Lu P. "*Enhanced Mechanical Properties of Graphene-Based Poly(vinyl alcohol) Composites*". Macromolecules. 2010;**43**(5):2357-63.
[32] Lu HH, Cooper Jr JA, Manuel S, Freeman JW, Attawia MA, Ko FK, Laurencin CT. "*Anterior cruciate ligament regeneration using braided*

biodegradable scaffolds: in vitro optimization studies". Biomaterials. 2005;**26**(23):4805-16.
[33] Jonathan NC. "*Liquid-Phase Exfoliation of Nanotubes and Graphene*". Advanced Functional Materials. 2009;**19**(23):3680-95.
[34] Lotya M, King PJ, Khan U, De S, Coleman JN. "*High-Concentration, Surfactant-Stabilized Graphene Dispersions*". ACS Nano. 2010;**4**(6):3155-62.
[35] Khan U, O'Neill A, Lotya M, De S, Coleman JN. "*High-Concentration Solvent Exfoliation of Graphene*". Small. 2010;**6**(7):864-71.
[36] Bourlinos AB, Georgakilas V, Zboril R, Steriotis TA, Stubos AK. "*Liquid-Phase Exfoliation of Graphite Towards Solubilized Graphenes*". Small. 2009;**5**(16):1841-5.
[37] Aboutalebi SH, Gudarzi MM, Zheng QB, Kim J-K. "*Spontaneous Formation of Liquid Crystals in Ultralarge Graphene Oxide Dispersions*". Advanced Functional Materials. 2011;**21**(15):2978-88.
[38] Hernandez Y, Lotya M, Rickard D, Bergin SD, Coleman JN. "*Measurement of Multicomponent Solubility Parameters for Graphene Facilitates Solvent Discovery*". Langmuir. 2009;**26**(5):3208-13.
[39] Bergin SD, Sun Z, Streich P, Hamilton J, Coleman JN. "*New Solvents for Nanotubes: Approaching the Dispersibility of Surfactants*". The Journal of Physical Chemistry C. 2009;**114**(1):231-7.
[40] Blake P, Brimicombe PD, Nair RR, Booth TJ, Jiang D, Schedin F, Ponomarenko LA, Morozov SV, Gleeson HF, Hill EW, Geim AK, Novoselov KS. "*Graphene-Based Liquid Crystal Device*". Nano Letters. 2008;**8**(6):1704-8.
[41] Coleman JN. "*Liquid Exfoliation of Defect-Free Graphene*". Accounts of Chemical Research. 2012;**46**(1):14-22.
[42] Bergin SD, Sun Z, Streich P, Hamilton J, Coleman JN. "*New Solvents for Nanotubes: Approaching the Dispersibility of Surfactants*". J Phys Chem C. 2010;**114**(1):231-7.
[43] Sun Z, Hasan T, Torrisi F, Popa D, Privitera G, Wang F, Bonaccorso F, Basko DM, Ferrari AC. "*Graphene Mode-Locked Ultrafast Laser*". ACS Nano. 2010;**4**(2):803-10.
[44] Ferrari AC, Meyer JC, Scardaci V, Casiraghi C, Lazzeri M, Mauri F, Piscanec S, Jiang D, Novoselov KS, Roth S, Geim AK. "*Raman Spectrum of Graphene and Graphene Layers*". Physical Review Letters. 2006;**97**(18):187401.
[45] Meyer JC, Geim AK, Katsnelson MI, Novoselov KS, Obergfell D, Roth S, Girit C, Zettl A. "*On the roughness of single- and bi-layer graphene membranes*". Solid State Communications. 2007;**143**(1–2):101-9.
[46] Olek M, Ostrander J, Jurga S, Möhwald H, Kotov N, Kempa K, Giersig M. "*Layer-by-Layer Assembled Composites from Multiwall Carbon Nanotubes with Different Morphologies*". Nano Letters. 2004;**4**(10):1889-95.
[47] Sweetman LJ, Nghiem L, Chironi I, Triani G, in het Panhuis M, Ralph SF. "*Synthesis, properties and water permeability of SWNT buckypapers*". Journal of Materials Chemistry. 2012;**22**(27):13800-10.
[48] Yan M, Tallman DE, Bierwagen GP. "*Role of oxygen in the galvanic interaction between polypyrrole and aluminum alloy*". Electrochimica Acta. 2008;**54**(2):220-7.
[49] Aboutalebi SH, Aminorroaya-Yamini S, Nevirkovets I, Konstantinov K, Liu HK. "*Enhanced Hydrogen Storage in Graphene Oxide-MWCNTs Composite at Room Temperature*". Adv Energy Mater. 2012;**2**(12):1439-46.

[50] Aboutalebi SH, Chidembo AT, Salari M, Konstantinov K, Wexler D, Liu HK, Dou SX. "*Comparison of GO, GO/MWCNTs composite and MWCNTs as potential electrode materials for supercapacitors*". Energ Environ Sci. 2011;**4**(5):1855-65.
[51] Polschikov SV, Nedorezova PM, Klyamkina AN, Kovalchuk AA, Aladyshev AM, Shchegolikhin AN, Shevchenko VG, Muradyan VE. "*Composite materials of graphene nanoplatelets and polypropylene, prepared by in situ polymerization*". Journal of Applied Polymer Science. 2013;**127**(2):904-11.
[52] Li Z, Zhou M-R, Zhang T, Zhang J, Yang L, Zhou Z-n. "*The Facile Synthesis of Graphene Nanoplatelets and Lead Styphnate Composites for the Depressed Electrostatic Hazards*". Journal of Materials Chemistry A. 2013.
[53] Yoon O, Sohn I, Kim D, Lee N-E. "*Enhancement of thermomechanical properties of poly(D,L-lactic-co-glycolic acid) and graphene oxide composite films for scaffolds*". Macromol Res. 2012;**20**(8):789-94.
[54] Kilbride BE, Coleman JN, Fraysse J, Fournet P, Cadek M, Drury A, Hutzler S, Roth S, Blau WJ. "*Experimental observation of scaling laws for alternating current and direct current conductivity in polymer-carbon nanotube composite thin films*". Journal of Applied Physics. 2002;**92**(7):4024-30.
[55] Stout DA, Basu B, Webster TJ. "*Poly(lactic–co-glycolic acid): Carbon nanofiber composites for myocardial tissue engineering applications*". Acta Biomaterialia. 2011;**7**(8):3101-12.
[56] Hualin Zhang, Zhiqing Chen. "*Fabrication and Characterization of Electrospun PLGA/MWNTs/ Hydroxyapatite Biocomposite Scaffolds for Bone Tissue Engineering*". Journal of Bioactive and Compatible Polymers. 2010;**25**(3):241-59.
[57] T. A, Hassan M.S, Nam K., Bing Y.Y., Barakat A. N, Khil M, Kim H, . "*Preparation, characterization, and cytotoxicity of CPT/Fe2O3-embedded PLGA ultrafine composite fibers: a synergistic approach to develop promising anticancer material*". International Journal of Nanomedicine. 2012;**7**:1659-70.
[58] Aviss K.J., Gough J.E., Downes S., " *Aligned electrospun polymer fibres for skeletal muscle regeneration*". European Cells and Materials. 2010;**19**:193-204.
[59] Li Y, Feng L, Shi X, Wang X, Yang Y, Yang K, Liu T, Yang G, Liu Z. "*Surface coating-dependent cytotoxicity and degradation of graphene derivatives: Towards the design of non-toxic, degradable nano-graphene*". Small. 2014;**10**(8):1544-54.
[60] Yang K, Wan J, Zhang S, Tian B, Zhang Y, Liu Z. "*The influence of surface chemistry and size of nanoscale graphene oxide on photothermal therapy of cancer using ultra-low laser power*". Biomaterials. 2012;**33**(7):2206-14.

5 SUMMARY AND CONCLUSION

The main aim of this thesis was to design and develop three-dimensional conducting biomaterials using wet-spinning and electrospinning in order to be utilised in biomedical applications. Multifunctional conducting wet-spun fibres such as PEDOT:PSS-CHI, PEDOT:PSS-CHI-PPy.Cipro and PLGA-graphene were fabricated. In addition, a novel spinning strategy which combines electrospinning and wet-spinning was developed to fabricate PEDOT:PSS-CHI-PLGA nanostructured fibres. All of the materials developed and fibres produced were thoroughly studied for their spinnability, mechanical properties, electrical conductivity, electrochemical behaviour and *in vitro* biocompatibility properties. Some of the potential applications of these fibres were demonstrated such as controlled drug release and as supports for cellular growth. The outcome and conclusions of this thesis are summarised and reviewed in the following sections:-

Chapter 2: Multi-functional conducting wet-spun fibres for controlled release of ciprofloxacin

The fabrication of conducting fibres using the conducting polymer PEDOT:PSS was performed using the wet-spinning approach which was subsequently utilised for the controlled delivery of an anitibiotic, Ciprofloxacin. This work demonstrated that highly conducting wet-spun fibres of PEDOT:PSS can be fabricated when using chitosan as coagulation solution. It was found that optimal wet-spinning parameters including feed rate, coagulation composition and size of spinneret are key factors that affect the production of continuous and conducting fibres. Although, chitosan was utilized as coagulation agent to form PEDOT:PSS fibres, it was found that chitosan only contributed around 3.5 % of the total mass of PEDOT:PSS-CHI. This low proportion of chitosan ensured that the conductivity of the fibres formed was not

compromised. The fibres demonstrated electrical conductivity of 56 ± 7 Scm^{-1} after treatment with ethylene glycol.

The high conductivity of these fibres facilitated their subsequent use as an electrode upon which it was possible to electrochemically synthesis a second layer of conducting polymer (polypyrrole) containing the antibiotic ciprofloxacin hydrochloride (Ppy.cipro) as a dopant. The thickness of the Ppy.Cipro layer was tuned by varying current density and time of electropolymerisation, which also resulted in different loadings of drug in the Ppy.Cipro layer. The cyclic voltammogram (CV) of fibres demonstrated electro-activity in PBS, which was essential for the further applications of the fibres to control drug release. The cyclic voltammogram of PEDOT:PSS-CHI-Ppy.Cipro fibres revealed oxidation and reduction peaks at +0.2 V and -0.1 V, respectively, that were utilised later on for the electrical stimulation of fibres to control cipro release. The impedance spectrum of fibres in PBS showed their lower resistivity (~2.8 $k\Omega/cm^2$) at 1 kHz (relevant frequency of biological activities) compared with Pt wire (~ 10.3 $k\Omega/cm^2$), thus confirming the suitability of the fibres as Pt wire replacement.

The release of cipro from the fibres was controlled using electrical stimulation over a 72 hr timeframe. The release profile demonstrated a doubling of the mass of cipro released when the fibres were electrically held in their reduced state compared to the passive (non-stimulated) state. It was also shown that it is possible to reduce the passive release by 20% by applying a voltage that held the fibre in an oxidised state. Moreover, the ability to switch between reduced and oxidised states of the fibres to

control the turning on/off of the cipro release demonstrated the potential of these fibres to modulate the release profiles.

The antibacterial efficacy of cipro (in the fibre as well as when released) was tested to confirm that the antibiotic property of the cipro was retained after electrochemical polymerisation and electrically stimulated release. The presence of a zone of inhibition surrounding the fibres (PEDOT:PSS-CHI-Ppy.Cipro) against two different types of bacteria (*S. pyogenes* and *E.coli*) demonstrated the antibacterial property of the fibres after electrochemical polymerisation. In addition, different sizes of zone of inhibitions were found when the release aliquots were in contact with *S. pyogenes* and *E.coli* which correlated with the amount of cipro released from the fibre (contained in each aliquot). These results confirmed that the antibacterial property of cipro was retained.

The biocompatibility of PEDOT:PSS-CHI and PEDOT:PSS-CHI-Ppy.Cipro fibres was tested using the B35 neuroblastoma cells model. The results demonstrated that neither the fibres or the released cipro are toxic for neural cells, however, it was observed that the neural cells did not attach to the surface of either the PEDOT:PSS-CHI nor PEDOT:PSS-CHI-Ppy.Cipro fibres well and preferred to agglomerate to each other rather than spread along the fibres.

The PEDOT:PSS-CHI-Ppy.Cipro fibres, because of their favourable physical and electrochemical behaviour as well as antibacterial and biocompatibility properties, demonstrate their suitability for use in biomedical applications.

Chapter 3: Combined wet-spinning and electrospinning: new fabrication method to enhance bio-compatibility of conducting fibres

A novel fabrication technique was developed in an attempt to improve the biocompatibility of PEDOT:PSS-CHI wet-spun fibres and enhance the adhesion of B35 neural cells to the fibres. The wet-spinning system was modified by introducing an electrospinning component to the method. Combined wet-spinning and electrospinning was utilised as a new technique to fabricate a conducting or non-conducting 3D architecture depending on the requirements of the final structure.

The combined simultaneous wet-spinning and electrospinning method put to use the two techniques whereby the fabricated micro wet-spun conducting PEDOT:PSS-CHI fibres are covered with a porous PLGA electrospun layer. The physical characterisation of these PEDOT:PSS-CHI-PLGA fibres revealed a porous PLGA electrospun sheath with diameter of 1.64 ± 0.6 μm which was wrapped continuously around the wet-spun fibre. The thickness of the PLGA electrospun sheath could be tuned by varying the electrospinning pumping rate. The electrochemical characterisation (CV in PBS) of the fibres showed that the electrospun sheath does not hinder the transfer of ions from the PBS into the conducting PEDOT:PSS-CHI micro-fibre core.

The drug delivery application of these novel fibres was demonstrated using ciprofloxacin release from the PLGA electrospun sheath. The release profile indicated that the cipro release within the first 28 days was due to diffusion of cipro from the PLGA electrospun sheath. Neural cell attachment onto fibres was revealed by fluorescent imaging techniques and confirmed cell attachment to the surface of

fibres and that the cells also migrated into the electrospun sheath, proliferating and differentiating into the structure. Moreover, the electrospun sheets acted as a guide for neural cells since the size and specific geometry of PLGA electrospun sheets facilitated the attachment of the axons of the B35 neural cells that mimicked the direction of the fibres.

This chapter demonstrated a novel and facile technique for the production of PEDOT:PSS-CHI-PLGA fibres, characterisations of these novel fibres as well as their capability to release drug or support cell growth.

Chapter 4: Wet-spinning of multifunctional PLGA-graphene fibres

The production and application of graphene in fabricating conducting bio-fibres were the main aims of this chapter. The production method of graphene was liquid phase exfoliation of graphene in organic solvent through bath sonication. It was found that the concentration and quality of the produced graphene was dependent on various parameters such as solvent and the sonication time. Initial solid-state exfoliation of graphite, through thermal expansion of graphite, facilitated the diffusion of solvent between the graphene layers and resulted in more efficient solvent exfoliation of graphene.

It was demonstrated that NMP, which was reported to be the most efficient solvent for graphene, is not effective when expanded graphite is used as precursor. However, cyclohexyl-pyrrolidone (CHP) effectively dispersed high concentrations of graphene (up to 5 mg/ml) at much lower sonication times compared to literature reports on solvent exfoliation of graphene. It is suggested in this thesis that the origin of this phenomenon is due to the difference between defects and functionalities in natural

graphite and expanded graphite. Raman spectroscopy studies showed that natural graphite contains a portion of defects and functionalities, represented by the D band in its Raman spectra, whereas the spectra of expanded graphite does not contain a D band. It has been established that, as the sonication time increased it was possible to disperse more graphene into the solvent; until achieving the highest concentration at ~5 mg/ml after 96 hr sonication. Transmission electron microscopy (TEM) analysis showed that the graphene dispersion contained both monolayer and multilayers graphene. The processability of the solvent exfoliated graphene was shown by preparing free-standing robust, flexible and highly conducting graphene paper using vacuum filtration. SEM analysis confirmed that the free-standing graphene paper contain graphene flakes that are well-aligned in the plane of the paper. The comparison between the Raman spectra (2D peak) of graphite and graphene free-standing paper shows that, while the graphene needs aggregates to form the paper, the flakes do not restack in a fully ordered assembly similar to graphite. Raman study of the free-standing graphene paper showed 2D bands reported for graphene flakes of three to five layers. The free-standing graphene paper also had a superior conductivity to those previously reported; which was due to the defect free nature of expanded graphite (graphene precursor).

The high conductivity of the produced graphene made this material an excellent choice for the production of highly conducting composites. Therefore, the solvent exfoliated graphene was added to PLGA to produce an electrically conductive composite. The wet-spinning method was used to spin electrically conductive and robust graphene-PLGA composite fibres. Systematic control of graphene loading in the spinning solution was achieved by dissolving the required amount of PLGA to

the graphene stock dispersion. The addition of PLGA to the graphene dispersion did not have an adverse effect on graphene dispersion quality. Comparing the viscosities of wet-spinnable PLGA with PLGA-graphene solutions suggested that at least 1.5 wt. % of PLGA in the composite spinning solution is required for successful wet-spinning to occur and a fibre to form. This composition resulted in the highest mass loading of graphene of 25 wt. % in the dried fibres (verified by TGA studies). The PLGA fibre displayed very high strain, however when graphene was added, the fibre strain decreased while modulus and ultimate stress increased significantly. The significant drop of strain along with the introduction of conductivity suggests the formation of a graphene network within the fibres. By adding graphene to the PLGA fibres, conductivity was induced and increased with increasing graphene loading. The CV of PLGA-graphene fibre in PBS confirmed the electroactive property of fibres.

The biocompatibility of the fibres was studied through calcein AM staining on C2C12 cells. Results showed that cells could attach to the fibres and spread along their structures and that the specific geometry of the structure (fibre) guided cells to mimic the direction of fibres (also confirmed by Cryo-SEM studies). The ability to guide the direction of the cells growth is an attractive feature of these fibres. Quantitative viability of the C2C12 myoblast cells on the fibres, evaluated using Pico green assay, confirmed the *in vitro* biocompatibility of the fibres.